

# A model of phase fluctuations in a lattice $d$ -wave superconductor: application to the Cooper pair charge-density-wave in underdoped cuprates

Ashot Melikyan and Zlatko Tešanović  
*Department of Physics and Astronomy,*  
*Johns Hopkins University, Baltimore, MD 21218, USA*  
 (September 7, 2018)

We introduce and study an XY-type model of thermal and quantum phase fluctuations in a two-dimensional correlated lattice  $d$ -wave superconductor based on the QED<sub>3</sub> effective theory of high temperature superconductors. General features of and selected results obtained within this model were reported earlier in an abbreviated format (Z. Tešanović, cond-mat/0405235). The model is geared toward describing not only the long distance but also the *intermediate* lengthscale physics of underdoped cuprates. In particular, we elucidate the dynamical origin and investigate specific features of the charge-density-wave of Cooper pairs, which we argue is the state behind the periodic charge density modulation discovered in recent scanning-tunneling-microscopy experiments. We illustrate how Mott-Hubbard correlations near half-filling suppress superfluid density and favor an incompressible state which breaks translational symmetry of the underlying atomic lattice. We show how the formation of the Cooper pair charge-density-wave in such a strongly quantum fluctuating superconductor can naturally be understood as an Abrikosov-Hofstadter problem in a type-II *dual* superconductor, with the role of the dual magnetic field played by the electron density. The resulting Abrikosov lattice of dual vortices translates into the periodic modulation of the Bogoliubov-deGennes gap function and the electronic density. We numerically study the energetics of various Abrikosov-Hofstadter dual vortex arrays and compute their detailed signatures in the single-particle local tunneling density of states. A  $4 \times 4$  checkerboard-type modulation pattern naturally arises as an energetically favored ground state at and near the  $x = 1/8$  doping and produces the local density of states in good agreement with experimental observations.

PACS numbers:

## I. INTRODUCTION

Several recent experiments<sup>1,2,3</sup> support the proposal that the pseudogap state in underdoped cuprates should be viewed as a phase-disordered superconductor<sup>4</sup>. The effective theory based on this viewpoint was derived in Ref. 5: One starts with the observation<sup>6</sup> that in a phase fluctuating cuprate superconductor the Cooper pairing amplitude is large and robust, resulting in a short coherence length  $\xi \sim k_F^{-1}$  and small, tight cores for *singly quantized* (anti)vortices. As a result, the phase fluctuations are greatly enhanced, with  $hc/2e$  vortex and antivortex excitations, their cores containing hardly any electrons, quantum tunneling from place to place with the greatest of ease, scrambling off-diagonal order in the process – incidentally, this is the obvious interpretation of the Nernst effect experiments<sup>2</sup>. Simultaneously, the largely inert pairing amplitude takes on a dual responsibility of suppressing multiply quantized (anti)vortices, which require larger cores and cost more kinetic energy, while continuously maintaining the pseudogap effect in the single electron excitation spectrum. The theory of Ref. 5 uses this large  $d$ -wave pairing pseudogap  $\Delta$  to set the stage upon which the low-energy degrees of freedom, identified as electrons organized into Cooper pairs and BdG nodal fermions, and fluctuating  $hc/2e$  vortex-antivortex pairs, mutually interact via two emergent non-compact U(1) gauge fields,  $v_\mu$  and  $a_\mu$ .  $v$  and  $a$  couple to

electronic charge and spin degrees of freedom, respectively, and mediate interactions which are responsible for the three major phases of the theory<sup>5,7</sup>: A  $d$ -wave superconductor, an insulating spin-density wave (SDW), which at half-filling turns into a Mott-Hubbard-Neel antiferromagnet), and an intermediate “algebraic Fermi liquid”, a non-Fermi liquid phase characterized by critical, power-law correlations of nodal fermions.

In the context of the above physical picture, the recent discovery in scanning tunneling microscopy (STM) experiments<sup>8,9,10</sup> of the “electron crystal”, manifested by a periodic modulation of the local density of states (DOS), and the subsequent insightful theoretical analysis<sup>11</sup> of this modulation in terms of the *pair* density-wave, comes not entirely unexpected. Such modulation originates from the charge Berry phase term involving  $v_0$ <sup>5,12</sup>, the time-like component of  $v_\mu$ , and the long-distance physics behind it bears some resemblance to that of the elementary bosons, like <sup>4</sup>He (Ref. 13). As the quantum phase fluctuations become very strong, they occasion a suppression of the compressibility of the underlying electron system, via the phase-particle number uncertainty relation  $\Delta\varphi\Delta N \gtrsim 1$ , whose effective theory manifestation is precisely the above charge Berry phase. Once the off-diagonal order disappears, the system inevitably turns incompressible and the diagonal positional order sets in, leading to a Mott insulating state. The resulting charge-density-wave of Cooper pairs (CPCDW)<sup>12</sup> causes a periodic modulation of the electron density and the size

of the pseudogap  $\Delta$  and induces a similarly modulated local tunneling DOS. In this context, the observed “electron crystal” state<sup>9</sup> should be identified as a CPCDW.

While the above CPCDW scenario is almost certainly qualitatively correct, the ultimate test of the theory is whether it can explain and predict some of the *specific details* of the modulation patterns as they are actually observed in cuprates. This brings us to the main theme of this paper. Typically, when constructing an effective low energy theory of a condensed matter system, we are solely concerned with the long distance, low energy behavior. In the present case, however, this will not suffice. The modulation in question is associated with length and energy scales which are *intermediate*, between the short distance scale physics of a single lattice spacing and the ultimate long distance behavior. Our aim should thus be to construct a description which will be valid not only over very long lengthscales but also on the scale of several lattice spacings, which are the periodicities observed in experiments<sup>8,9,10</sup>. Furthermore, we ideally should be aiming for a “bosonized” version of the theory, within which a mean-field type approximation for the CPCDW state could be gainfully formulated. A natural question that needs to be answered first is what should be the objects that play the role of these bosons?

One choice is to designate *real-space* pairs of electrons (or holes) as such “elementary” bosons and to endow them with some “manageable”, i.e. pairwise and short-ranged, effective interactions. Such a model indeed generically leads to a phase diagram with compressible superfluid and incompressible Wigner crystal states just as our long-distance argument has suggested. This picture of real-space pairs arises within the SO(5)-based theory<sup>14,15</sup>, where the low energy sector of the theory assumes the form of hard-core plaquette bosons with nearest and next-nearest neighbor interactions. When one is dealing with extremely strongly bound *real space* *s*-wave or *d*-wave pairs this is undoubtedly the natural choice. In our view, however, in cuprates one is faced not with the real-space pairs but with the *momentum space* Cooper pairs. Apparently, one encounters here an echo of the great historical debate on Blatt-Schafroth versus BCS pairs – while certain long distance features are the same in both limits, many crucial properties are quite different<sup>16</sup>. To be sure, the Cooper pairs in cuprates are not far from the real-space boundary; the coupling is strong, the BCS coherence length is short, and the fluctuations are greatly enhanced. Still, there is a simple litmus test that places cuprates squarely on the BCS side: they are *d*-wave superconductors *with nodal fermions*.

This being the case, constructing a theory with Cooper pairs as “elementary” bosons turns into a daunting enterprise. Cooper pairs in nodal *d*-wave superconductors are highly non-local objects in the real space, and the effective theory in terms of their center-of-mass coordinates will reflect this non-locality in an essential way, with complicated intrinsically multi-body, extended-range interactions. The basic idea behind the QED<sub>3</sub> theory<sup>5</sup> is that

in these circumstances the role of “elementary” bosons should be accorded to *vortices* instead of Cooper pairs. Vortices in cuprates, with their small cores, are simple real space objects and the effective theory of quantum fluctuating vortex-antivortex pairs can be written in the form that is local and far simpler to analyze. In this dual language the formation of the CDW of Cooper pairs translates – via the charge Berry phase discussed above – to the familiar Abrikosov-Hofstadter problem in a dual superconductor<sup>12,17</sup>. The solution of this problem intimately reflects the non-local character of Cooper pairs and their interactions, and the specific CPCDW modulation patterns that arise in such theory are generally *different* from those of a real-space pair density wave. These two limits, the Cooper versus the real-space pairs, correspond to two different regimes of a dual superconductor, reminiscent of the strongly type-II versus strongly type-I regimes in ordinary superconductors. This difference is fundamental and, while both descriptions are legitimate, only one has a chance of being relevant for cuprates.

A well-informed reader will immediately protest that the key tenet of the QED<sub>3</sub> theory is that we *cannot* write down a useful “bosonized” version of the theory at all – the nodal BdG fermions in a fluctuating *d*-wave superconductor must be kept as an integral part of the quantum dynamics in underdoped cuprates. This, while true, mostly reflects the central role of nodal fermions in the *spin* channel. In contrast, the formation of CPCDW is predominantly a *charge* sector affair and there, provided the theory is reexpressed in terms of vortex-antivortex fluctuations – i.e. properly “dualized” – the effect of nodal fermions is less singular and definitely treatable. This gives one hope that a suitably “bosonized” dual version of the charge sector might be devised which will provide us with a faithful representation of underdoped cuprates. This is the main task we undertake in this paper.

To this end, following a brief review of the QED<sub>3</sub> theory in Section II, we propose in Section III a simple but realistic XY-type model of a thermally phase-fluctuating *d*-wave superconductor. Starting from this model we derive its effective Coulomb gas representation in terms of vortex-antivortex pairs. This representation is employed in Section IV to construct an effective action for quantum fluctuations of vortex-antivortex pairs and derive its field theory representation in terms of a dual type-II superconductor, incorporating the effect of nodal fermions. In Section V, we discuss some general features of this dual type-II superconductor and relate our results to the recent STM experiments<sup>8,9,10</sup>. This section is written in the style that seeks to elucidate basic concepts at the expense of overbearing mathematics; we hope the presentation can be followed by a general reader. After this we plunge in Section VI into a detailed study of the dual Abrikosov-Hofstadter-like problem which arises in the mean-field approximation applied to a dual superconductor and which regulates various properties of the CPCDW state. This particular variant of the Abrikosov-

Hofstadter problem arises from the said charge Berry phase effect: In the dual representation quantum bosons representing fluctuating vortex-antivortex pairs experience an overall *dual* magnetic field, generated by Cooper pairs, whose flux per plaquette of the (dual) CuO<sub>2</sub> lattice is set by doping:  $f = p/q = (1 - x)/2$ . Finally, a brief summary of our results and conclusions are presented in Section VII.

## II. BRIEF REVIEW OF THE QED<sub>3</sub> THEORY

The purpose of this section is mainly pedagogical: Before we move on to our main topic, we provide some background on the QED<sub>3</sub> effective theory of the pairing pseudogap in underdoped cuprates. This will serve to motivate our interest in constructing an XY-type model of fluctuating *d*-wave superconductors and to make a casual reader aware of the connection between the theoretical notions discussed in the rest of this paper and the actual physics of real electrons in CuO<sub>2</sub> planes. The readers well versed in the art of construction of effective field theories or those already familiar with the approach of Ref. 5 can safely jump directly to Section III.

The effective theory<sup>5</sup> of a strongly fluctuating  $d_{x^2-y^2}$ -wave superconductor represents the interactions of fermions with  $hc/2e$  vortex-antivortex excitations in terms of two non-compact emergent gauge fields,  $v_\mu$  and  $a_\mu^i$ . The Lagrangian  $\mathcal{L} = \mathcal{L}_f + \mathcal{L}_0$  is

$$\bar{\Psi}[D_0 + iv_0 - ieA_0 + \frac{(\mathbf{D} + i\mathbf{v} - ie\mathbf{A})^2}{2m} - \mu]\Psi - i\Delta\Psi^T\sigma_2\hat{\eta}\Psi + c.c. + \mathcal{L}_0[v, a] \quad , \quad (1)$$

where  $\bar{\Psi} = (\bar{\psi}_\uparrow, \bar{\psi}_\downarrow)$ ,  $\sigma_i$ 's are the Pauli matrices,  $\Delta$  is the amplitude of the  $d_{x^2-y^2}$  pairing pseudogap,  $A_\mu$  is the external electromagnetic gauge field,  $D_\mu = \partial_\mu + i2a_\mu^i(\sigma_i/2)$  is SU(2) covariant derivative and  $\hat{\eta} \equiv D_x^2 - D_y^2$ .  $\mathcal{L}_0[v, a]$  is generated by the Jacobian of the Franz-Tešanović (FT) singular gauge transformation:

$$\exp\left(-\int_0^\beta d\tau \int d^2r \mathcal{L}_0[v_\mu, a_\mu^i]\right) = \int d\Omega_{\hat{\mathbf{n}}} \sum_{A,B} \int \mathcal{D}\varphi(\mathbf{r}, \tau) \times 2^{-N_i} \delta[(w/\pi) - (n_A + n_B)] \delta[(\tilde{F}^i/\pi) - G_{A,B}^i] \quad , \quad (2)$$

where  $2\pi n_{A,B} = \partial \times \partial\varphi_{A,B}$ ,  $w = \partial \times v$ ,  $\tilde{F}_\lambda^i = \frac{1}{2}\epsilon_{\lambda\mu\nu}F_{\mu\nu}^i$ ,  $F_{\mu\nu}^i = \partial_\mu a_\nu^i - \partial_\nu a_\mu^i + 2\epsilon^{ijk}a_\mu^j a_\nu^k$ ,  $G_{A,B}^i = \Omega(\hat{\mathbf{n}})^{ij}m_j$ ,  $m_j = (0, 0, (n_A - n_B))$ ,  $\Omega(\hat{\mathbf{n}})$  rotates the spin quantization axis from  $\hat{\mathbf{z}}$  to  $\hat{\mathbf{n}}$ , and  $\int d\Omega_{\hat{\mathbf{n}}}$  is the integral over such rotations.

Its menacing appearance notwithstanding, the physics behind (1) is actually quite clear. In  $\mathcal{L}_f$ , which is just the effective *d*-wave pairing Lagrangian, the original electrons  $c_\sigma(x)$ , with the spin quantized along an *arbitrary* direction  $\hat{\mathbf{n}}$ , have been turned into topological fermions  $\bar{\Psi} = (\bar{\psi}_\uparrow, \bar{\psi}_\downarrow)$  through the application of the FT transformation:  $(\bar{c}_\uparrow, \bar{c}_\downarrow) \rightarrow (\exp(i\varphi_A)\bar{\psi}_\uparrow, \exp(i\varphi_B)\bar{\psi}_\downarrow)$ , where

$\exp(i\varphi_A(x) + i\varphi_B(x))$  equals  $\exp(i\varphi(x))$ , the center-of-mass fluctuating superconducting phase (see Ref. 5 for details). The main purpose of this transformation is to strip the awkward phase factor  $\exp(i\varphi(x))$  from the center-of-mass gap function, leaving behind a *d*-wave pseudogap amplitude  $\Delta$  and two gauge fields,  $v$  and  $a^i$ , which mimic the effects of phase fluctuations. The Jacobian given by  $\mathcal{L}_0[v, a^i]$  (2) insures that the fluctuations in *continuous* fields  $v$  and  $a^i$  faithfully represent configurations of *discrete* (anti)vortices. Note that topological fermions do not carry a definite charge and are neutral on the average – they do, however, carry a definite spin  $S = \frac{1}{2}$ , reflecting the fact that the spin SU(2) symmetry remains intact in a spin-singlet superconductor. As a consequence, the spin density operator  $S_z = \bar{c}_\uparrow c_\uparrow - \bar{c}_\downarrow c_\downarrow = \bar{\psi}_\uparrow \psi_\uparrow - \bar{\psi}_\downarrow \psi_\downarrow$  is an invariant of the FT transformation.

The two gauge fields,  $v$  and  $a^i$ , are the main dynamical agents of the theory. They describe the interactions of fermionic BdG quasiparticles with vortex-antivortex pair excitations in the fluctuating superconducting phase  $\varphi(x)$ . A U(1) gauge field  $v_\mu$  is the quantum fluctuating superflow and enters the non-conserved charge channel. In the presence of the external electromagnetic field  $A_\mu$ , one has  $v_\mu \rightarrow v_\mu - eA_\mu$  everywhere in  $\mathcal{L}_f$  (1) (but *not* in  $\mathcal{L}_0$ ), to maintain the local gauge symmetry of Maxwell electrodynamics. The Jacobian  $\mathcal{L}_0$  (2) is the exception since it is a purely mathematical object, generated by the change of variables from discrete (anti)vortex coordinates to continuous fields  $v$  (and  $a^i$ ).  $v_\mu$  appearing in  $\mathcal{L}_0$  contains only the vortex part of the superflow and is intrinsically gauge invariant. This point is of much importance since it is the state of the fluctuating (anti)vortices, manifested through  $\mathcal{L}_0[v, a^i]$ , which determines the state of our system as a whole, as we will see momentarily.

By comparison to  $v$ , an SU(2) gauge field  $a_\mu^i$  is of a more intricate origin. It encodes topological frustration experienced by BdG quasiparticles as they encircle  $hc/2e$  vortices; the frustration arises from the  $\pm 1$  phase factors picked up by fermions moving through the spacetime filled with fluctuating vortex-antivortex pairs. These phase factors, unlike those produced by superflow and emulated by  $v$ , are insensitive to vorticity and depend only on the spacetime configuration of vortex loops, not on their internal orientation: if we picture a fixed set of closed loops in 2+1-dimensional spacetime we can change the orientation of any of the loops any which way without affecting the topological phase factors, although the ones associated with superflow will change dramatically. This crucial symmetry of the original problem dictates the manner in which  $a^i$  couples to fermions in the above effective theory<sup>5</sup>. Its topological origin is betrayed by its coupling to a *conserved* quantum number – in spin-singlet superconductors this is a quasiparticle spin – and the absence of direct coupling to the non-conserved charge channel. By strict rules of the effective theory, such minimal coupling to BdG quasiparticles is what endows  $a_\mu^i$  with its ultimate punch at the low-

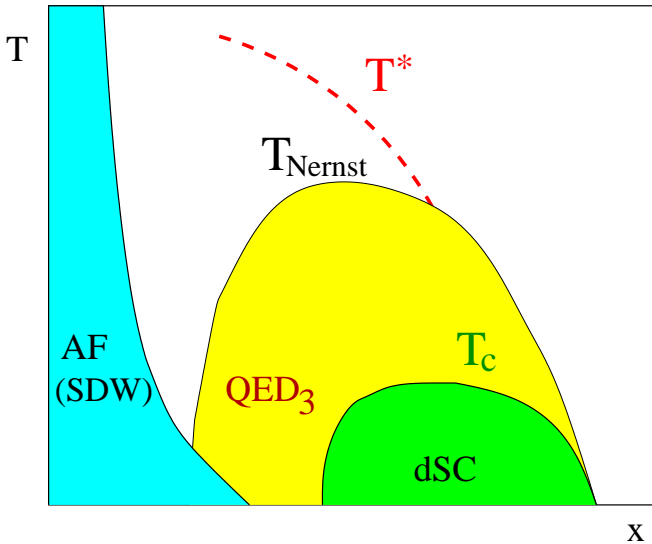


FIG. 1: The phase diagram of cuprates following from the QED<sub>3</sub> theory. Under the  $T_{\text{Nernst}}$  dome, the Nernst effect experiments<sup>2</sup> indicate strong vortex-antivortex fluctuations; this is where the conditions for the applicability of the theory are met. As the doping is reduced, the superconducting ground state is followed by an “algebraic” Fermi liquid, a non-Fermi liquid state described by the symmetric phase of QED<sub>3</sub> and characterized by critical, power-law correlations<sup>23</sup>. At yet lower doping, the BdG chiral symmetry is broken, resulting in an incommensurate antiferromagnet (SDW), which eventually morphs into the Neel antiferromagnet at half-filling. Depending on material parameters (anisotropy, strength of residual interactions, degree of interlayer coupling, etc.) of a particular HTS system, the transition between a superconductor and a SDW could be a direct one, without the intervening chiral symmetric ground state. The way CPCDW, the main subject of this paper, fits into this phase diagram is detailed later in the text.

est energies. While in this limit  $v_\mu$  – which couples to fermions in the non-minimal, non-gauge invariant way – turns massive and ultimately irrelevant,  $a_\mu^i$  ends up generating the interacting infrared (IR) critical point of QED<sub>3</sub> theory which regulates the low energy fermiology of the pseudogap state.

$\mathcal{L}$  (1) manifestly displays the U(1) charge and SU(2) spin global symmetries, and is useful for general considerations. To perform explicit calculations in the above theory one must face up to a bit of algebra that goes into computing  $\mathcal{L}_0[v, a^i]$ . The main technical obstacle is provided by two constraints: *i*) the sources of  $a_\mu^i$  should be an SU(2) gauge equivalent of half-flux Dirac strings, and *ii*) these sources are permanently confined to the sources of  $v_\mu$ , which themselves are also half-flux Dirac strings. The confined objects formed by these two half-string species are nothing but the physical fluctuating  $hc/2e$  vortex excitations. These constraints are the main source of technical hurdles encountered in trying to reduce (1) to a more manageable form – nevertheless, it is imperative they be carefully enforced lest we lose

the essential physics of the original problem. The constraints can be solved by introducing two dual complex fields  $\Phi(x) = |\Phi|e^{i\phi}$  and  $\Phi_s(x) = |\Phi_s|e^{i\phi_s}$  to provide coherent functional integral representation of the half-strings corresponding to  $v_\mu$  and  $a_\mu^i$ , respectively. In this dual language the half-strings are simply the worldlines of dual bosons  $\Phi$  and  $\Phi_s$  propagating through (2 + 1)-dimensional spacetime. It is important to stress that this is just a mathematical tool used to properly couple vortex-antivortex pair fluctuations to the electronic degrees of freedom – readers less intimate with the technology of dualization will find it explained in detail in the Appendix. The confinement of the two species of half-strings into  $hc/2e$  (anti)vortices is accomplished by demanding  $|\Phi(x)| = |\Phi_s(x)|$ . This finally results in  $\mathcal{L}_0$  expressed as

$$\exp\left(-\int_0^\beta d\tau \int d^2r \mathcal{L}_0[v_\mu, a_\mu^i]\right) \rightarrow \int d\Omega_{\hat{n}} \int \mathcal{D}[\Phi, \phi_s, A_d, \kappa^i] \times \mathcal{C}^{-1}[|\Phi|] \exp\left\{\int d^3x (i2A_d \cdot w + i2\kappa^i \cdot \tilde{F}^i - \mathcal{L}_d)\right\}, \quad (3)$$

where  $\mathcal{L}_d[\Phi, A_d, \kappa^i]$  is a dual Lagrangian given by

$$m_d^2|\Phi|^2 + |(\partial_\mu - i2\pi A_{d\mu})\Phi|^2 + \frac{g}{2}|\Phi|^4 + |\Phi|^2(\partial_\mu\phi_s - 2\pi\Omega^{i3}\kappa_\mu^i)^2, \quad (4)$$

and  $\mathcal{C}[|\Phi|]$  is a normalization factor determined by

$$\int d\Omega_{\hat{n}} \mathcal{D}[a^i, \phi_s, \kappa^i] \exp\{i2\kappa^i \cdot \tilde{F}^i + |\Phi|^2(\partial_\mu\phi_s - 2\pi\Omega^{i3}\kappa_\mu^i)^2\}. \quad (5)$$

Here  $A_d$  and  $\kappa^i$  are the charge and spin dual gauge fields, respectively, having been introduced to enforce the two  $\delta$ -functions in (2). Relative to our notation here, in Ref. 12 both gauge fields are rescaled as  $A_d(\kappa^i) \rightarrow 2\pi A_d(\kappa^i)$ . Notice that  $A_d$  and  $\kappa^i$  couple to  $v$  and  $a^i$  as  $\exp(i2A_d \cdot w + i2\kappa^i \cdot \tilde{F}^i) = \exp(i2A_d \cdot (\partial \times v) + i\kappa_\lambda^i \epsilon_{\lambda\mu\nu} (\partial_\mu a_\nu^i - \partial_\nu a_\mu^i + 2\epsilon^{ijk} a_\mu^j a_\nu^k))$  (3).

At this point, one should take note of the following convenient property of  $\mathcal{L}$  (1,3), one that will prove handy repeatedly as we go along:  $A_d$  and  $\kappa^i$  provide – via the above coupling to  $v$  and  $a^i$  – the only link of communication between the fermionic matter Lagrangian  $\mathcal{L}_f$  and the vortex-antivortex state Jacobian  $\mathcal{L}_0$ . This way of formulating the theory is more than a mere mathematical nicety: It is particularly well-suited for the strongly fluctuating superconductor which nonetheless does *not* belong to the extreme strongly bound limit of real-space pairs, when they can be viewed as “elementary” bosons. Such extreme limit of “preformed” pairs or pair “molecules” is frequently invoked, inappropriately in our view, to describe the cuprates. Were the cuprates in this extreme limit, there would be *no* gapless nodal quasiparticle excitations, the situation manifestly at odds

with the available experimental information<sup>19</sup>. In addition, such demise of nodal fermions would rob the effective low-energy theory of any *spin* degrees of freedom, a most undesirable theoretical feature in the context of all we know about the cuprates.

In a superconductor, the vortex-antivortex pairs are bound and the dual bosons representing vortex loop worldlines are in the “normal” (i.e., non-superfluid state):  $\langle \Phi \rangle = \langle \Phi_s \rangle = 0$  (see the Appendix). Consequently, both dual gauge fields are  $A_d$  and  $\kappa^i$  are massless; this is as it should be in the dual normal state. This implies that upon integration over  $A_d$  and  $\kappa^i$  both  $v_\mu$  and  $a_\mu^i$  will be *massive*:  $\mathcal{L}_0 \rightarrow M_0^2 v_0^2 + M_\perp^2 \mathbf{v}^2 + (v \rightarrow a)$ , where  $M_0^2 \propto M_\perp^2 \sim \xi_d$ , the dual correlation length. As advertised above, the massive character of  $v$  immediately makes the system a physical superconductor: If we introduce a static external source vector potential  $\mathbf{A}^{ex}(\mathbf{q})$ , the response to this perturbation is determined by the fermionic “mean-field” stiffness originating from  $\mathcal{L}_f$  and the “intrinsic” stiffness set by  $\mathcal{L}_0$ , whichever is *smaller*. In a strongly fluctuating superconductor this in practice means  $\mathcal{L}_0$ . The mass  $M_\perp^2(x, T)$  of the Doppler gauge field  $\mathbf{v}$  in  $\mathcal{L}_0$  is effectively the helicity modulus of such a superconductor and determines its superfluid density  $\rho_s$ , reduced far below what would follow from  $\mathcal{L}_f$  alone. In a similar vein, the mass  $M_0^2(x, T)$  of  $v_0$  sets the compressibility of the system  $\chi_c$ , again far smaller than the value for the non-interacting system of electrons at the same density:

$$\begin{aligned} \rho_s &\sim \lim_{\mathbf{q} \rightarrow 0} \frac{\delta^2 E_0}{\delta \mathbf{A}^{ex}(\mathbf{q}) \delta \mathbf{A}^{ex}(-\mathbf{q})} = \frac{\Pi_f^{jj}(\mathbf{q}) M_\perp^2}{\Pi_f^{jj}(\mathbf{q}) + M_\perp^2} \sim M_\perp^2, \\ \chi_c &\sim \lim_{\mathbf{q} \rightarrow 0} \frac{\delta^2 E_0}{\delta A_0^{ex}(\mathbf{q}) \delta A_0^{ex}(-\mathbf{q})} = \frac{\Pi_f^{\rho\rho}(\mathbf{q}) M_0^2}{\Pi_f^{\rho\rho}(\mathbf{q}) + M_0^2} \sim M_0^2 \end{aligned} \quad (6)$$

where  $E_0$  is the ground state energy and  $\Pi_f^{jj}(\mathbf{q}; x, T)$  and  $\Pi_f^{\rho\rho}(\mathbf{q}; x, T)$  are the current-current and density-density responses of the fermionic Lagrangian  $\mathcal{L}_f$ , respectively.

Evidently, the “intrinsic” stiffness of  $v$  as it appears in  $\mathcal{L}_0$  encodes at the level of the effective theory the strong Mott-Hubbard short-range correlations which are the root cause of reduced compressibility and superfluid density and enhanced phase fluctuations in underdoped cuprates. This is entirely consistent with the spirit of the effective theory and should be contrasted with the application of a Gutzwiller-type projector to a mean-field BCS state, to which it is clearly superior: In the latter approach one is suppressing on-site double occupancy by a local projector mimicking correlations that are *already* included at the level of the renormalized “mean-field” fermionic Lagrangian  $\mathcal{L}_f$  in (1), i.e. they are built-in into  $\Pi_f^{jj}$  and  $\Pi_f^{\rho\rho}$  (6). In this approach the superconductivity is always present at  $T = 0$  as long as the doping is finite, albeit with a reduced superfluid density. In contrast, within the effective theory (1), the microscopic Mott-Hubbard correlations are *additionally* echoed by the appearance of well-defined vortex-antivortex exci-

tations, whose core size is kept small by a large pairing pseudogap  $\Delta$ . Such vortex-antivortex excitations further suppress superfluid density from its renormalized “mean-field” value and ultimately destroy the off-diagonal long range order (ODLRO) altogether – even at  $T = 0$  and finite doping – all the while remaining sharply defined with no perceptible reduction in  $\Delta$ .

As the vortex-antivortex pairs unbind, the superconductivity is replaced by the dual superfluid order:  $\langle \Phi \rangle \neq 0$ ,  $\langle \Phi_s \rangle \neq 0$ , and  $v_\mu$  and  $a_\mu^i$  turn massless:  $\mathcal{L}_0 \rightarrow c_0 \xi (\nabla v_0)^2 + c \xi (\nabla \times \mathbf{v})^2 + (v \rightarrow a)$ , where  $\xi(x, T \rightarrow 0)$  is the superconducting correlation length,  $c_0$  and  $c$  are numerical constants, and we have used radiation gauge  $\nabla \cdot \mathbf{v} = 0$ . Physically, the massless character of  $v_\mu$  and  $a_\mu^i$  describes the admixing of *free* quantum vortex-antivortex excitations into the ground state of the system which started as a *d*-wave superconductor. Now, it is clear from Eq. (6) that the response to  $\mathbf{A}^{ex}(\mathbf{q})$  is *entirely* determined by  $\mathcal{L}_0$ . The massless character of  $\mathbf{v}$  in  $\mathcal{L}_0$  implies the vanishing of the helicity modulus and superfluid density, despite the fact that the contribution from  $\mathcal{L}_f$  to both remains *finite* and hardly changes through the transition. Similarly, the response to  $A_0^{ex}(\mathbf{q})$  vanishes as well, since  $v_0$  is now massless. Thus, the system simultaneously loses superfluidity ( $\rho_s \rightarrow 0$ ) and turns incompressible ( $\chi_c \sim c_0 \xi |\mathbf{q}|^2 \rightarrow 0$ ) for doping smaller than some critical  $x_c$ .

Note that the theory<sup>5</sup> predicts a universal relation between the superfluid density  $\rho_s$  and the fluctuation diamagnetic susceptibility  $\chi_{\text{dia}}$  in underdoped cuprates, as  $T \rightarrow 0$ . Right before the superconductivity disappears, for  $x > x_c$ , the discussion surrounding Eq. (6) implies  $\rho_s \sim M_\perp^2 \sim 1/\xi_d$ . Similarly, in the region of strong superconducting fluctuations for  $x < x_c$ ,  $M_\perp^2$  in (6) is replaced by  $c\xi \mathbf{q}^2$  as is clear from the previous paragraph. The prefactor  $c\xi$  is nothing but the diamagnetic susceptibility  $\chi_{\text{dia}} \sim c\xi$ . Assuming that the superconducting correlation length and its dual are proportional to each other,  $\xi \sim \xi_d$ , one finally obtains  $\chi_{\text{dia}} \sim \rho_s^{-1}$ . In the case where strong phase fluctuations deviate from “relativistic” behavior, the dynamical critical exponent  $z \neq 1$  needs to be introduced and the above expressions generalized to  $\rho_s \sim M_\perp^2 \sim 1/\xi_d^z$ ,  $\chi_{\text{dia}} \sim \xi_d^{2-z}$ , and  $\chi_{\text{dia}} \sim \rho_s^{(z-2)/z}$ . Experimental observation of such a universal relation between  $\rho_s$  and  $\chi_{\text{dia}}$  would provide a powerful evidence for the dominance of *quantum* phase fluctuations in the pseudogap state of underdoped cuprates.

In the “dual mean-field” approximation  $\langle \Phi \rangle = \langle \Phi_s \rangle = \Phi$  one finds:

$$\begin{aligned} \mathcal{L}_0 &= \frac{1}{4\pi^2 |\Phi|^2} (\partial \times v)^2 + \mathcal{L}_0^a[a^i]; \\ e^{-\int d^3x \mathcal{L}_0^a} &= \mathcal{C}^{-1} \int \mathcal{D}\kappa^i \exp\left\{ \int d^3x (i2\kappa^i \cdot \tilde{F}^i + \mathcal{R}[\kappa^i]) \right\}, \end{aligned} \quad (7)$$

where  $\int d^3x \mathcal{R} \equiv \ln \int d\Omega_{\hat{\mathbf{n}}} \exp(-4\pi^2 \int d^3x |\Phi|^2 (\kappa_\mu^i \hat{n}_i)^2)$ .

$\mathcal{L}_0^a[a^i]$  appears somewhat unwieldy, chiefly through its non-local character. The non-locality is the penalty we

pay for staying faithful to the underlying physics: While the topological origin of  $a^i$  demands coupling to the conserved SU(2) spin three-currents, its sources are permanently confined to Dirac half-strings of the superflow Doppler field  $v$ , which by its very definition is a non-compact U(1) gauge field (see below). The manifestly SU(2) invariant form (1) subjected to these constraints is therefore even more elegant than it is useful.

The situation, however, can be remedied entirely by a judicious choice of gauge:  $a_\mu^1 = a_\mu^2 = 0$ ,  $a_\mu^3 = a_\mu$ . In this “spin-axial” gauge – which amounts to selecting a fixed (but arbitrary) spin quantization axis – the integration over  $\kappa_i$  can be performed and  $\mathcal{L}_0^a$  (7) reduces to a simple local Maxwellian:

$$\mathcal{L}_0[v, a] \rightarrow \frac{1}{4\pi^2|\Phi|^2}(\partial \times v)^2 + \frac{1}{4\pi^2|\Phi|^2}(\partial \times a)^2 \quad , \quad (8)$$

where  $\Phi$  is the dual order parameter of the pseudogap state, i.e. the condensate of loops formed by vortex-antivortex creation and annihilation processes in (2+1)-dimensional Euclidean spacetime. This is the quantum version of the Kosterlitz-Thouless unbound vortex-antivortex pairs and is discussed in detail in the Appendix. The effective Lagrangian  $\mathcal{L} = \mathcal{L}_f + \mathcal{L}_0[v, a]$  of the quantum fluctuating  $d$ -wave superconductor finally takes the form:

$$\bar{\Psi}[D_0 + iv_0 - ieA_0 + \frac{(\mathbf{D} + i\mathbf{v} - ie\mathbf{A})^2}{2m} - \mu]\Psi - i\Delta\Psi^T\sigma_2\hat{\eta}\Psi + \text{c.c.} + \mathcal{L}_0[v, a] \quad , \quad (9)$$

where  $D_\mu \rightarrow \partial_\mu + ia_\mu\sigma_3$ , other quantities remain as defined below Eq. (1), and  $\mathcal{L}_0[v, a]$  of the pseudogap state is given by Eq. (8). More generally, the full spin-axial gauge expression for  $\mathcal{L}_0[v, a]$  in (9), valid both in the pseudogap ( $\langle\Phi\rangle \neq 0$ ) and superconducting ( $\langle\Phi\rangle = 0$ ) states, is:

$$\exp\left(-\int_0^\beta d\tau \int d^2r \mathcal{L}_0[v_\mu, a_\mu]\right) \rightarrow \int \mathcal{D}[\Phi, \phi_s, A_d, \kappa] \times \mathcal{C}^{-1}[|\Phi|] \exp\left\{\int d^3x (i2A_d \cdot w + i2\kappa \cdot \tilde{F} - \mathcal{L}_d)\right\} \quad , \quad (10)$$

where dual Lagrangian  $\mathcal{L}_d[\Phi, A_d, \kappa]$  is

$$m_d^2|\Phi|^2 + |(\partial_\mu - i2\pi A_{d\mu})\Phi|^2 + \frac{g}{2}|\Phi|^4 + |\Phi|^2(\partial_\mu\phi_s - 2\pi\kappa_\mu)^2 \quad , \quad (11)$$

and normalization factor  $\mathcal{C}[|\Phi|]$  equals

$$\int \mathcal{D}[a, \phi_s, \kappa] \exp\{i2\kappa \cdot \tilde{F} + |\Phi|^2(\partial_\mu\phi_s - 2\pi\kappa_\mu)^2\} \quad . \quad (12)$$

Again,  $A_d$  and  $\kappa$  are the charge and spin dual gauge fields, respectively, which, in the spin-axial gauge, couple to  $v$  and  $a$  as  $\exp(i2A_d \cdot w + i2\kappa \cdot \tilde{F}) = \exp(i2A_d \cdot (\partial \times v) + i\kappa_\lambda \epsilon_{\lambda\mu\nu}(\partial_\mu a_\nu - \partial_\nu a_\mu))$  (10).

The above is just the standard form of the QED<sub>3</sub> theory discussed earlier<sup>5</sup>. It resurfaces here as a particular gauge edition of a more symmetric, but also far more cumbersome description – fortunately, in contrast to its high symmetry parent, the Lagrangian (9) itself is eminently treatable<sup>20</sup>.

A committed reader should note that the ultimate non-compact U(1) gauge theory form of  $\mathcal{L}$  (9) arises as a natural consequence of the constraints described above. Once the sources of  $v$  and  $a$  are confined into physical  $hc/2e$  vortices, the non-compact U(1) character is the shared fate for both. While we do have the choice of selecting the singular gauge in which to represent the Berry gauge field  $a$ , there is no similar choice for  $v$ , which must be a non-compact U(1) gauge field. It is then only natural to use the FT gauge and represent  $a$  as a non-compact U(1) field as well, in order to straightforwardly enforce the confinement of their respective sources<sup>21</sup>. The non-compactness in this context reflects nothing but an elementary property of a phase-fluctuating superconductor: The conservation of a topological vortex charge  $\partial \cdot n = 0 = \partial \cdot n_{A,B}$ <sup>22</sup>.

We end this section with the following remarks: In explicit calculations with (9) or its lattice equivalent, it is often useful to separate the low energy nodal BdG quasiparticle excitations from the rest of the electronic degrees of freedom by linearizing  $\mathcal{L}_f$  near the nodes. The nodal fermions  $\psi_{\sigma,\alpha}$ , where  $\alpha = 1, \bar{1}, 2$  and  $\bar{2}$  is a node index, can then be arranged into  $N$  four-component BdG-Dirac spinors following the conventions of Ref. 5, where  $N = 2$  for a single CuO<sub>2</sub> layer. These massless Dirac-like objects carry no overall charge and are at zero chemical potential – reflecting the fact that pairing in the particle-particle channel always pins the  $d$ -wave nodes to the true chemical potential – and can be thought of as the particle-hole excitations of the BCS “vacuum”. They, however, can be polarized and their polarization will renormalize the fluctuations of the Doppler gauge field  $v$ , the point which will be emphasized later. Furthermore, the nodal fermions carry spin  $S = \frac{1}{2}$  and interact strongly with the Berry gauge field  $a$  to which they are minimally coupled. In contrast, the rest of the electronic degrees of freedom, which we label “anti-nodal” fermions,  $\psi_{\sigma,(\alpha\beta)}$ , where  $\langle\alpha\beta\rangle = \langle 12\rangle, \langle 2\bar{1}\rangle, \langle \bar{1}\bar{2}\rangle$ , and  $\langle \bar{2}1\rangle$ , are combined into spin-singlet Cooper pairs and do not contribute significantly to the spin channel. On the other hand, these anti-nodal fermions have finite density and carry the overall electric charge. Their coupling to  $v$  is the dynamical driving force behind the formation of the CPCDW. Meanwhile, the nodal fermions are not affected by the CPCDW at the leading order – their low energy effective theory is still the symmetric QED<sub>3</sub> even though the translational symmetry is broken by the CPCDW<sup>12</sup>.

The presence of these massless Dirac-like excitations in  $\mathcal{L}_f$  is at the heart of the QED<sub>3</sub> theory of cuprates<sup>5</sup>. QED<sub>3</sub> theory is an effective low energy description of a fluctuating  $d_{x^2-y^2}$ -wave superconductor, gradually losing phase coherence by progressive admixing of quantum vortex-antivortex fluctuations into its ground state. All

the while, even as the ODLRO is lost, the amplitude of the BdG gap function remains finite and largely undisturbed as the doping is reduced toward half-filling as depicted in Fig. 1. How is this possible? A nodal  $d_{x^2-y^2}$ -wave superconductor – in contrast to its fully gapped cousin or a conventional s-wave superconductor – possesses *two* fundamental symmetries in its ground state; the familiar one is just the presence of the ODLRO, shared by all superconductors. In addition, there is a more subtle symmetry of its low energy fermionic spectrum which is exclusively tied to the presence of nodes. This symmetry is *emergent*, in the sense that it is not a symmetry of the full microscopic Hamiltonian but only of its low energy nodal sector, and is little more than the freedom intrinsic to arranging two-component nodal BdG spinors into four-component massless Dirac fermions<sup>5</sup> – by analogy to the field theory we call this symmetry *chiral*. The QED<sub>3</sub> theory first formulates and then answers in precise mathematical terms the following question: can a nodal  $d_{x^2-y^2}$ -wave superconductor lose ODLRO but nonetheless retain the BdG chiral symmetry of its low energy fermionic spectrum<sup>5</sup>? In conventional BCS theory the answer is a straightforward “no”: as the gap goes to zero all vestiges of the superconducting state are erased and one recovers a Fermi liquid normal state. However, in a strongly quantum fluctuating superconductor considered here, which loses ODLRO via vortex-antivortex unbinding, the answer is a remarkable “yes”. The chirally *symmetric*, IR *critical* phase of QED<sub>3</sub> is the explicit realization of this new, non-Fermi liquid state of quantum matter, with the phase order of a  $d_{x^2-y^2}$ -wave superconductor gone but the chiral symmetry of fermionic excitations left in its wake. While these excitations are incoherent, being strongly scattered by the massless Berry gauge field, the BdG chiral symmetry of the low energy sector remains intact<sup>23</sup>. Importantly, as interactions get too strong – the case in point being the cuprates at very low dopings – the BdG chiral symmetry will be eventually spontaneously broken, leading to antiferromagnetism and possibly other fully gapped states<sup>5,7</sup>. Nonetheless, the BdG chiral symmetry breaking is not fundamentally tied to the loss of ODLRO: different HTS materials are likely to have different  $T = 0$  phase diagrams with larger or smaller portions of a stable critical “normal” state – described by the symmetric QED<sub>3</sub> – sandwiched between a superconductor and an antiferromagnet (SDW) (Fig. 1). In all cases, provided our starting assumption of the predominantly pairing nature of the pseudogap is correct, the symmetric QED<sub>3</sub> emerges as the underlying effective theory of underdoped cuprates, echoing the role played by Landau Fermi liquid theory in conventional metals.

### III. THERMAL (“CLASSICAL”) PHASE FLUCTUATIONS

Our first goal is to introduce an XY model type representation of thermal (or “classical”) phase fluctuations.

To this end we first observe that in cuprates, we are dealing with a  $d$ -wave superconductor on a tightly bound two-dimensional CuO<sub>2</sub> lattice (the black lattice in Fig. 2). The simplest starting point is the lattice  $d$ -wave superconductor (LdSC) model discussed in detail by Vafeek *et al.*<sup>18</sup>. The model describes fermions hopping between nearest neighbor sites  $\langle ij \rangle$  on a square lattice with a renormalized matrix element  $t^*$  and contains a nearest neighbor spin-singlet pairing term with an effective coupling constant  $\lambda_{\text{eff}}$  adjusted to stabilize the  $d_{x^2-y^2}$  state with the maximum pairing gap  $\Delta$ :

$$H_{\text{LdSC}} = -t^* \sum_{\langle ij \rangle, \sigma} c_{i\sigma}^\dagger c_{j\sigma} + \sum_{\langle ij \rangle} \Delta_{ij} [c_{i\uparrow}^\dagger c_{j\downarrow}^\dagger - c_{i\downarrow}^\dagger c_{j\uparrow}^\dagger] + (\text{c.c.}) \\ + (1/\lambda_{\text{eff}}) \sum_{\langle ij \rangle} |\Delta_{ij}|^2 + (\dots) \quad , \quad (13)$$

where  $(\dots)$  denotes various residual interaction terms.  $c_{i\sigma}^\dagger$  and  $c_{i\sigma}$  are creation and annihilation operators of some *effective* electron states, appropriate for energy scales below and around  $\Delta$ , which *already include* renormalizations generated by integration of higher energy configurations, particularly those associated with strong Mott-Hubbard correlations. This effective LdSC model is phenomenological but can be justified within a more microscopic approach, an example being the one based on a  $t - J$ -style effective Hamiltonian. The complex gap function is defined on the bonds of the CuO<sub>2</sub> (black) lattice:  $\Delta_{ij} = A_{ij} \exp(i\theta_{ij})$ . The amplitude  $A_{ij}$  is frozen below the pseudogap energy scale  $\Delta$  and equals  $A_{ij} = \pm\Delta$  along horizontal (vertical) bonds. Thus, the  $d$ -wave character of the pairing has been incorporated directly into  $A_{ij}$  from the start.

What remains are the fluctuations of the bond phase  $\theta_{ij}$ . It is advantageous to represent these *bond* phase fluctuations in terms of *site* fluctuations by identifying  $\exp(i\theta_{ij}) \rightarrow \exp(i\varphi_k)$ , where  $\varphi_k$  is a site phase variable associated with the middle of the bond  $\langle ij \rangle$ . Consequently, we are now dealing with the set of *site* phases  $\varphi_k$  located at the vertices of the blue lattice in Fig. 2. Note that the blue lattice has twice as many sites as the original CuO<sub>2</sub> lattice or its dual. This is an important point and will be discussed shortly.

We can now integrate over the fermions in the LdSC model and generate various couplings among phase factors  $\exp(i\varphi_k)$  residing on different “blue” sites. The result is the minimal site XY-type model Hamiltonian representing a fluctuating classical lattice  $d$ -wave superconductor:

$$\mathcal{H}_{XY}^d = -J \sum_{nn} \cos(\varphi_i - \varphi_j) - J_1 \sum_{rnnn} \cos(\varphi_i - \varphi_j) \\ - J_2 \sum_{bnnn} \cos(\varphi_i - \varphi_j) \quad , \quad (14)$$

where  $\sum_{nn}$  runs over nearest neighbors on the blue lattice while  $\sum_{rnnn}$  and  $\sum_{bnnn}$  run over red and black



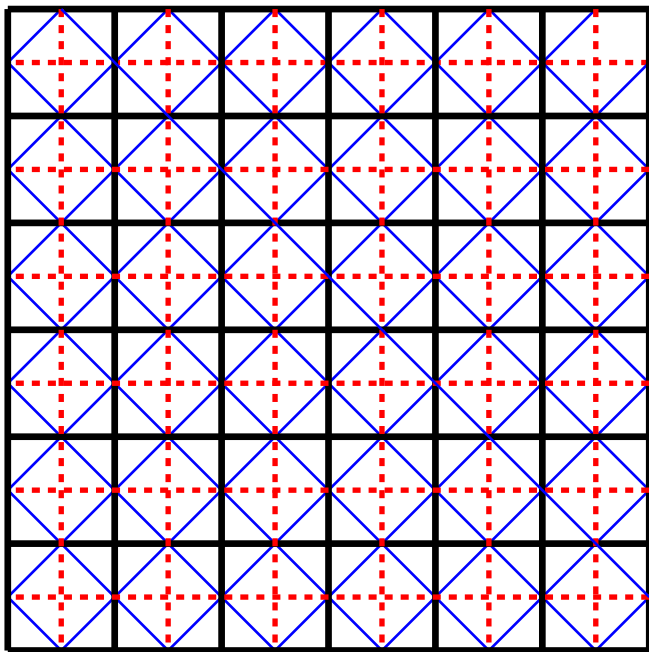


FIG. 2:  $\text{CuO}_2$  lattice represented by thick black lines (vertices are copper atoms and oxygens are in the middle of each bond). The nodes of the blue lattice (thin solid lines) represent sites of our “effective” XY model (14), with the phase factor  $\exp(i\varphi_i)$  located at each blue vertex. The dual of the copper lattice is shown in red dashed lines. The nearest neighbor coupling on the blue lattice is denoted by  $J$  (blue link) and the two next-nearest neighbor couplings are  $J_1$  (red link) and  $J_2$  (black link). Generically,  $J_1 \neq J_2$  and the translational symmetry of the blue lattice is broken by the “checkerboard” array of “red” and “black” plaquettes, as is evident from the figure. This doubles up the unit cell which then coincides with that of the original (black)  $\text{CuO}_2$  lattice, as it should be.

next-nearest neighbor bonds depicted in Fig. 2, respectively. The couplings beyond next-nearest neighbors are neglected<sup>24</sup> in (14). Such more distant couplings are not important for the basic physics which is of interest to us here, and their effect can be simulated by a judicious choice of  $J_1$  and  $J_2$  – the reader should be warned that the situation changes when  $T \rightarrow 0$  as will be discussed in the next section. Keeping  $J_1$  and  $J_2$ , however, is essential. If only  $J$  is kept in (14), the translational symmetry of the blue lattice would be left intact and we would find ourselves in a situation more symmetric than warranted by the microscopic physics of a  $d$ -wave superconductor. In this sense  $J_1$  and  $J_2$  or, more precisely, their difference  $J_1 - J_2 \neq 0$ , are dangerously irrelevant couplings and should be included in any approach which aims to describe the physics at intermediate lengthscales.

In general, near half-filling,  $J$ ,  $J_1$  and  $J_2$  tend to be all positive and mutually different. This ensures that the ground state is indeed a  $d$ -wave superconductor (the reader should recall that  $d$ -wave signs had already been absorbed into  $A_{ij}$ ’s so the ground state is an XY ferromagnet instead of an antiferromagnet – the antiferromag-

net would be an extended  $s$ -wave state.). The explicit values of  $J$ ,  $J_1$  and  $J_2$  can be computed in a particular model. In this paper we treat them as adjustable parameters.

### A. Vortex-antivortex Coulomb gas representation of $\mathcal{H}_{XY}^d$

The fact that  $J_1 \neq J_2$  breaks translational symmetry of the blue lattice. This is as it should be since the blue lattice has twice as many sites as the original  $\text{CuO}_2$  lattice. This is an important point to which we will return shortly. Now, however, let us assume for the moment that  $J_1 = J_2$ . This assumption is used strictly for pedagogical purposes. Then, the blue lattice has a full translational symmetry and it is straightforward to derive the effective Coulomb gas representation for fluctuating vortex-antivortex pairs. Here we follow the derivation of Ref. 25. The cosine functions in (14) are expanded to second order and one obtains the effective continuum theory:

$$\mathcal{H}_{cont} = \frac{1}{2} \tilde{J} \int d^2r |\nabla\varphi(\mathbf{r})|^2 + (\dots) , \quad (15)$$

where  $\tilde{J} = J + J_1 + J_2$  and  $\varphi(\mathbf{r})$  is the continuum version of the site phase  $\varphi_i$  on the blue lattice.  $(\dots)$  denotes higher order terms in the expansion of the cosine function. As usual, the superfluid velocity part  $v(\mathbf{r}) = \nabla\varphi(\mathbf{r})$  is separated into a regular (XY spin-wave) part and a singular (vortex) part  $(\nabla\varphi)_v$ :

$$v(\mathbf{r}) = \nabla\chi(\mathbf{r}) + 2\pi(\hat{z} \times \nabla) \int d^2r' n(\mathbf{r}') G(r, r') , \quad (16)$$

where  $\chi$  is a regular free field and  $n(\mathbf{r})$  is the density of topological vortex charge:  $n(\mathbf{r}) = \sum_i \delta(\mathbf{r} - \mathbf{r}_i^v) - \sum_j \delta(\mathbf{r} - \mathbf{r}_j^a)$ , with  $\mathbf{r}_i^v$  and  $\mathbf{r}_j^a$  being the positions of vortex and antivortex defects, respectively. We are limiting ourselves to  $\pm 1$  vortex charges but higher charges are easily included.  $G(r, r')$  is the 2D electrostatic Green’s function which satisfies:

$$\nabla^2 G(r, r') = \delta(\mathbf{r} - \mathbf{r}') . \quad (17)$$

Far from systems boundaries, the solution of (17) is:

$$G(r, r') = \frac{1}{2\pi} \ln(|\mathbf{r} - \mathbf{r}'|/a) + C , \quad (18)$$

where  $a$  is the UV cutoff, of the order of the (blue) lattice spacing and  $C$  is an integration constant, to be associated with the core energy.

This ultimately gives the vortex part of the Hamiltonian as:

$$\mathcal{H}_v = 2\pi^2 \tilde{J} \int d^2r d^2r' d^2r'' n(\mathbf{r}') n(\mathbf{r}'') \nabla G(r, r') \cdot \nabla G(r, r'') , \quad (19)$$



After integration by parts this results in the desired Coulomb gas representation of  $\mathcal{H}_v$ :

$$-\pi\tilde{J} \int d^2r d^2r' n(\mathbf{r})n(\mathbf{r}') \ln(|\mathbf{r} - \mathbf{r}'|/a) + E_c \int d^2r n^2(\mathbf{r}) , \quad (20)$$

where  $E_c \sim C$  is the core energy. Note that the integrals in the first part of (20) include only the regions outside vortex cores (the size of which is  $\sim a^2$ ).

How is the above derivation affected if we now restore  $J_1 \neq J_2$ , as is the case in real cuprates? The long distance part remains the same since  $J_1 - J_2$  enters only at the  $O(k^4)$  order of the gradient expansion of cosine functions in (14), i.e.  $J_1 - J_2 \neq 0$  affects only the terms denoted by  $(\dots)$  in  $\mathcal{H}_{cont}$  (15). So, the strength of the Coulomb interaction between (anti)vortices in  $\mathcal{H}_v$  (20) is still given by  $\tilde{J} = J + J_1 + J_2$ . The core energy changes, however. This change can be traced back to (17) and (18); depending on whether the vortex core is placed in a red (i.e., containing the red cross in Fig. 2) or a black plaquette of the blue lattice, the constant of integration  $C$  will generally be different. This is just the reflection of the fact that for  $J_1 \neq J_2$  the original translational symmetry of the blue lattice is broken down to the *checkerboard* pattern as is obvious from Fig. 2. So, Eq. (18) must be replaced by:

$$G(r, r') = \frac{1}{2\pi} \ln(|\mathbf{r} - \mathbf{r}'|/a) + C_{r(b)} . \quad (21)$$

$G(r, r')$  is just the electrostatic potential at point  $\mathbf{r}$  produced by a vortex charge at  $\mathbf{r}'$ . Since not all locations for  $\mathbf{r}'$  are equivalent, there are two constants of integration  $C_r \neq C_b$  ( $C_r - C_b \sim J_1 - J_2$ ), corresponding to whether  $\mathbf{r}'$  is in the red or black plaquettes of the blue lattice (Fig. 2). Retracing the steps leading to the Coulomb gas representation we finally obtain:

$$\mathcal{H}_v^d = -\pi\tilde{J} \int d^2r \int d^2r' n(\mathbf{r})n(\mathbf{r}') \ln(|\mathbf{r} - \mathbf{r}'|/a) + E_c^r \int d^2r n^2(\mathbf{r}) + E_c^b \int d^2r n^2(\mathbf{r}) , \quad (22)$$

where  $E_c^{r(b)}$  are the core energies of (anti)vortices located in red (black) plaquettes and  $E_c^r - E_c^b \sim J_1 - J_2$ .  $E_c^{r(b)}$  are treated as adjustable parameters, chosen to best reproduce the energetics of the original Hamiltonian (14). The explicit lattice version of (20) follows from Ref. 26, where a duality transformation and a Migdal-style renormalization procedure have been applied to the XY model:

$$\mathcal{H}_v^d = -\pi\tilde{J} \sum_{\mathbf{r} \neq \mathbf{r}'} s(\mathbf{r})s(\mathbf{r}') \ln(|\mathbf{r} - \mathbf{r}'|/a) + E_c^r \sum_{\mathbf{r} \in \mathcal{R}} s^2(\mathbf{r}) + E_c^b \sum_{\mathbf{r} \in \mathcal{B}} s^2(\mathbf{r}) . \quad (23)$$

In (23)  $s(\mathbf{r}) = 0, \pm 1(\pm 2, \pm 3, \dots)$  and  $\mathbf{r}$  are summed over the red ( $\mathcal{R}$ ) and black ( $\mathcal{B}$ ) sites of the lattice dual to

the blue lattice in Fig. 2. Eq. (23) can be viewed as a convenient lattice regularization of (22). It is rederived in the Appendix with the help of Villain approximation.

We can also recast  $\mathcal{H}_v$  in a form which interpolates between the continuum (22) and lattice (23) Coulomb gases. For convenience, we now limit our attention to only  $\pm 1$  vortex charges (vortices and antivortices) since these are the relevant excitations in the pseudogap regime. The underlying lattice in (23) is “smoothed out” into a periodic potential  $V(\mathbf{r})$  whose minima are located in the plaquettes of the blue lattice (at vertices of the dual blue lattice). The precise form of  $V(\mathbf{r})$  can be computed in a continuum model of realistic cuprates involving local atomic orbitals, self-consistent computations of the pseudogap  $\Delta$ , etc. and is not important for our purposes; only its overall symmetry matters and the fact that it is sufficiently “smooth”. This finally produces:

$$\mathcal{H}_v^d = -\pi\tilde{J} \int d^2r \int d^2r' n(\mathbf{r})n(\mathbf{r}') \ln(|\mathbf{r} - \mathbf{r}'|/a) + \int d^2r V(\mathbf{r})\rho(\mathbf{r}) , \quad (24)$$

where  $n(\mathbf{r})$  is the vortex charge density as before and  $\rho(\mathbf{r}) = \sum_i \delta(\mathbf{r} - \mathbf{r}_i^v) + \sum_j \delta(\mathbf{r} - \mathbf{r}_j^a)$  is the vortex particle density *irrespective* of vortex charge. If  $E_c^r = E_c^b$ , the periodicity of  $V(\mathbf{r})$  coincides with that of the blue lattice – the value at the minimum is basically  $E_c^r = E_c^b$ . On the other hand, if  $E_c^r \neq E_c^b$  as is the case in real cuprates,  $V(\mathbf{r})$  has a *checkerboard* symmetry on the blue lattice, with *two* different kinds of local extrema; the red one, at energy set by  $E_c^r$  and a black one, at energy  $E_c^b$  (this is all depicted in Fig. 2).

The most important consequence of these two different local extrema of  $V(\mathbf{r})$  is that there are two special locations for the position of vortices; on the original  $\text{CuO}_2$  lattice of Fig. 2 these correspond to vortices either residing in its plaquettes or at its vertices. On general grounds, we expect one of these positions to be the absolute minimum while the other assumes the role of either a locally stable minimum or a saddle point with an unstable direction. Whether  $E_c^r < E_c^b$  or the other way around and whether the higher energy is a local minimum or a saddle point, however, can be answered with certainty only within a model more macroscopic than the one used here. In particular, a specific analysis of the electronic structure of a strongly correlated vortex core is necessary which goes far beyond the XY-type model used in this paper. For our purposes  $E_c^r$  and  $E_c^b$  can be treated as adjustable parameters and it suffices only to know that the microscopic physics selects either the red or the black plaquettes in Fig. 2 as the favored vortex core sites and relegates the other to either the metastable or a weakly unstable status.

#### IV. QUANTUM PHASE FLUCTUATIONS

The previous discussion pertains to the thermal (or classical) 2D XY model. The key difference from the usual Coulomb gas representation for vortex-antivortex pairs turned out to be the inequivalence of vortex core positions on the blue lattice (Fig. 2), which served to recover the translational symmetry of the original CuO<sub>2</sub> lattice. This effect was represented by the blue lattice potential  $V(\mathbf{r})$  in the vortex Hamiltonian (24).

To obtain the *quantum* version of the fluctuation problem or an effective (2+1)D XY-type model we need to include the imaginary time dependence in  $\varphi_i \rightarrow \varphi_i(\tau)$ . In general, this will result in vortex-antivortex pairs propagating through imaginary (Euclidean) time, as vortex cores move from one plaquette to another through a sequence of quantum tunneling processes. There are two aspects of such motion: The first is the tunneling of the vortex core. This is a “microscopic” process, in the sense that a detailed continuum model, with self-consistently computed core structure, is needed to describe it quantitatively. For the purposes of this paper, all we need to know is that one of the final components characterizing such a tunneling process is the “mass”  $M$  of the vortex core as it moves through imaginary time<sup>27</sup>. This implies a term

$$\frac{1}{2} \int_0^\beta d\tau \sum_i M \left( \frac{d\mathbf{r}_i^{v(a)}}{d\tau} \right)^2 \quad (25)$$

in the quantum mechanical vortex action, where  $\mathbf{r}_i^{v(a)}(\tau)$  is the position of the  $i$ th (anti)vortex in the CuO<sub>2</sub> plane at time  $\tau$ . Note that  $M$  is here just another parameter in the theory which, like  $J$ ,  $J_1$ , and  $J_2$ , is more microscopic than our model<sup>27</sup>. However, the microscopic physics of the cuprates clearly points to  $M$  being far smaller than in conventional superconductors. Cuprates are strongly coupled systems, with a short coherence length  $\xi \sim k_F^{-1}$  and the vortex core of only several lattice spacings in size. Consequently, there are only a few electrons “inside a core” at any given time, making (anti)vortices “light” and highly quantum objects, with strong zero-point fluctuations. Furthermore, the core excitations appear to be gapped<sup>28</sup> by the combination of strong coupling and local Mott-Hubbard correlations<sup>29,30,31,32,33</sup>. This has an important implication for the second component of the core tunneling process, the familiar Bardeen-Stephen form of dissipation, which is such a ubiquitous and dominating effect in conventional superconductors. In conventional systems the core is hundreds of nanometers in diameter and contains thousands of electrons.  $M$  is large in such a superconductor and, as a vortex attempts to tunnel to a different site, its motion is damped by these thousands of effectively normal electrons, resulting in significant Bardeen-Stephen dissipation and high viscosity. The motion of such a huge, strongly damped object is effectively classical. Vortices in underdoped cuprates are precisely the opposite, with small  $M$ , the Bardeen-Stephen dissipation

nearly absent and a very low viscosity. In this sense, the quantum motion of a vortex core in underdoped cuprates is closer to superfluid <sup>4</sup>He than to other, conventional superconductors<sup>34</sup>. We are therefore justified in assuming that it is adequately described by (25) and ignoring small vortex core viscosity for the rest of this paper<sup>35</sup>. The special feature of the cuprates, however, is the presence of gapless nodal quasiparticles away from the cores which generate their own peculiar brand of (weak) dissipation – such effect is discussed and included later in this section.

The second aspect of the vortex propagation through imaginary time involves the motion of the superflow velocity field surrounding the vortex *outside* its core, i.e., in the region of space where the magnitude of  $\Delta$  is approximately uniform. This is a long range effect and, unlike the vortex core energies, mass, or Bardeen-Stephen dissipation, exhibits certain universal features, shared by all superconductors and superfluids. For example, in superfluid <sup>4</sup>He this effect would result in a Magnus force acting on a vortex. In a superconductor, the effect arises from the time derivative of the phase in the regions of uniform  $\Delta$ . The origin of such time derivative and its physical consequences are most easily appreciated by considering an ordinary (fictitious) strongly fluctuating  $s$ -wave superconductor with a phase factor  $\exp(i\phi_i(\tau))$  at each *site* of the CuO<sub>2</sub> lattice. For reader’s benefit we discuss this case first as a pedagogical warm-up for what lies ahead.

##### A. Pedagogical exercise: quantum fluctuating $s$ -wave superconductor

After performing the FT transformation and forgetting the double valuedness problem (ignoring the Berry gauge field  $a$ ) since we are concentrating on the charge channel, the quantum action will contain a purely imaginary term (see Section II):

$$\frac{i}{2} \int_0^\beta d\tau \sum_i (n_{i\uparrow}(\tau) + n_{i\downarrow}(\tau)) \partial_\tau \phi_i \quad , \quad (26)$$

where  $n_{i\sigma} \equiv \bar{\psi}_{i\sigma} \psi_{i\sigma}$ . It is useful to split the electron density into its average and the fluctuating parts:  $n = n_\uparrow + n_\downarrow \rightarrow \bar{n} + \delta n$ . The average part is unimportant for the spin-wave phase due to the periodicity of  $\phi_i(\tau)$  in the interval  $[0, \beta]$ . In the vortex part of the phase, however, this average density acts as a *magnetic flux*  $\frac{1}{2}\bar{n}$  seen by (anti)vortices<sup>13</sup>. This first time derivative is just the charge Berry phase and it couples to (half of) the total electronic charge density. After the fermions are integrated out, the fluctuating part of the density will simply generate a  $\phi_i^2$  term whose stiffness is set by the fermionic compressibility.

For simplicity, we will first ignore the charge Berry phase and set  $\bar{n} = 0 \pmod{2}$ . This results in a (2+1)D

XY model:

$$\mathcal{L}_{XY} = \frac{1}{2}K_0 \sum_i \dot{\phi}_i^2 - J \sum_{nn} \cos(\phi_i - \phi_j) , \quad (27)$$

where  $K_0$  is effectively the fermionic charge susceptibility (compressibility):  $K_0 \sim \chi_c \sim \langle \delta n_i^2 \rangle$ . Again, we expand the cosine to the leading order (the same results are obtained in the Villain approximation, see Appendix) and separate the regular and singular (vortex) contributions to  $\partial_\mu \phi \rightarrow \partial_\mu \chi + (\partial_\mu \varphi)_v$ . As a result,  $\mathcal{L}_{XY}$  is transformed into

$$\frac{1}{2}K_\mu (\partial_\mu \phi)^2 \rightarrow iW_\mu \partial_\mu \chi + iW_\mu (\partial_\mu \phi)_v + \frac{1}{2}K_\mu^{-1} W_\mu^2 , \quad (28)$$

where  $K_\mu = (K_0, K, K)$  and  $W$  is a real Hubbard-Stratonovich three-vector field. The integral over the free field  $\chi$  can be carried out, producing the constraint  $\partial \cdot W = 0$ . The constraint is solved by demanding that  $W = \partial \times A_d$ , where  $A_d$  will soon assume the meaning of the dual gauge field. The vortex part is now manipulated into:

$$\begin{aligned} \mathcal{L}_{XY} &\rightarrow i(\partial \times A_d) \cdot (\partial \phi)_v + \frac{1}{2}K_\mu^{-1} (\partial \times A_d)_\mu^2 \\ &\rightarrow -2\pi i A_d \cdot n + \frac{1}{2}K_\mu^{-1} (\partial \times A_d)_\mu^2 , \quad (29) \end{aligned}$$

where the integration by parts and  $\partial \times (\partial \phi)_v = 2\pi n$  have been used and  $n_\mu$  is the vorticity in the (2+1) dimensional spacetime (vorticity, by its very nature, is conserved:  $\partial \cdot n = 0$ ). Now, we use the standard transition from Feynman path integrals to coherent functional integrals<sup>36</sup>. A relativistic vortex boson complex field  $\Phi(x)$  is introduced, whose worldlines in (2+1) dimensional spacetime coincide with fluctuating vortex loops (see the Appendix for a more detailed account). The first term in (29) is just the current of these relativistic vortex particles coupled to a vector potential  $A_d$ . Furthermore, vortices have some intrinsic line action  $\int ds \mathcal{S}_0$ , coming from core terms (and/or lattice regularization) which supply the (2+1) kinetic term. In the end, one obtains a dual Lagrangian:

$$\mathcal{L}_d = |(\partial + i2\pi A_d)\Phi|^2 + m^2(\mathbf{r})|\Phi|^2 + \frac{g}{2}|\Phi|^4 + \frac{K_\mu^{-1}}{2}(\partial \times A_d)_\mu^2, \quad (30)$$

where  $g > 0$  is a short range repulsion describing the penalty for vortex core overlap. The mass term will in general be spatially modulated, reflecting the underlying lattice potential, as in (24). A detailed derivation of the above dual Lagrangian can be found in the Appendix.

It is useful to underscore the following relation between the steps that led to (30) and the formalism discussed in Section II, which is coached in the language closer to the original electrons: Only the familiar long range Biot-Savart (anti)vortex interactions, mediated by dual gauge field  $A_d$ , arise from the fermionic action in Section II and Refs. 12,38. This corresponds to large regions of space

where the pseudogap  $\Delta$  is large and approximately uniform. In contrast, small (anti)vortex core regions, where  $\Delta$  might exhibit significant non-uniformity, supply the the core kinetic part (25), vortex core energy and the short range core repulsion term ( $g$ ), which are all stored in the ‘‘Jacobian’’ for  $v$  and  $a$  gauge fields. This is significant since it enables us to deal rather straightforwardly with the charge Berry phase which now must be restored.

First, notice that the self-action of  $A_d$ , which was introduced in this section through a Hubbard-Stratonovich decoupling in Eq. (28), actually follows ‘‘microscopically’’ from the integration over the fermions and the gauge field  $v$  in Section II and<sup>12</sup>. There  $A_d$  was introduced as a field enforcing a  $\delta$ -function constraint  $\delta[(\partial \times v)/\pi - n]$  but the physics is precisely the same, the formal difference being just the order in which we integrate the fermionic matter. Once we restore the Berry phase term  $(i/2) \int d^3x \bar{n} (\partial_\tau \phi)_v$  back to the action, we note that in the formalism of Section II and<sup>12</sup> none of the fields in the dual Lagrangian (30) couples to it directly. Instead, it is  $v_0$  that enters the Berry phase via the  $\delta$ -function constraint  $\partial_\tau \phi \rightarrow v_0$ . The Berry phase term will then affect (30) via the coupling of  $v_0$  to the spatial part of  $A_d$ , i.e., the dual magnetic induction  $\mathbf{B}_d = \nabla \times \mathbf{A}_d$ .

The above observations suggest that it useful to separate out the saddle point part of  $v$  as:  $v \rightarrow -i\bar{v} + \delta v$ . The saddle point part  $\bar{v}$  is determined by minimizing the total action (the ‘‘-’’ sign is chosen so that  $\bar{v}_0$  couples to the electron density as a chemical potential). Of course, if there were no Berry phase term we would have  $\bar{v} = 0$ . With the Berry phase term included  $\bar{v} = 0$  but  $\bar{v}_0$  is now finite. Observe from Eqs. (1,2) of Ref. 12 that the saddle point equation for  $\bar{v}_0$  simply reduces to:  $\frac{1}{2}\bar{n} = \mathbf{B}_d = \nabla \times \mathbf{A}_d$  (note that, relative to our notation, dual gauge field in Ref. 12 is rescaled as  $A_d \rightarrow 2\pi A_d$ ). So, with the Berry phase included, the final form of the dual theory still remains given by Eq. (30) but must be appended by the constraint  $\frac{1}{2}\langle n(x) \rangle = \langle \mathbf{B}_d(x) \rangle$ .

If we now apply the dual mean-field approximation to (28) one obtains  $\mathcal{F}_{mf}$  given by:

$$|(\nabla + i2\pi \mathbf{A}_d)\Phi|^2 + m^2(\mathbf{r})|\Phi|^2 + \frac{g}{2}|\Phi|^4 + \frac{K_0^{-1}}{2}\mathbf{B}_d^2 , \quad (31)$$

with the constraint taking the form  $\mathbf{B}_d(\mathbf{r}) = \frac{1}{2}\langle n(\mathbf{r}) \rangle$ . One immediately recognizes (31) as the Abrikosov-Hofstadter problem for a dual type-II superconductor – we are in type-II regime<sup>37</sup> since small compressibility implies large dual Ginzburg parameter  $\kappa_d \sim 1/\sqrt{K_0} \sim 1/\sqrt{\chi_c}$  – subjected to the overall (dual) magnetic field flux per plaquette of the dual lattice,  $f$ , given by  $f = p/q = (1-x)/2$ , where  $x$  is doping. Note that at half-filling  $\bar{n} = 1 \Rightarrow f = 1/2$ . The solution that minimizes (31) at half-filling is a checkerboard array of vortices and antivortices in  $\Phi$ , with the associated modulation in  $\mathbf{B}_d(\mathbf{r}) = \frac{1}{2}\langle n(\mathbf{r}) \rangle$ , as discussed in Refs. 12,38. This is nothing but the dual equivalent of a CPCDW in an  $s$ -wave superconductor at half-filling, with a two-fold degenerate array of alternating enhanced and suppressed

charge densities on sites of the original lattice. An overwhelming analytic and numerical support exists for this state being the actual ground state of the negative  $U$  Hubbard model<sup>39</sup>, the prototypical theoretical toy model in this category. This gives us confidence that the mean-field approximation captures basic features of the problem.

## B. Quantum fluctuating $d$ -wave superconductor

The above pedagogical exercise applies to an idealized strongly fluctuating  $s$ -wave superconductor and its associated ordinary (2+1)D XY model. What about our  $d$ -wave lattice superconductor (LdSC) and its effective XY-type model (14), with the bond phases mapped into site phases on the blue lattice? Again, we go from  $\exp(i\theta_{ij})$  to  $\exp(i\varphi_k)$  as before. The cosine part of (27) is replaced by  $\mathcal{H}_{XY}^d$  (14) and is handled in the same way as for the classical case. This will ultimately result in a modulated potential  $V(\mathbf{r})$  of Eq. (24). In the context of the dual theory (30) this will translate into a position-dependent mass term  $m^2(\mathbf{r})|\Phi(x)|^2$  in the dual Lagrangian (30) except now this mass term has the checkerboard symmetry on the blue lattice, with  $m_r^2$  in the red plaquettes different from  $m_b^2$  in the black plaquettes ( $m_r^2 - m_b^2 \sim E_c^r - E_c^b$ ). Including the constraint on the overall dual induction  $\mathbf{B}_d$  seems to complete the process.

Alas, the situation is a bit more involved. First, the time derivative part and the Berry phase are more complicated. The difficulty arises since the *bond* superconducting phase  $\theta_{ij}$  of a LdSC couples in a more complicated way to the *site* fermionic variables. However, we can still deal with this by enlisting the help of the FT gauge transformation which screens the long-range part of  $\theta_{ij}$  by  $\frac{1}{2}\phi_i + \frac{1}{2}\phi_j$ , where  $\phi_i$  are the phases in the fermionic fields. After this transformation (we are again ignoring  $a_\mu$  which we can put back in at the end) one obtains  $i\frac{1}{2}n_i\partial_\tau\phi_i$  at each site of the  $\text{CuO}_2$  lattice. This translates into  $i\frac{1}{8}n_i\partial_\tau\phi_i + i\frac{1}{8}n_j\partial_\tau\phi_j$  for each bond  $\langle ij \rangle$  of the  $\text{CuO}_2$  lattice. This bond expression can be rewritten as:

$$\begin{aligned} \frac{i}{8}[n_i + n_j]\frac{1}{2}(\partial_\tau\phi_i + \partial_\tau\phi_j) + \frac{i}{8}[n_i - n_j]\frac{1}{2}(\partial_\tau\phi_i - \partial_\tau\phi_j) \\ \cong \frac{i}{8}[n_i + n_j]\partial_\tau\theta_{ij} + (\dots) \quad , \quad (32) \end{aligned}$$

where  $(\dots)$  contains higher order derivatives and is typically not important in the discussion of critical phenomena (but see below). In the end, following our replacement of bond phases on  $\text{CuO}_2$  lattice with site phases on the blue lattice  $\theta_{ij} \rightarrow \varphi_k$  we finally obtain the Berry phase term of our lattice  $d$ -wave superconductor:

$$\frac{i}{8}[n_i + n_j]\partial_\tau\varphi_k \rightarrow \frac{i}{8}[\bar{n}_i + \bar{n}_j]\partial_\tau\varphi_k + \frac{i}{8}\delta\Delta_{ij}\partial_\tau\varphi_k \quad . \quad (33)$$

The expression (32) seems too good to be true and it is – the replacement  $\theta_{ij} \rightarrow \frac{1}{2}\phi_i + \frac{1}{2}\phi_j$  holds only far away

from vortices, when the phases change slowly between nearby bonds (sites). In general, the bond phase of the LdSC will not couple to the electron densities in a simple way suggested by (32). Still, we have gained an important insight; its coupling to the *overall* electron density represented by the leading term in (33) is effectively exact. This follows directly from the electrodynamic gauge invariance which mandates that both regular and singular configurations of the phase must have the same first time derivative in the action. For arbitrarily smoothly varying phase, with no vortices present, the replacement  $\theta_{ij} \rightarrow \frac{1}{2}\phi_i + \frac{1}{2}\phi_j$  is accurate to any desired degree and the Berry phase given by the leading term in (33) follows. Incidentally, this result is not spoiled by the higher order terms, represented by  $(\dots)$  in (32), since they do not contribute to the *overall* dual magnetic field, by virtue of  $\bar{n}_i - \bar{n}_j = 0$ . We, however, cannot claim with the same degree of certainty that  $\delta\Delta_{ij}$  is in a simple relationship to variations in the electronic densities on sites  $i$  and  $j$  as (32) would have it<sup>40</sup>. Instead, we should view  $\delta\Delta_{ij}$  in (33) as a Hubbard-Stratonovich field used to decouple the  $\theta_{ij}^2$  term in the quantum action. This makes  $\delta\Delta_{ij}$  inherently a *bond* field whose spatial modulation translates into variation in the pseudogap  $\Delta$  and will be naturally related to the dual induction  $\mathbf{B}_d$  below<sup>41</sup>. This is different from our pedagogical  $s$ -wave exercise where the modulation in  $\mathbf{B}_d$  was directly related to the variation in the electronic density.

The second source of complication is more intricate and relates to the fact that, as  $T \rightarrow 0$ , we must be concerned about nodal fermions. In the  $s$ -wave case and the finite temperature  $d$ -wave XY-type model (14) we know that coupling constants  $J$ ,  $J_1$ ,  $J_2$ , and so on, are finite or at least can be made so in simple, reasonably realistic models. In general, we need to keep only several of the nearby neighbor couplings to capture the basic physics. There is a tacit assumption that such expansion is in fact well-behaved. In the quantum  $d$ -wave case, however, the expansion in near neighbor couplings is not possible – at  $T = 0$  its presumed analytic structure is obliterated by gapless nodal fermions. Naturally, after the electrons are integrated out we will still be left with some effective action for the phase degrees of freedom  $\theta_{ij}(\tau)$  but this action will be both non-local and non-analytic in terms of differences of phases on various bonds. The only option appears to be to keep the gapless fermionic excitations in the theory. This in itself of course is perfectly fine but it does not advance our stated goal of “bosonizing” the CPCDW problem a least bit. Note that the issue here is not the Berry gauge field  $a$  and its coupling to nodal fermions – even when we ignore coupling of vortices to spin by setting  $a \rightarrow 0$  and concentrate solely on the charge sector as we have done so far, the gapless BdG quasiparticles still produce non-analytic contributions to the phase-only action. In short, what one has here is more than a problem; it is a calamity. The implication is nothing less but that there is *no* usable XY-type model for the charge sector of a quantum  $d$ -wave

superconductor, the optimistic title of the present paper notwithstanding.

Fortunately, there is a way out of this conundrum. While indeed we cannot write down a simple XY-like model for the fluctuating phases it turns out that the dual version of the theory can be modified in a relatively straightforward way to incorporate the non-analyticity caused by nodal fermions. To see how this is accomplished we go back to Section II and use our division of electronic degrees of freedom into low-energy nodal ( $\psi_{\sigma,\alpha}$ ) and “high-energy” anti-nodal fermions, tightly bound into spin-singlet Cooper pairs ( $\psi_{\sigma,\langle\alpha\beta\rangle}$ ). Imagine for a moment that we ignore nodal fermions altogether, by, for example, setting the number of Dirac nodal flavors  $N \rightarrow 0$  (in a single  $\text{CuO}_2$  plane  $N = 2$ ). Exact integration over anti-nodal electrons  $c_{\sigma,\langle\alpha\beta\rangle}$  leads to an XY-type model precisely of the type discussed at the beginning of this subsection. Since anti-nodal electrons are fully gapped the effective Hamiltonian has the conjectured form (14) with *finite* couplings  $J$ ,  $J_1$  and  $J_2$ , and with higher order terms which decay sufficiently rapidly. The explicit values of  $J$ ,  $J_1$  and  $J_2$  at  $T = 0$  might be difficult to determine but not more so than for an  $s$ -wave superconductor. Furthermore, since anti-nodal fermions carry all the charge density, the Berry phase term remains as determined earlier and so does the timelike stiffness of  $\varphi_i$ . Derivation of the dual theory proceeds as envisioned, with all the short range effects stored in vortex core terms and ultimately in  $m^2(\mathbf{r})$ , and with only remaining long range interactions mediated by the dual gauge field  $A_d$ . We now restore nodal fermions ( $N \neq 0$ ); as already emphasized, the only coupling of nodal fermions to the dual theory is via the gauge fields  $v$  and  $a$ . Since we are ignoring the spin channel we can neglect  $a$ . As far as  $v$  is concerned, including nodal fermions leads to a non-local, non-analytic correction to its stiffness, expressed as

$$v_\mu K_\mu v_\mu \rightarrow v_\mu (K_\mu \delta_{\mu\nu} + N Q_{\mu\nu}) v_\nu \quad ,$$

where  $K_\mu$  is determined by anti-nodal electrons.  $Q_{\mu\nu}(q)$  is the contribution from nodal fermions, linear in  $q$  and in general quite complicated. We give here few simpler limits:  $Q_{00}(0, \omega_n) = c|\omega_n|$ ,  $Q_{0i} = Q_{i0} = 0$ ,  $Q_{xx}(\mathbf{q}, 0) = Q_{yy}(\mathbf{q}, 0) = -cq_>$ ,  $Q_{xy}(\mathbf{q}, 0) = Q_{yx}(\mathbf{q}, 0) = -cq_<\text{sgn}(q_x, q_y)$ , where  $q_> = \max(|q_x|, |q_y|)$ ,  $q_< = \min(|q_x|, |q_y|)$  and  $c \sim \pi^2/16\sqrt{2}^{43}$ .

In the language of dual theory, this translates into a modified self-action for the dual gauge field:

$$\begin{aligned} & \frac{1}{2}(\partial \times A_d)_\mu K_\mu^{-1}(\partial \times A_d)_\mu \\ & \rightarrow \frac{1}{2}(\partial \times A_d)_\mu [K_\mu \delta_{\mu\nu} + N Q_{\mu\nu}]^{-1}(\partial \times A_d)_\nu \quad , \quad (34) \end{aligned}$$

where  $[K_\mu \delta_{\mu\nu} + N Q_{\mu\nu}]^{-1}$  is the tensor inverse of  $K_\mu \delta_{\mu\nu} + N Q_{\mu\nu}$ . This action is clearly more complicated than its Maxwellian  $s$ -wave counterpart but nevertheless decidedly manageable – most importantly, the part of the dual action involving dual boson field  $\Phi$  remains *unaffected*. Note that nodal fermions induce *subleading* but

still long-ranged interactions between vortices, in addition to the familiar Biot-Savart interactions. These interactions have square symmetry on the blue lattice, reflecting their nodal origin. Furthermore, when  $A_d$  is integrated over, they will produce a peculiar dissipative term  $\sim |\omega_n|v_0^2$  which describes the damping of collective quantum vorticity fluctuations by gapless nodal quasiparticles. The importance of this effect is secondary relative to the mass term for  $v_0$  which is always generated by anti-nodal fermions, basically because the density of states  $N(E)$  for nodal fermions vanishes as  $E \rightarrow 0$ . However, given the smallness of traditional Bardeen-Stephen core viscosity this “nodal” mechanism is an important source of dissipation of vortex motion in underdoped cuprates. Since our focus in the present paper is dual mean-field theory, this dissipative term will play no direct role.

Armed with the above analysis we can finally write down the Lagrangian of the quantum XY-type model describing a LdSC:

$$\begin{aligned} \mathcal{L}_{XY}^d &= i \sum_i f_i \dot{\varphi}_i + \frac{K_0}{2} \sum_i \dot{\varphi}_i^2 + \mathcal{H}_{XY}^d + \mathcal{L}_{\text{nodal}} + \mathcal{L}_{\text{core}} \\ &= i \sum_i f_i \dot{\varphi}_i + \frac{K_0}{2} \sum_i \dot{\varphi}_i^2 - J \sum_{nn} \cos(\varphi_i - \varphi_j) \\ &\quad - J_1 \sum_{rnnn} \cos(\varphi_i - \varphi_j) - J_2 \sum_{bnnn} \cos(\varphi_i - \varphi_j) \\ &\quad + \mathcal{L}_{\text{nodal}}[\cos(\varphi_i - \varphi_j)] + \mathcal{L}_{\text{core}} \quad , \quad (35) \end{aligned}$$

where the sums run over sites  $i$  of the blue lattice and the notation is the same as below Eq. (14),  $f_i = \frac{1}{8}(\bar{n}_k + \bar{n}_j)$  with  $k, j$  being the end sites of bond  $i$ , the time-like phase stiffness  $K_0$  results from the Hubbard-Stratonovich integration over  $\delta\Delta_{ij}$  as detailed above, and  $\mathcal{L}_{\text{core}}$  contains core terms coming from a small region around the (anti)vortex where  $\Delta$  itself is significantly suppressed, an example being (25). The explicit form of  $\mathcal{L}_{\text{nodal}}[\cos(\varphi_i - \varphi_j)]$  in the XY model language is unknown but it is a non-analytic, non-local functional of  $\cos(\varphi_i - \varphi_j)$ ; its effect will be incorporated once we arrive at the dual description, following the above arguments. Note that the short range parts of cosine functions and time derivative in (35) will be subsumed into  $\mathcal{L}_{\text{core}}$  once we go to continuum or Villain representations of the problem, as described elsewhere in the paper. Furthermore, observe that at half-filling the dual flux per plaquette of the blue lattice has an *intrinsic* checkerboard pattern:  $f = 1/2$  for black plaquettes and  $f = 0$  for red plaquettes. This is a direct consequence of  $\varphi(\tau)$  being a bond phase, residing on the blue lattice sites in Fig. 2, its Berry phase given by Eq. (33). Thus, in the quantum problem, the Berry phase *combines* with the next-nearest neighbor bonds (for  $J_1 \neq J_2$ ) in breaking translational symmetry of the blue lattice down to the checkerboard pattern of Fig. 2. The average flux through the unit cell on the blue lattice is  $f = 1/2$  which is just as it should be since there are two plaquettes of the blue lattice per single plaquette of the original black lattice and the dual flux per

plaquette of the CuO<sub>2</sub> lattice is  $f = 1/2$  at half-filling.

It is now straightforward to derive a dual representation of (35) by retracing the path that led from (27) to (30). In this fashion we obtain the dual Lagrangian of the (2+1)D XY model appropriate for a strongly fluctuating  $d$ -wave superconductor near half-filling<sup>44</sup>:

$$\mathcal{L}_d = |(\partial + i2\pi A_d)\Phi|^2 + m^2(\mathbf{r})|\Phi|^2 + \frac{g}{2}|\Phi|^4 + \frac{1}{2}(\partial \times A_d)_\mu [K_\mu \delta_{\mu\nu} + NQ_{\mu\nu}]^{-1} (\partial \times A_d)_\nu + (\dots) , \quad (36)$$

where  $\partial \times A_d$  satisfies the constraint arising from the charge Berry phase. The dual Lagrangian for a  $d$ -wave superconductor (36) differs from its  $s$ -wave counterpart (30) in the following important respects: *i*) the periodicity of the mass potential is different and reflects the checkerboard periodicity on the (dual) blue lattice set by our vortex core potential  $V(\mathbf{r})$ , *ii*) the self-action for the dual gauge field contains non-local, non-analytic contribution of nodal fermions, *iii*) the modulation of the dual flux  $\mathbf{B}_d$  relates to the variation in the pseudogap  $\delta\Delta_{ij}$  (as opposed to the electronic density  $\delta n_i$ ) via the constraint  $\delta\mathbf{B}_d(\mathbf{r}) \sim (1/16)\langle\delta\Delta_{ij}(\mathbf{r})\rangle$ , and *iv*) at doping  $x$ , the overall dual flux through the unit cell of the blue lattice imposed by the Berry phase constraint is  $f = p/q = (1-x)/2$ , comprised of  $f = p/q = (1-x)/2$  at a black plaquette and  $f = 0$  at a red one. We therefore expect the results for stable CPCDW states to be different from those of a hypothetical strongly fluctuating  $s$ -wave superconductor. Also, note that  $K_0$  is now set by  $K_0 \sim \langle|\delta\Delta_{ij}|^2\rangle$ , which is still related to fermion compressibility<sup>40</sup> and still relatively small since the basic aspect of our approach is that amplitude fluctuations in  $\Delta_{ij}$  are suppressed. This implies our dual superconductor remains in the type-II regime ( $\kappa_d \sim 1/\sqrt{K_0} \gg 1$ ). Finally,  $(\dots)$  denotes higher order terms which have been neglected. For those readers who find the above road to (36) perhaps a bit too slick, we give a detailed step-by-step derivation in the Appendix.

An important point should be noted here: The neglected higher order terms  $(\dots)$  involve higher order kinetic terms, additional intermediate range interactions, short range current-current interactions and numerous other contributions. All are irrelevant in the sense of critical behavior. In our problem, however, we are not interested only in the critical behavior. In particular, we would like to determine the charge modulation of the CPCDW on lengthscales which are not extremely long compared to the CuO<sub>2</sub> lattice constant. These additional terms could be important for this purpose. Particularly significant in this respect are the higher order corrections to the Berry phase (32) which, while not affecting the value of overall  $f$ , do influence the form of the effective dual Abrikosov-Hofstadter problem that ensues.

The strategy of keeping a large number of otherwise irrelevant terms is not a practical one. We will therefore introduce a simplification here which is actually quite nat-

ural and allows us to retain the essential realistic features of the original model and maintain the particle-hole symmetry as well. Consider a situation where  $m^2(\mathbf{r})$  in (36) is very strongly modulated. This is a ‘‘tight-binding’’ limit, universally considered appropriate for cuprates, and we can simply view quantum (anti)vortices as being able to hop only between the nearby plaquettes of the blue lattice, as is clearly implicit in (35). Furthermore, we assume that the two extrema in  $m^2(\mathbf{r})$  are separated by an energy scale larger than such hopping. This is a perfectly reasonable assumption since it illustrates an already important characteristic of our effective model, the fact that red and black plaquettes of the blue lattice are intrinsically not equivalent (by the form of the Berry phase and  $J_1 \neq J_2$ ). Under these circumstances we can rewrite the dual Lagrangian in a tight-binding form:

$$\begin{aligned} \mathcal{L}_d = & \sum_r |(\partial_\tau + i2\pi A_{d0})\Phi_r|^2 + \sum_b |(\partial_\tau + i2\pi A_{d0})\Phi_b|^2 \\ & - \sum_{\langle rr' \rangle} t_{rr'} \exp(i2\pi \int_r^{r'} ds \cdot \mathbf{A}_d) \Phi_r^* \Phi_{r'} \\ & - \sum_{\langle rb \rangle} t_{rb} \exp(i2\pi \int_r^b ds \cdot \mathbf{A}_d) \Phi_r^* \Phi_b - (\text{c.c.}) \\ & + \sum_r (m_r^2 |\Phi_r|^2 + \frac{g}{2} |\Phi_r|^4) + \sum_b (m_b^2 |\Phi_b|^2 + \frac{g}{2} |\Phi_b|^4) \\ & + \frac{1}{2} (\partial \times A_d)_\mu [K_\mu \delta_{\mu\nu} + NQ_{\mu\nu}]^{-1} (\partial \times A_d)_\nu + (\dots) , \quad (37) \end{aligned}$$

where vortex boson fields  $\Phi_{r(b)}$  reside on red (black) plaquettes of the blue lattice,  $t_{rr(b)}$  is the vortex hopping between the nearest red-red(black) neighbors,  $\exp(i2\pi \int_r^{r'(b)} ds \cdot \mathbf{A}_d)$  are the appropriate Peierls factors,  $|m_r^2 - m_b^2| \gg t_{rb}$  (core energies on red and black plaquettes are significantly different), and  $\nabla \times \mathbf{A}_d$  in the last term is the lattice flux of the dual magnetic field, equal  $f = p/q = (1-x)/2$  per unit cell of the original CuO<sub>2</sub> lattice. We have also assumed that it is the red plaquettes that are favored by vortex cores, making it unnecessary to include  $t_{bb}$  explicitly. The assumption  $E_r \ll E_b$  appears naturally warranted by the overall symmetry of the problem but, should the details of microscopic physics intervene and reverse the situation in favor of the black plaquettes, all one needs to do is exchange labels  $r \leftrightarrow b$  (note that  $m_r^2 < 0$ ,  $m_b^2 > 0$  in a dual superconductor).

The resulting tight-binding dual Hamiltonian:

$$\begin{aligned}
\mathcal{H}_d = & - \sum_{\langle rr' \rangle} t_{rr'} \exp(i2\pi \int_r^{r'} ds \cdot \mathbf{A}_d) \Phi_r^* \Phi_{r'} \\
& - \sum_{\langle rb \rangle} t_{rb} \exp(i2\pi \int_r^b ds \cdot \mathbf{A}_d) \Phi_r^* \Phi_b - (\text{c.c.}) + \\
& + \sum_r (m_r^2 |\Phi_r|^2 + \frac{g}{2} |\Phi_r|^4) \\
& + \sum_b (m_b^2 |\Phi_b|^2 + \frac{g}{2} |\Phi_b|^4) + (\dots) \tag{38}
\end{aligned}$$

will be analyzed in two limits: for  $t_{rr} \gg t_{rb}^2/|m_r^2 - m_b^2|$ , in which case we can simply set  $t_{rb} \rightarrow 0$ , the effective Hofstadter problem assumes the form equivalent to the standard  $s$ -wave case defined on the sites of the red lattice (Fig. 2). Importantly, however, the relation between the modulation in  $\mathbf{B}_d$  and  $\delta\Delta_{ij}$  remains *different* from the  $s$ -wave case and peculiar to a  $d$ -wave, as explained above. We will call this limit an H1 model. Similarly, in the opposite case  $t_{rr} \ll t_{rb}^2/|m_r^2 - m_b^2|$  we can set  $t_{rr} \rightarrow 0$  and obtain an effective Hofstadter problem with hoppings between red and black sites only. Note that this situation is *not* equivalent to the standard  $s$ -wave case: In order to hop from one red plaquette to another a vortex must go through a black site, picking up a Peierls phase factor different from the one for a conventional direct red-to-red hop. In considering these Peierls factors we must exercise caution since the “assisted” hops between red plaquettes pass directly through the dual fluxes  $f = p/q = (1-x)/2$  located on black sites. By infinitesimally displacing the said flux, one is back to the situation where all closed paths of hops are composed of fluxes  $f = p/q = (1-x)/2$  through black and  $f = 0$  through red plaquettes of the blue lattice. The resulting Hamiltonian has an exact particle-hole symmetry around half-filling ( $x \rightarrow -x$ ), as it should. We call this the H2 model. Finally, still in the limit  $t_{rr} \ll t_{rb}^2/|m_r^2 - m_b^2|$  with  $t_{rr} \rightarrow 0$ , we can “spread” the dual flux so it is uniformly distributed throughout each blue lattice plaquette and equal  $f = p/q = (1-x)/4$ . In this situation, dubbed an H3 model, the  $x \rightarrow -x$  symmetry is obeyed only approximately, for small  $x$  (near half-filling), but this is all we are interested in. We have established by explicit computations that the H3 model satisfies the particle-hole symmetry at some Hofstadter fractions  $f$  while it does not appear to do so at others; it is for this reason that we tend stay away from the H3 model in this paper. The reader should note that the issue of how to deal with dual fluxes when hopping through black plaquettes arises only in tight-binding models H2 and H3 (but not H1!) – the original dual Lagrangian (36) is free of such issues and has manifest  $x \rightarrow -x$  symmetry. The down side, of course, is that such a continuum theory is far more difficult to solve, both analytically and numerically.

The Hamiltonian (38), in its three editions H1, H2, and (to a limited extent!) H3, defines probably the simplest

dual version of the Hofstadter problem which appropriately builds in the  $d$ -wave character of the fluctuating lattice superconductor and the essential phenomenology of the pseudogap state in underdoped cuprates. The extra terms ( $\dots$ ) can still be used for fine-tuning (for example,  $g \rightarrow g_r, g_b$ , additional  $|\Phi_r|^2 |\Phi_b|^2$  repulsions, etc.) but the important particle-hole symmetry around half-filling is already present without them. All the detailed numerical calculations reported in the latter pages of this paper and described in Ref. 12 use the mean-field version of (38) and the three models based on it, H1 ( $t_{rr} \gg t_{rb}^2/|m_r^2 - m_b^2|$ ) and H2 and H3 ( $t_{rr} \ll t_{rb}^2/|m_r^2 - m_b^2|$ ), as the point of departure.

## V. DUAL SUPERCONDUCTOR AND COOPER PAIR CDW IN UNDERDOPED CUPRATES

The previous sections concentrated on the derivation of the effective quantum XY-type model for phase fluctuations in underdoped cuprates and its dual counterpart (36) and (37). In this section we pause to take stock of where we are with respect to the real world and to consider some general features of the physical picture that emerges from Eqs. (36,37). First, the dual superconductor (36) describes the physics of strongly fluctuating superconductors in terms of a complex bosonic field  $\Phi$ , which creates and annihilates quantum vortex-antivortex pairs viewed as “charged” relativistic particles (vortices) and antiparticles (antivortices) – this is depicted in Fig. 3. The conserved “charge” is just the vorticity associated with these topological defects, +1 for vortices and -1 for antivortices, and the gauge field coupled to it is nothing but  $A_d$ . Physically,  $A_d$  describes the familiar logarithmic interactions between (anti)vortices. We stress that the dual description is just a convenient mathematical tool: Its main advantage is that it allows a theorist to access a strongly quantum fluctuating regime of a superconductor, where the superfluid density  $\rho_s$  at  $T = 0$  can be very small or even vanish, while the pairing pseudogap  $\Delta$  remains large. According to the theory of Ref. 5 this is the regime that governs the properties of the pseudogap state in underdoped cuprates. This regime is entirely inaccessible by more conventional theoretical approaches which use the mean-field BCS state as the starting point around which to compute fluctuation corrections.

The dual superconductor description predicts two basic phases of cuprates:  $\langle \Phi \rangle = 0$  is just the familiar superconducting state. Quantum and thermal vortex-antivortex pair fluctuations are present (and thus  $\langle |\Phi|^2 \rangle \neq 0$ ) but these pairs are always bound, resulting in a finite, but considerably suppressed superfluid density. As vortex-antivortex pairs unbind at some doping  $x = x_c$ , the superfluid density goes to zero and the superconducting state is replaced by its dual counterpart,  $\langle \Phi \rangle \neq 0$ . The meaning of dual ODLRO is actually quite simple: Finite  $\langle \Phi \rangle$  means that vortex loops (loops of vortex-antivortex pairs being created and annihilated in



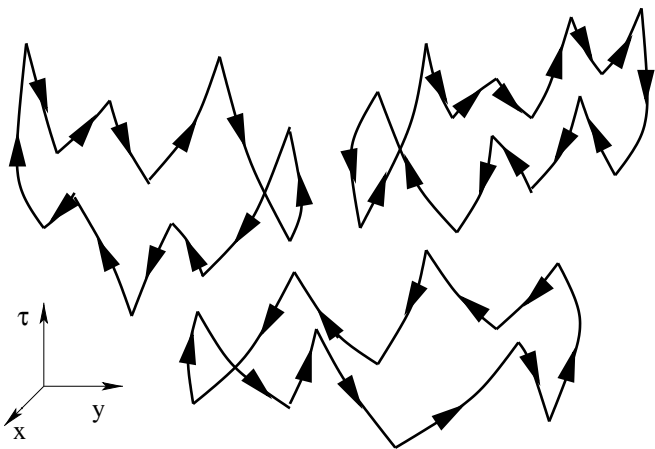


FIG. 3: Quantum fluctuations of vortex-antivortex pairs.  $xy$ -plane is the  $\text{CuO}_2$  layer and  $\tau$ -axis shows direction of imaginary time. Vortices (arrows pointing upwards) and antivortices (arrows pointing downwards) are always created and annihilated in pairs. Note that the structures arising from linked creation-annihilation events form oriented loops carrying  $\pm 1$  vorticity. These loops are just the virtual particle-antiparticle creation and annihilation processes in the quantum vacuum of the relativistic bosonic field  $\Phi(x)$ , as described in the text and the Appendix.  $\Phi$  is our *dual* order parameter: In a physical superconductor such vorticity loops are finite and  $\langle \Phi \rangle = 0$ . Note that the intersections of such finite loops with the  $xy$ -plane at any given time  $\tau$  define a set of bound vortex-antivortex dipoles in the  $\text{CuO}_2$  layer. The superconducting order is lost when vortex-antivortex pairs unbind and the average size of the above vorticity loops diverges – some of the loops become as large as the system size. This is the pseudogap state, with  $\langle \Phi \rangle \neq 0$ . The reader should note the following amusing aside: The above figure can easily be adapted to depict the low energy *fermionic* excitations of theory (1). The creation and annihilation processes now describe spin up (arrows pointing upwards) and spin down (arrows pointing downwards) quasi-particle excitations from the BCS-type spin-singlet vacuum. The loops carry a well-defined spin and can be thought of as relativistic BdG Dirac particles/antiparticles – their massless character in a nodal  $d$ -wave superconductor implies the presence of loops of arbitrarily large size. These fermionic loops move in the background of fluctuating vortex loops discussed above, their mutual interactions encoded in gauge fields  $v$  and  $a$ . This is a pictorial representation of the theory (1).

(2+1) dimensional spacetime) can now extended over the whole sample, i.e. the worldline of a dual relativistic boson can make its way from any point to infinity (see Fig. 3). The presence of such unbound vortex-antivortex excitations directly implies vanishing helicity modulus and thus the absence of the Meissner effect and  $\rho_s = 0$  (see Section II for details). The phase diagram of a dual superconductor as it applies to cuprates is shown in Fig. 4.

In the dual mean-field approximation, just as in a conventional one, we ignore fluctuations in  $\Phi$  and minimize the action specified by (36) with respect to a complex function  $\Phi(\mathbf{r})$ . In a physical superconductor ( $x > x_c$ )

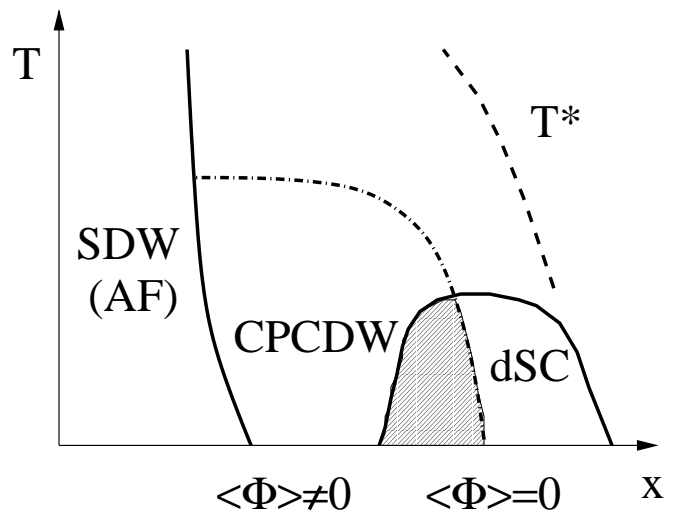


FIG. 4: The schematic phase diagram of underdoped cuprates in the theory of Refs. 5,12.  $T^*$  denotes the pseudogap temperature ( $T^* \sim \Delta$ ). Dual superconducting order (finite  $\langle \Phi \rangle$ ) implies the absence of the true, physical superconductivity. Conversely, the absence of dual order ( $\langle \Phi \rangle = 0$ ) corresponds to the physical superconductor. The shaded area represents the region of coexistence between a strongly fluctuating superconductor and a CPCDW state, which will generally occur in the dual theory. This region of “supersolid” behavior is characterized by  $\langle \Phi \rangle = 0$  but finite  $\langle |\Phi|^2 \rangle$ , which is modulated within the  $\text{CuO}_2$  layer according to our theory of a dual superconductor. The precise size of a coexistence region, however, is difficult to estimate from the mean-field theory and a more elaborate approach, including fluctuations in  $\Phi$  and  $A_d$ , needs to be employed. Finally, the finite temperature phase boundary of the CPCDW (dashed-dotted line) should not be taken quantitatively apart from the fact that it is located below  $T^*$ .

$\Phi(\mathbf{r}) = 0$ . For  $x < x_c$ , the minimum action corresponds to finite  $\Phi(\mathbf{r})$ . However, since the charge Berry phase translates into a dual magnetic field  $\mathbf{B}_d$  this finite  $\Phi(\mathbf{r})$  must contain  $N_d$  vortices, where  $N_d$  is the number of the dual flux quanta piercing the system. Note that this number is nothing but half of the total number of electrons  $N_d = N/2$ , the factor of one half being due to the fact that we are considering Cooper pairs. In a tight binding representation (37) this implies a dual flux  $f = p/q = (1 - x)/2$  per each  $\text{CuO}_2$  unit cell. The presence of such vortex array in  $\Phi(\mathbf{r})$  will be accompanied by spatial variation in  $B_d(\mathbf{r})$ , which translates into the modulation of the pseudogap  $\delta\Delta_{ij}$  and thus into a CDW of Cooper pairs (CPCDW). Consequently, in the vocabulary of the dual mean-field approximation, the question of formation and the structure of the CPCDW is equivalent to finding the Abrikosov vortex array on a tight binding lattice, i.e. the Abrikosov-Hofstadter problem defined by (37,38). The formation of CPCDW results in a modulation of the local tunneling DOS and one is led to identify the “electron crystal” state observed in STM experiments<sup>8,9,10</sup> as the CPCDW.

Our task is to determine the specific pattern in which the vortices in  $\Phi(\mathbf{r})$  arrange themselves to minimize the expectation value of the dual Hamiltonian (38). Once this is known we can determine the modulation in the dual induction  $\mathbf{B}_d$  and the structure of the CPCDW follows from the  $\mathbf{B}_d \leftrightarrow \delta\Delta_{ij}$  correspondence. In this section we are interested in general qualitative results and we therefore focus on the H1 model where such results are more transparent. The H2 and H3 models turn out to be more opaque and have to be studied numerically as soon as one is away from half-filling.

The solution of the Abrikosov-Hofstadter problem is obtained as follows: one first sets  $g = 0$  in (38) and finds the ground state of the resulting quadratic Hofstadter Hamiltonian  $\mathcal{H}_d(g = 0)$  given by

$$-\sum_{\langle rr' \rangle} t_{rr'} e^{2\pi i \int_r^{r'} ds \cdot \mathbf{A}_d} \Phi_r^* \Phi_{r'} - \sum_{\langle rb \rangle} t_{rb} e^{2\pi i \int_r^b ds \cdot \mathbf{A}_d} \Phi_r^* \Phi_b - (\text{c.c.}) + \sum_r m_r^2 |\Phi_r|^2 + \sum_b m_b^2 |\Phi_b|^2 . \quad (39)$$

At flux  $f = p/q$  the ground state is  $q$ -fold degenerate and we denote it by  $\Phi^{(q)}(\mathbf{r})$ . One then turns on finite  $g$ , forms a linear combination of these degenerate states  $\sum_q \alpha_q \Phi^{(q)}(\mathbf{r})$ , and determines variationally the set of coefficients  $\{\alpha_q\}$  which minimizes the full Hamiltonian (38). With  $\{\alpha_q\}$  fixed in this fashion the only remaining degeneracy in the ground state consists of lattice translations and rotations. Once the ground state  $\Phi^{(0)}$  is found, the magnetic induction  $\mathbf{B}_d$  follows from Maxwell equation:

$$\frac{\delta \mathcal{L}_d}{\delta \mathbf{A}_d} = \frac{1}{\tilde{K}_0} \Delta \times \delta \mathbf{B}_d(\mathbf{r}) - \mathbf{j}^\Phi = 0 , \quad (40)$$

where  $\mathcal{L}_d$  is given by Eq. (37),  $\delta \mathbf{B}_d = \Delta \times \mathbf{A}$ , and  $\mathbf{j}^\Phi$  is the current in the ground state of dual Hamiltonian (39) with the *uniform* dual flux  $f$ . All quantities in (40) are defined on the blue lattice of Fig. 2:  $\Delta$  is a lattice derivative,  $\mathbf{j}^\Phi$  and  $\mathbf{A}_d$  are link variables, and  $\mathbf{B}_d = \Delta \times \mathbf{A}_d$  is a site variable. The detailed definitions of all these objects are given in the next section. The non-local, non-analytic self-energy for the dual gauge field in (37) was replaced by an effective Maxwellian ( $K_\mu \rightarrow \tilde{K}_\mu$ ) – this approximation is valid for weak modulation  $\delta \mathbf{B}_d$ . We should stress that this way of determining the ground state  $\Phi^{(0)}$  and dual induction  $\mathbf{B}_d(\mathbf{r})$  is valid only if  $\tilde{K}_0$  is sufficiently small so that the dual Ginzburg parameter  $\kappa_d \sim 1/\sqrt{\tilde{K}_0}$  is sufficiently large – in underdoped cuprates this is a justified assumption since strong Mott-Hubbard correlations strongly suppress all charge density fluctuations. At higher modulation, i.e. for intermediate values of  $\kappa_d$ , the nodal contribution becomes more significant and its intrinsic square symmetry (see discussion around Eq. (34)) will act to orient  $\delta \mathbf{B}_d$  relative to the blue lattice. If this is the case, the interplay between this “nodal” effect and the one arising from the Abrikosov-Hofstadter problem itself can lead to interesting new patterns for the CPCDW state; a detailed study of such an interplay

is left for the future. Finally, from  $\delta \mathbf{B}_d(\mathbf{r}) \equiv \mathbf{B}_d(\mathbf{r}) - f$  we obtain  $\delta \Delta_{ij}$  which can be fed back into the electronic structure via the expressions given in Section II.

Notice that the above method of solving the problem corresponds to the strongly type-II regime of a dual superconductor ( $\kappa_d \gg 1$ ). In this limit, the CPCDW pattern is *primarily* given by the dual supercurrent  $\mathbf{j}^\Phi$  in the Maxwell equation (40), itself determined by the solution to the Abrikosov-Hofstadter problem (39). The modulation in  $\delta \mathbf{B}_d$  only reflects this pattern of vortices in  $\mathbf{j}^\Phi$  (40), and the dual magnetic energy is only a small fraction of the Abrikosov-Hofstadter condensation energy. Imagine now that we ask the following question: What are the interactions among vortices in  $\Phi$  that have resulted in  $\Phi^{(0)}$  being the ground state of the Abrikosov-Hofstadter problem? This question is analogous to the one inquiring about the interactions that have led to the triangular lattice of vortices in the continuum version of the problem, i.e. the interactions inherent in the famed Abrikosov participation ratio  $\beta_A$ . In both cases, these are far from pairwise and short-ranged – they are in fact intrinsically multi-body interactions, involving two-, three-, and multiple-body terms, all of comparable sizes and all long-ranged<sup>42</sup>. They can be thought of as the interactions among the center-of-mass coordinates of Cooper pairs. This should be contrasted with the picture of real-space pairs, interacting with some simple, pairwise and short-ranged interactions. The pair density-wave patterns in this case are determined not by the charge Berry phase and the Abrikosov-Hofstadter problem but by the Wigner-style crystallization. This is precisely the opposite limit of the Maxwell equation (40), in which it is the dual magnetic energy that determines the pattern rather than simply reflecting the one set by the Abrikosov-Hofstadter condensation energy, encoded in  $\Phi^{(0)}$ , and communicated by  $\mathbf{j}^\Phi$ . This is clearly seen in the Wigner crystal limit: consider an array of real-space pairs fixed in their positions. Such particles carry a unit dual flux and are completely *invisible* to vortices. As a result  $\mathbf{j}^\Phi = 0$  and (40) turns into the minimization of the dual magnetic energy. In the real-space pair limit this dual magnetic energy is nothing but the original assumed interactions between the pair bosons:  $\frac{1}{2} \sum_{ij} V(\mathbf{r}_i - \mathbf{r}_j) = \frac{1}{2} \int d^2 r d^2 r' \mathbf{B}_d(\mathbf{r}) V(\mathbf{r} - \mathbf{r}') \mathbf{B}_d(\mathbf{r}')$ , since  $\mathbf{B}_d(\mathbf{r}) = \sum_i \delta(\mathbf{r} - \mathbf{r}_i)$ , where  $\{\mathbf{r}_i\}$  are the pairs' positions – this is just the minimization of the potential energy in the Wigner problem. Consequently, the two descriptions, that of the Cooper pairs versus the real-space pairs, correspond to the two *opposite* limits of (40, 39), the first to the strongly type-II, the second to the strongly type-I limit of a dual superconductor. The density-wave patterns associated with these two limits are generally different and can be distinguished in experiments.

We now resume our discussion of the Abrikosov-Hofstadter problem. The simplest case, for all models, is  $f = 1/2$  or  $x = 0$ . For the H1 model, the (anti)vortices prefer red plaquette locations and  $\Phi_r$  will be large compared to  $\Phi_b$ , which can be safely ignored. The resulting

dual vortex array at half-filling is depicted in Fig. 5. The structure is a checkerboard with vortices in  $\Phi_r$  located on alternating black plaquettes. There is a single dual vortex per two unit cells of the  $\text{CuO}_2$  lattice, as expected for  $f = 1/2$ . Such close packing of dual vortices results in “empty” black plaquettes actually being occupied by dual antivortices (manifestation of the fact that our  $f = 1/2$  Hofstadter problem does not break the dual version of time reversal invariance). There is, however, *no* modulation in bond variables  $\delta\Delta_{ij}$  located on vertices of the blue lattice due to its peculiar relation to dual magnetic induction  $\mathbf{B}_d$  – all blue sites are in a perfectly symmetric relation to the dual vortex-antivortex checkerboard pattern on black plaquettes, as is obvious from Fig. 5. This implies  $\delta\Delta_{ij} = 0$  and the pseudogap  $\Delta$  remains uniform despite  $\Phi(\mathbf{r}) \neq 0$ . From this one would tend to conclude that there will be no CPCDW and no modulation in the local DOS. Still, there is a clear lattice translational symmetry breaking in the dual sector as evident from Figs. 5 and 6. Consequently, if we go beyond the leading derivatives, for example by including corrections to the Berry phase discussed around (26), we expect that a weak checkerboard modulation will develop in quantities like the electron density  $\delta n_i$ . The above is a special feature of the fluctuating LdSC which, however, is altered when we include the spin channel in our consideration. The Berry gauge field  $a_\mu$  must then be restored – its coupling to nodal fermions induces antiferromagnetic order at half-filling and thus breaks the above symmetry in the leading order by a commensurate spin-density wave (SDW)<sup>7, 5</sup>.

As the system is doped  $f$  decreases away from  $1/2$  according to  $f = p/q = (1-x)/2$ . The ground state energy of (38) is particularly low for dopings such that  $q$  is a small integer, (integer)<sup>2</sup> or a multiple of 2, reflecting the square symmetry of the  $\text{CuO}_2$  planes. Such dopings are thus identified as “major fractions” in the sense of the Abrikosov-Hofstadter problem. In the window of doping which is of interest in cuprates, these fractions are  $7/16$ ,  $4/9$ ,  $3/7$ ,  $6/13$ ,  $11/24$ ,  $15/32$ ,  $13/32$ ,  $29/64$ ,  $27/64$ ,  $\dots$ , corresponding to dopings  $x = 0.125$  ( $1/8$ ),  $0.111$  ( $1/9$ ),  $0.143$  ( $1/7$ ),  $0.077$  ( $1/13$ ),  $0.083$  ( $1/12$ ),  $0.0625$  ( $1/16$ ),  $0.1875$  ( $3/16$ ),  $0.09375$  ( $3/32$ ),  $0.15625$  ( $5/32$ ), etc. Other potentially prominent fractions, like  $1/4$ ,  $1/3$ ,  $2/5$ , or  $3/8$ , are associated with dopings outside the underdoped regime of strong vortex-antivortex fluctuations. In general, we expect that particularly low energy states correspond to fractions such that the pattern of dual vortices in  $\Phi$  can be easily accommodated by the underlying  $\text{CuO}_2$  lattice. Furthermore, we expect that the quartic repulsion in (38) will favor the most uniform array of dual vortices that can be constructed from the  $q$ -dimensional degenerate Hofstadter manifold. In the window of dopings one deals with in cuprates, these conditions single out doping  $x = 0.125$  ( $f = 7/16$ ) as a particularly prominent fraction. At  $x = 0.125$  ( $q = 16$ ), the dual vortex pattern and the accompanying modulation in  $\mathbf{B}_d$  can take advantage of a  $4 \times 4$  elementary block which, when ori-

ented along the  $x(y)$  direction, fits neatly into plaquettes of the dual lattice, as depicted in Fig. 5. This  $4 \times 4$  elementary block embedded into the original  $\text{CuO}_2$  lattice and containing 7 dual vortices ( $f = 7/16$ ) is clearly the most prominent geometrical structure among all the ones we have found in our study, both in its intrinsic simplicity and its favorable commensuration with the underlying atomic lattice. It is bound to be among the highly energetically preferred states in underdoped cuprates, as it is indeed found in the next section.

Before we turn to the details of this energetics, we investigate the signature in the electronic structure of the above  $4 \times 4$  elementary block. Such signature could be detected in the STM experiments of the type performed in Refs. 8,9,10. To this end, we compute the dual induction  $\mathbf{B}_d$  associated with the pattern of 7 dual vortices in Fig. 5 and from it the spatial modulation of the  $d$ -wave pseudogap  $\delta\Delta_{ij}$  on each bond within the  $4 \times 4$  supercell. With  $\Delta$  thus fixed, we evaluated the local density of BdG fermion states of our LdSC model. The results are shown in Figs. 7-9. Note that we do our computations in the “supersolid” region of the phase diagram in Fig. 4. This enables us to use the BdG formalism with only moderate smearing in the coherence peaks coming from the gauge fields  $v$  and  $a$  and it also allows for rather direct comparison with experiments. The downside is that we have to assume that the modulation profile in  $\mathbf{B}_d$  remains the same as determined from our dual mean-field arguments. Considering the high symmetry of elementary block in Fig. 5 this appears to be a rather minor assumption.

## VI. DUAL ABRIKOSOV-HOFSTADTER PROBLEM

In this section we present the results of numerical analysis of the H1 model. Within this model the values of the matter field  $\Phi(\mathbf{r})$  on the black sites are suppressed by very large  $m_b^2$ , and  $\Phi(\mathbf{r})$  effectively lives on the lattice dual to the original copper lattice, that is on the red sites in Fig. 2. Therefore, the dual fluxes reside inside the red plaquettes, shown in Fig. 11. In this section we will drop the subscript  $d$  in order to make notation more compact and use  $\mathbf{A}(\mathbf{r})$  for the vector potential corresponding to a uniform dual magnetic flux equal to  $f = p/q$ . Modulation of the field, which will be determined numerically, is described by  $\delta\mathbf{A}(\mathbf{r})$ . Within mean-field approximation, our problem then is reduced to minimization of the following Ginzburg-Landau lattice functional:

$$\mathcal{H}_d = -t \sum_{\mathbf{r}, \delta} e^{i\mathbf{A}_{\mathbf{r}, \mathbf{r}+\delta} + i\delta\mathbf{A}_{\mathbf{r}, \mathbf{r}+\delta}} \Phi^*(\mathbf{r})\Phi(\mathbf{r} + \delta) + \sum_{\mathbf{r}} \left( m^2 |\Phi(\mathbf{r})|^2 + \frac{g}{2} |\Phi(\mathbf{r})|^4 \right) + \frac{\kappa_d^2}{2} \sum_{\mathbf{r}} \delta B_d^2(\mathbf{r}) \quad , \quad (41)$$

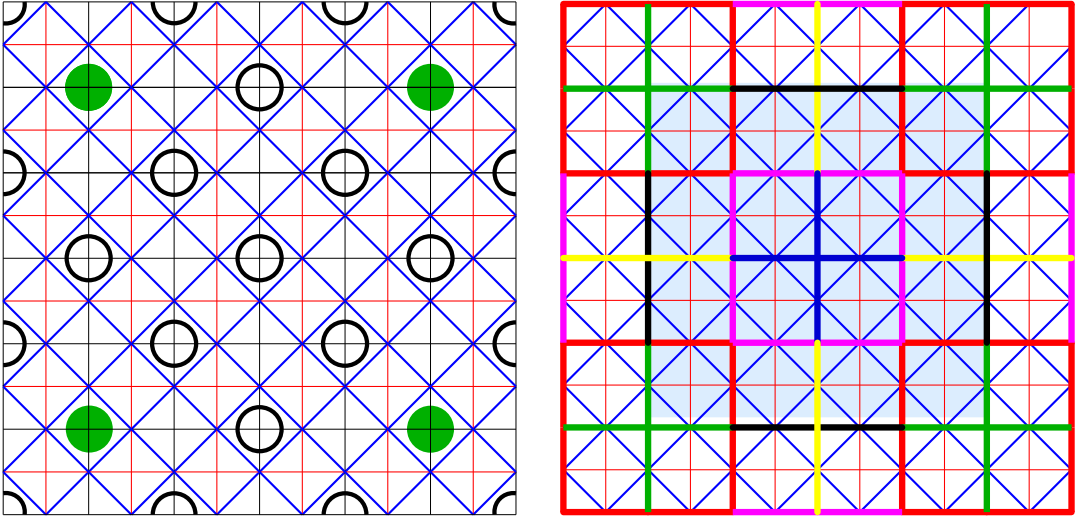


FIG. 5: Left panel: the circles depict the checkerboard array of vortices in  $\Phi$  forming the ground state of Hamiltonian H1 at half-filling ( $f = 1/2$  per plaquette of the atomic lattice). The empty black plaquettes are actually occupied by dual antivortices, brought into existence by a simple geometric constraint on the phase of  $\Phi$  in such a checkerboard array. The full green circles denote “dual vortex holes”<sup>5</sup>, i.e. the dual vortices that are missing relative to the half-filling checkerboard pattern once the system is doped to  $x = 1/8$  ( $f = 7/16$ ). The centers of these green circles form a square which defines the  $4 \times 4$  elementary block of 7 dual vortices (black circles) per 16 sites of the  $\text{CuO}_2$  lattice discussed in text. Right panel: the most general distribution of modulations  $\delta\Delta_{ij}$  consistent with the vortex pattern just described. The green “crosses” correspond to “dual vortex holes”. In general, there are six<sup>48</sup> phenomenological parameters  $\delta\Delta_{ij}$  shown in different colors. The number of inequivalent sites of the black lattice is also six (see Fig. 7).

where  $m^2 = m_r^2$ ,  $\delta = \{\pm\hat{x}, \pm\hat{y}\}$ , the link variables  $\mathcal{A}$  are defined as

$$\mathcal{A}_{\mathbf{r}, \mathbf{r}+\delta} = \int_{\mathbf{r}}^{\mathbf{r}+\delta} d\mathbf{r} \cdot \mathbf{A} \quad . \quad (42)$$

Note that from this point on, we absorb the factors of  $2\pi$  into the definition of  $\mathbf{A}$  for numerical convenience and to conform with the Abrikosov dimensionless notation<sup>37</sup>. The modulated part of the flux  $\delta B_d(\mathbf{r})$  is given by the circulation of the corresponding  $\delta\mathcal{A}$  around each plaquette as

$$\delta\mathcal{A}_{\mathbf{r}, \mathbf{r}+\hat{x}} + \delta\mathcal{A}_{\mathbf{r}+\hat{x}, \mathbf{r}+\hat{x}+\hat{y}} + \delta\mathcal{A}_{\mathbf{r}+\hat{x}+\hat{y}, \mathbf{r}+\hat{y}} + \delta\mathcal{A}_{\mathbf{r}+\hat{y}, \mathbf{r}} \quad . \quad (43)$$

The minimization of  $\mathcal{H}_d$  with respect to the link variables  $\delta\mathcal{A}$  is equivalent to the solution of the following set of equations:

$$\begin{aligned} 0 &= 2t|\Phi(\mathbf{r})||\Phi(\mathbf{r}+\hat{x})|\sin(\mathcal{A}_{\mathbf{r}, \mathbf{r}+\hat{x}} + \delta\mathcal{A}_{\mathbf{r}, \mathbf{r}+\hat{x}} + \alpha_{\mathbf{r}+\hat{x}} - \alpha_{\mathbf{r}}) \\ &\quad + \kappa_d^2(\delta B_d(\mathbf{r}) - \delta B_d(\mathbf{r}-\hat{y})) \\ 0 &= 2t|\Phi(\mathbf{r})||\Phi(\mathbf{r}+\hat{y})|\sin(\mathcal{A}_{\mathbf{r}, \mathbf{r}+\hat{y}} + \delta\mathcal{A}_{\mathbf{r}, \mathbf{r}+\hat{y}} + \alpha_{\mathbf{r}+\hat{y}} - \alpha_{\mathbf{r}}) \\ &\quad + \kappa_d^2(\delta B_d(\mathbf{r}-\hat{x}) - \delta B_d(\mathbf{r})) \quad , \end{aligned} \quad (44)$$

where  $\alpha_{\mathbf{r}}$  is the phase of the dual matter field  $\Phi(\mathbf{r})$ . Since the last terms in equations (44) can be identified as  $x$  and  $y$  components of the lattice curl, these are the lattice analogs of the (dual) Maxwell’s equations in two dimensions, providing explicit lattice realization of Eq. (40).

Before we present the results of the numerical computation, we will discuss briefly the structure of the solutions that should be expected on general symmetry

grounds. In the limit of infinite  $\kappa_d$  the gauge field  $\delta\mathcal{A}$  does not fluctuate, and only  $\Phi(\mathbf{r})$  should be varied in minimizing  $\mathcal{H}_d$ . To understand why the solution for a general filling is inhomogeneous consider first a case of  $g = 0$ . Then the functional  $\mathcal{H}_d$  simply describes a particle on a tight-binding lattice moving in a uniform magnetic field  $\bar{f}$ . The corresponding Hamiltonian is

$$\hat{H}_{\text{Hof}}\Phi(\mathbf{r}) = -t \sum_{\delta=\pm\hat{x}, \pm\hat{y}} e^{i\mathcal{A}_{\mathbf{r}, \mathbf{r}+\delta}} \Phi(\mathbf{r}+\delta) + m^2\Phi(\mathbf{r}) \quad .$$

The minimization of the functional  $\mathcal{H}_d$  is closely related to finding the ground states of Hamiltonian  $\hat{H}_{\text{Hof}}$ . Note that although the dual magnetic field felt by the particles is perfectly uniform, the gauge-field  $\mathbf{A}(\mathbf{r})$  is not, regardless of the gauge used. Indeed, if this were the case the circulation of the vector potential  $\mathbf{A}$  around the primitive plaquette would be zero by periodicity, which is not possible as the circulation is equal to the flux of the magnetic field  $2\pi p/q$  through the plaquette. Thus, the Hamiltonian  $H_{\text{Hof}}$  does not commute with the usual lattice translation operators. Instead, as noted by Peierls long time ago, magnetic translation operators  $T_{\mathbf{R}}$ , generating lattice translations complemented by simultaneous gauge transformations, must be constructed in order to commute with  $\hat{H}_{\text{Hof}}$ .

Unlike the ordinary translations, operators  $T_{\mathbf{R}}$  do not commute. Rather, operators  $T_{\mathbf{R}}$  form a ray representation of the translation group. The theory for irreducible ray representations of the translation group was

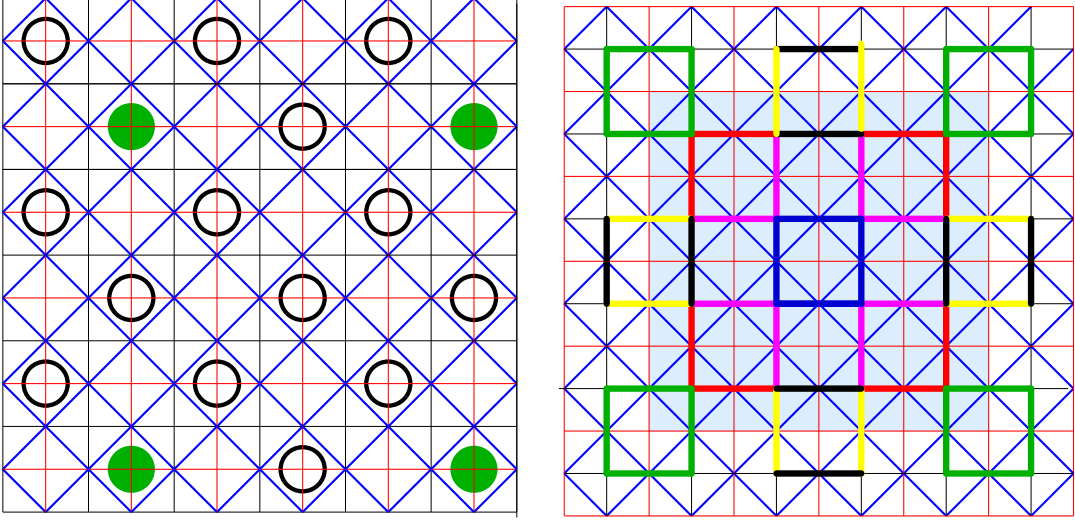


FIG. 6: The same as Fig. 5 except now the role of red and black plaquettes is reversed. This corresponds to either  $E_c^b < E_c^r$  or the (anti)vortex core location at the black plaquette being a *local* minimum of the vortex lattice potential  $V(\mathbf{r})$ . In the latter case, the pictured array would be a metastable configuration of dual vortices at  $x = 0$  and  $x = 1/8$ , ultimately unstable to the true ground state at those dopings depicted in Fig. 5. The most general pattern of  $\delta\Delta_{ij}$  is shown on the right. In this case, the “dual vortex holes” (solid green circles) correspond to the centers of  $\delta\Delta_{ij}$  bonds shown in green. Note that in general there are six<sup>48</sup> distinct parameters controlling modulations of the pairing pseudogap  $\Delta_{ij}$ . The number of non-equivalent (black) sites, however, is three (see Fig. 8).

constructed by Brown<sup>45</sup>. Alternatively, one can use the magnetic translation group introduced by Zak<sup>46</sup>, and use the ordinary representations of that group to classify the eigenstates of the Hamiltonian.

On the lattice, the classification of the states is simple and for completeness, we demonstrate how the magnetic eigenstates can be constructed. Consider for example the Landau gauge  $A_x = 0$ ,  $A_y = 2\pi xp/q$ , in which the unit cell spans  $q$  elementary plaquettes in  $\hat{x}$ -direction. Then the Peierls factors  $\mathcal{A}_{\mathbf{r},\mathbf{r}+\hat{\delta}}$ , shown in Fig. 10, are periodic modulo  $2\pi$  with enlarged  $q \times 1$  unit cell. The Hamiltonian now can be written as

$$\hat{H}_{\text{Hof}}\Phi(x, y) = m^2\Phi(x, y) - t\left(\Phi(x+1, y) + \Phi(x-1, y) + \Phi(x, y+1)e^{2\pi i \frac{p}{q}x} + \Phi(x, y-1)e^{-2\pi i \frac{p}{q}x}\right).$$

The Hamiltonian, obviously, remains invariant under transformations  $\mathbf{r} \rightarrow \mathbf{r} + \hat{y}$  and  $\mathbf{r} \rightarrow \mathbf{r} + q\hat{x}$ . Consequently, it can be diagonalized with the usual Bloch conditions

$$\Phi(\mathbf{r} + q\hat{x}) = e^{iqk_x} \Phi(\mathbf{r}) \quad (45)$$

$$\Phi(\mathbf{r} + \hat{y}) = e^{ik_y} \Phi(\mathbf{r}), \quad (46)$$

where  $(k_x, k_y)$  is the crystal momentum defined in a Brillouin zone  $\frac{2\pi}{q} \times 2\pi$ . Using these conditions, we rewrite the equation for the eigenstates as

$$m^2g(x) - t\left(g(x+1) + g(x-1) + 2g(x)\cos(k_y + 2\pi xp/q)\right) = Eg(x), \quad (47)$$

where  $g(x) = \Phi(x, 0)$ . Now we have one-dimensional equation for  $g(x)$ , where  $x = 0, 1, 2, \dots, q-1$ , that has to be solved with Bloch condition

$$g(x+q) = e^{iqk_x}g(x).$$

Thus the problem of diagonalization is reduced to the diagonalization of  $q \times q$  matrix for each  $\mathbf{k}$ . Note, however, that we did not exhaust all the information contained in the magnetic translation operators, apart from translations by  $q$  lattice spacings in  $\hat{x}$  direction. Consider an eigenstate described by crystal momentum  $\mathbf{k}$  within the Brillouin zone and characterized with wavefunction  $g(x)$ . Then function  $g_1(x) = g(x+1)$  is also an eigenstate of the Hamiltonian  $\hat{H}_{\text{Hof}}$  with the same energy but with momentum  $(k_x, k_y + 2\pi p/q)$ . By repeating this operation, one finds that  $q$  states with crystal momenta described by the same  $k_x$  but different  $k_y$ :

$$k_y, k_y + 2\pi p/q, k_y + 4\pi p/q, \dots, k_y + (q-1)2\pi p/q$$

all have the same energy. Since  $p$  and  $q$  are mutually prime, this set coincides with

$$k_y, k_y + 2\pi/q, k_y + 4\pi/q, \dots, k_y + (q-1)2\pi/q.$$

Occasionally, in the theory of magnetic translation groups, this is expressed by using a reduced Brillouin zone of size  $(2\pi)^2/q^2$ , then every band is said to be  $q$ -fold degenerate. As a typical example, a dispersion for  $p/q = 1/4$  is shown in the right panel of Fig. 10.

In the gauge we just described, there are  $q$  degenerate minima described by wavefunctions  $\Phi_j(x, y)$  that

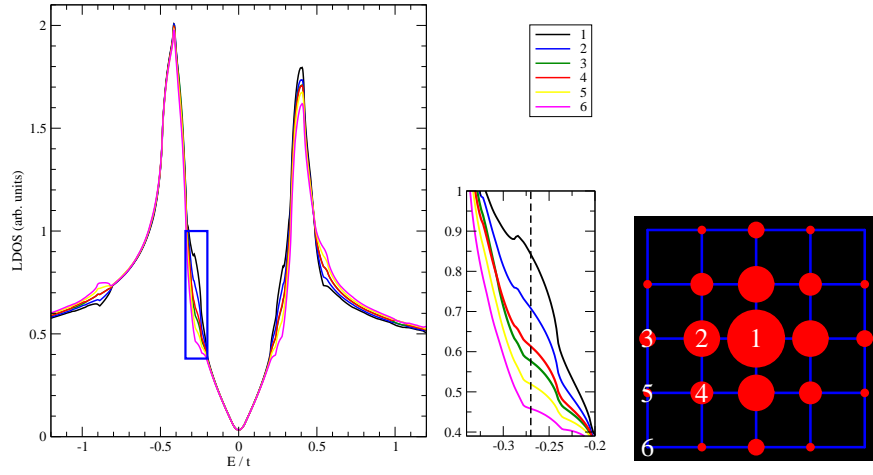


FIG. 7: The local density of states (LDOS) of the lattice  $d$ -wave superconductor with the modulated bond gap function  $\Delta_{ij}$  corresponding to the  $4 \times 4$  supercell structure of Fig. 5 at doping  $x = 1/8$ . The calculations are done within the LdSC model of phase fluctuations. Note that the fluctuations of the gauge fields  $v$  and  $a$  lead to small broadening of the peaks but produce no significant changes, as long as one is in the superconducting state. The parameters are  $t^* = 1.0$ ,  $\Delta = 0.1$  and the variation in  $\Delta$  from the weakest to the strongest bond is  $\pm 25\%$ . The portion enclosed within a rectangle is enlarged in the central panel. The numbers correspond to the locations of Cu atoms within a  $4 \times 4$  unit supercell on the  $\text{CuO}_2$  lattice depicted on the right panel. Note that Cu atom labeled 1 coincides with the location of the "dual vortex hole" in Fig. 5 (full green circle) where  $\Delta$  is the weakest, while the one labeled 6 corresponds to the Cu atom in the center of Fig. 5 which is surrounded by four strongest  $\Delta$ 's. The radii of the red circles indicate the magnitude of LDOS at  $E = -0.27t^*$  (dashed line in the central panel). This pattern of LDOS is very robust in our calculations and is precisely the tight-binding analogue of the checkerboard structure observed by Hanaguri et al<sup>9</sup> (note that on a tight-binding lattice, the Fourier transforms at wavevectors  $2\pi/4a_0$  and  $3 \times 2\pi/4a_0$  are not independent since  $3 \times 2\pi/4a_0$  and  $-2\pi/4a_0$  are equivalent). The symmetry of modulations in  $\Delta_{ij}$  corresponding to Fig. 5 imply that there are only six non-equivalent sites within the  $4 \times 4$  unit cell. Note that modulation pattern at energies above  $\Delta$  is actually *reversed* compared to the pattern at energies below  $\Delta$ . Finally, the nodes remain effectively intact, in accordance with Ref. 12. Finite LDOS at zero energy is entirely due to artificial broadening used to emulate finite experimental resolution. In the absence of such broadening, the LDOS remains zero within numerical accuracy (see Fig. 9).

are located at  $k_x = 0$  and  $k_y = 2\pi mp/q$ , where  $j = 0, 1, 2, \dots, (q-1)$ . Therefore, sufficiently close to the transition, the minimum of the functional  $\mathcal{H}_d$  should be sought as a linear combination of the  $q$  degenerate states  $\Phi_j(\mathbf{r})$  and our problem is equivalent to minimizing the Abrikosov participation ratio

$$\min \frac{\sum_{\mathbf{r}} |\Phi(\mathbf{r})|^4}{(\sum_{\mathbf{r}} |\Phi(\mathbf{r})|^2)^2}, \quad \text{where } \Phi(\mathbf{r}) = \sum_{j=1}^q C_j \Phi_j(\mathbf{r}). \quad (48)$$

Since  $k_x = 0$  for all  $\Phi_j(\mathbf{r})$ , any linear combination of functions  $\Phi_j(\mathbf{r})$  is periodic in  $x$ -direction:  $\Phi(\mathbf{r} + q\hat{x}) = \Phi(\mathbf{r})$ . In addition, for each of the  $q$  ground states,  $k_y$  is a multiple of  $2\pi/q$ , and consequently  $\Phi(\mathbf{r} + q\hat{y}) = \Phi(\mathbf{r})$ . From these two properties we find that any linear combination  $\sum_j C_j \Phi_j(\mathbf{r})$  must be periodic in the  $q \times q$  unit cell.

The minimization problem can be formulated equivalently in terms of coefficients  $C_j$ :

$$\mathcal{H}_d = E_0 \sum_j |C_j|^2 + \sum \Gamma_{j_1, j_2, j_3, j_4}^{(4)} C_{j_1}^* C_{j_2}^* C_{j_3} C_{j_4}, \quad (49)$$

where  $E_0$  is the ground state energy of  $\hat{H}_{\text{Hof}}$  following

from (47) and

$$\Gamma_{j_1, j_2, j_3, j_4}^{(4)} = \sum_{\mathbf{r}} \Phi_{j_1}^*(\mathbf{r}) \Phi_{j_2}^*(\mathbf{r}) \Phi_{j_3}(\mathbf{r}) \Phi_{j_4}(\mathbf{r}). \quad (50)$$

Note that (49) itself has Ginzburg-Landau form with  $q$  order parameters  $C_j$ . In our case, the form of the matrix  $\Gamma^{(4)}$  is dictated by our "microscopic" Hamiltonian  $\mathcal{H}_d$  and corresponds to the Abrikosov participation ratio (48). One could in principle generalize the theory by considering completely general form of  $\Gamma^{(4)}$  compatible with the overall symmetry requirements. Such procedure is equivalent to introducing long-ranged quartic interactions with general kernel  $K(\mathbf{r}, \mathbf{r}', \mathbf{r}'', \mathbf{r}''')$ :

$$\sum K(\mathbf{r}, \mathbf{r}', \mathbf{r}'', \mathbf{r}''') \Phi^*(\mathbf{r}) \Phi^*(\mathbf{r}') \Phi(\mathbf{r}'') \Phi(\mathbf{r}''').$$

Equation (49) is the most direct and convenient representation for numerical minimization of  $\mathcal{H}_d$  in the limit of infinite  $\kappa_d$ . However, in order to allow for intermediate values of  $\kappa_d$  and to be able to analyze the impact of various short-ranged terms describing interaction of dual fluxes  $\delta B_d(\mathbf{r})$ , we also have opted to follow a slightly different route: The numerical results that are presented below are produced by *direct* numerical minimization of functional (41) with respect to both the dual matter field

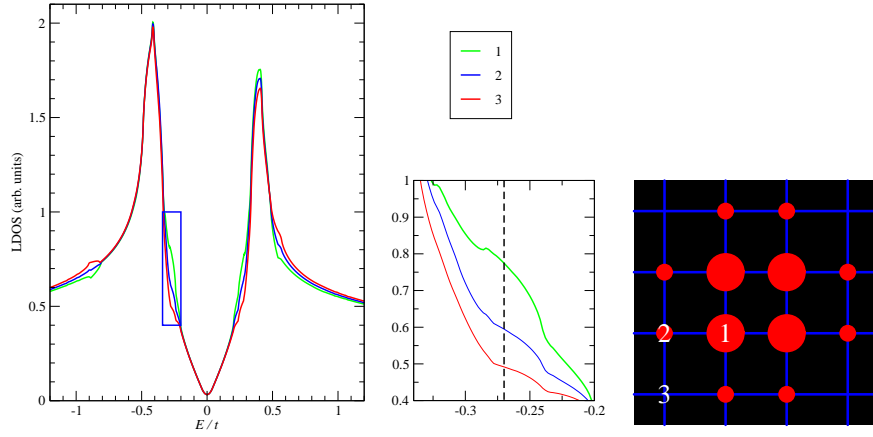


FIG. 8: Left panel: The local density of states (LDOS) of the lattice  $d$ -wave superconductor with the modulated bond gap function  $\Delta_{ij}$  corresponding to the  $4 \times 4$  supercell structure of Fig. 6 at doping  $x = 1/8$ . The parameters used are the same as in Fig. 7. Right panel: the local density of states at energy  $E = -0.27t$  (dashed line in the central panel). The radii of the circles are proportional to the LDOS at a given Cu atom. Note that inside the unit cell  $4 \times 4$  there are three (rather than six, as in Fig. 7) non-equivalent sites. Even in absence of any underlying theory, this pattern of modulation appears to correspond to CPCDW simply by visual inspection.

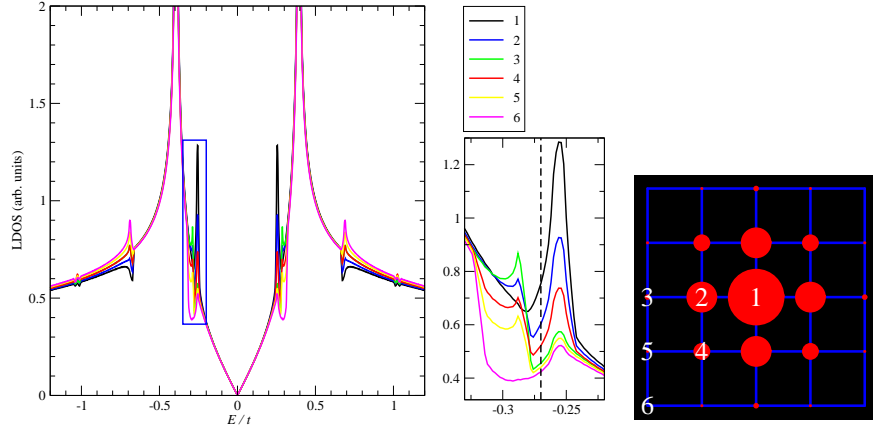


FIG. 9: The local density of states (LDOS) of the lattice  $d$ -wave superconductor with the modulated bond gap function  $\Delta_{ij}$  corresponding to the  $4 \times 4$  supercell structure of Fig. 5 at  $x = 1/8$ , computed under the assumption of perfect particle-hole symmetry for low-energy fermionic excitations. The parameters used are the same as in Fig. 7, with the exception of the broadening, which has been suppressed here in order to demonstrate that the nodes remain essentially unaffected by CPCDW<sup>12</sup>.

$\Phi$  and the link variables  $\delta A_\alpha$  by imposing periodic boundary conditions on  $N_x \times N_y$  blocks with varying  $N_x$  and  $N_y$ . At least in the vicinity of the transition, the largest unit cell one has to consider is  $q \times q$ . It should be stressed that we found identical results using both approaches whenever direct comparison is possible (sufficiently large  $\kappa_d$  and no additional short-ranged interactions between the fluxes).

We perform numerical minimization of functional (41) with respect to both the matter field  $\Phi(\mathbf{r})$  and the link variables  $\delta A_\alpha$  by imposing periodic boundary conditions on  $n \times m$  blocks with variable  $m$  and  $n$ . The number of independent variables grows as  $3mn$  and the largest unit cells we were able to consider are  $8 \times 8$ . We used the conjugate gradient minimization technique with as many

as  $10^4 - 10^5$  randomly chosen different starting points.

We remind the reader that since the dual matter field variables  $\Phi(\mathbf{r})$  in the H1 model live on the on red sites, the dual fluxes  $\delta B_d(\mathbf{r})$  reside inside the red plaquettes, shown in Fig. 11. Note that each link of the original copper lattice is shared by two red plaquettes and therefore the enhancement of the  $d$ -wave gap function  $\Delta$  should be interpreted as the average between the fluxes at the neighboring dual plaquettes. Thus, at half-filling  $f = \frac{1}{2}$  there is no modulation in  $\Delta$  and no charge density modulation emerging from our model H1 even though there is a checkerboard pattern in the dual flux. The checkerboard pattern remains the same for the entire range of parameters we were able to check. However, as explained in the previous section, since there is a definite symmetry



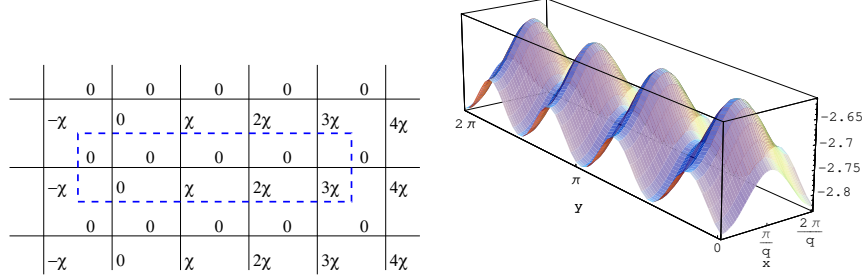


FIG. 10: Left panel: the Peierls link variables  $\mathcal{A}_{ij}$  in Landau gauge for  $q = 4$ .  $\chi$  denotes  $2\pi p/q$ . Both  $\mathcal{A}_{\mathbf{r},\mathbf{r}+\hat{x}}$  and  $\mathcal{A}_{\mathbf{r},\mathbf{r}+\hat{y}}$  are periodic in  $\hat{y}$ -direction. Although  $\mathcal{A}_{\mathbf{r},\mathbf{r}+\hat{y}}$  increases monotonically with  $x$ ,  $\exp(i\mathcal{A}_{\mathbf{r},\mathbf{r}+\hat{x}})$  is periodic with the unit cell shown by the dashed rectangle. Right panel: the dispersion  $E(k_x, k_y)$  of the lowest Hofstadter band for  $p/q = 1/4$  in units of  $t^*$ . There are  $q = 4$  ground states at  $k_x = 0$  and  $k_y = 2\pi j/q$ , where  $j = 0, 1, \dots, q - 1$ . For  $q = 4$  the energy of the ground states is  $E_0 = -2\sqrt{2}t$ .

breaking in the dual sector by the checkerboard array of  $\delta B_d(\mathbf{r})$  higher order derivatives and other terms not included in our dual Lagrangian are expected to generate a weak checkerboard modulation to accompany  $\delta B_d(\mathbf{r})$ .

At field characterized by  $f = p/q = 7/16$ , which within H1 model corresponds to doping  $x = 1/8$ , the structure of the configuration is considerably more complex. When restricted to a  $4 \times 4$  lattice, the resulting pattern is the square lattice of “crosses” separated by four unit cells, shown in Fig. 12. This configuration, however, is not the true global minimum. If a larger unit cell for modulations of the dual fluxes is allowed, the energy can be additionally lowered by  $\approx 0.5\%$  by distorting the ideal square pattern. The lowest energy we found corresponds to the quasi-triangular lattice of crosses shown in the right panel of Fig. 12. The lowest energy state that we find has the symmetry of this quasi-triangular pattern for all  $\kappa_d^2$  from 1.0 to  $10^5$ .

The smallness of the energy differences, involving only few percents of the overall Abrikosov-Hofstadter energy scale, indicates that the state that emerges victorious can be changed by the additional short range interactions and derivative terms which we have routinely neglected. Not surprisingly, therefore, the precise energetics of various low energy Abrikosov-Hofstadter states is decided by details. We find that inclusion of terms  $|\Phi(\mathbf{r})|^6$  and dual density-density interactions  $|\Phi(\mathbf{r})|^2|\Phi(\mathbf{r}+\delta)|^2$  with moderate coefficients does not change the patterns we described. On the other hand, the inclusion of the terms describing short-ranged interactions between the dual fluxes produces significant effects. An example of the typical pattern obtained by replacing the self-interaction term

$$\sum_{\mathbf{r}} \frac{1}{2} \kappa_d^2 (\delta B_d)^2 \quad (51)$$

by

$$\sum_{\mathbf{r}} \frac{1}{2} \kappa_d^2 (\delta B_d)^2 + \Gamma_0 \sum_{nn} \delta B_d(i) B_d(j) + \Gamma_1 \sum_{nnn} \delta B_d(i) B_d(j) \quad (52)$$

is shown in Fig. 13. The parameters  $\Gamma_0$  and  $\Gamma_1$  in (52) are chosen to make the distribution of the dual flux somewhat smoother than what is demanded by (51) only. This suffices to bring the energy of the square pattern in Fig. 13 from just above to just below that of the quasi-triangular pattern of Fig. 12. It is tempting to speculate that this slight additional “smoothing” of the dual flux represents the combined effects of nodal fermions and Coulomb interactions present in real systems. Note that the symmetry and the qualitative features of this pattern coincide with our  $4 \times 4$  “elementary” block conjectured to be the likely CPCDW ground state in the previous section (see Figs. 5 and 6). Once  $\delta B_d(i)$  are translated into  $\delta \Delta_{ij}$  the resulting pattern closely resembles the checkerboard distribution of local density of states of “electron crystal” observed in the STM experiments, as illustrated in Fig. 7.

Let us now consider this observed STM checkerboard pattern in more detail, in light of our theory. Obviously, our analysis being restricted to the tight-binding lattice, we cannot describe the local density of states (LDOS) at positions between the sites of Cu lattice – the peaks in our theoretical LDOS are always located on top of Cu atoms. In contrast, the STM measurements by Hanaguri *et al.*<sup>9</sup>, have much better spatial resolution and can image the actual continuous atomic orbitals. Our tight-binding lattice results for LDOS( $\mathbf{r}, E$ ) could be viewed as “coarse-grained” representation of the LDOS  $g(\mathbf{r}, E)$  observed experimentally:

$$\text{LDOS}(\mathbf{R}, E) \propto \int g(\mathbf{r}, E) d\mathbf{r} \quad ,$$

where the integral extends over a square of size  $a_0 \times a_0$  centered around Cu lattice site  $\mathbf{R}$ . Equivalently, the true continuum LDOS signal could be obtained by broadening our lattice LDOS around each Cu lattice site.

A prominent feature of the checkerboard pattern in STM measurements that has received much attention is the presence of a pronounced Fourier signal not only at wavevectors  $\frac{2\pi}{a_0}(\frac{1}{4}, 0)$  and  $\frac{2\pi}{a_0}(0, \frac{1}{4})$ , which correspond to the  $4a_0 \times 4a_0$  periodicity just described, but also at

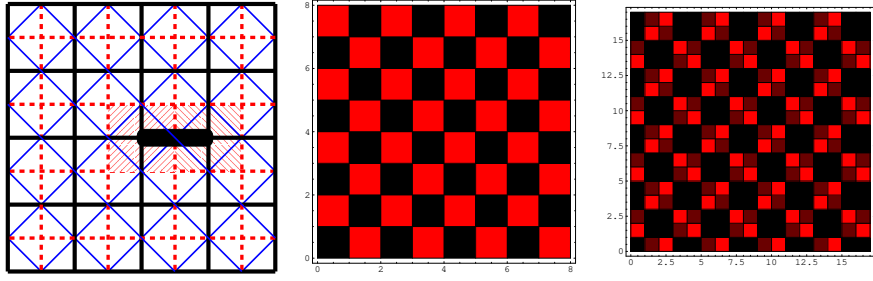


FIG. 11: Left panel: Any link of the black lattice (thick solid lines), which corresponds to  $\Delta_{ij}$ , is shared by two dual plaquettes shown in red. Within H1 model, therefore, the enhancement or suppression of  $\Delta_{ij}$  is determined by the average of the fluxes through the neighboring plaquettes of the dual lattice (red dashed lines). Central panel: distribution of  $\delta B_d$  at half filling. In units of  $t$ , the parameters used are  $\kappa_d^2 = 30.0$ ,  $m^2 = -1.0$ , and  $g = 2.0$ . The energy per site is  $-3.695$ . Right panel: distribution of  $\delta B_d$  at  $p/q = 1/4$ . In units of  $t$ , the parameters used are  $\kappa_d^2 = 30.0$ ,  $m^2 = -1.0$ , and  $g = 2.0$ . The energy per site is  $-3.564$ .

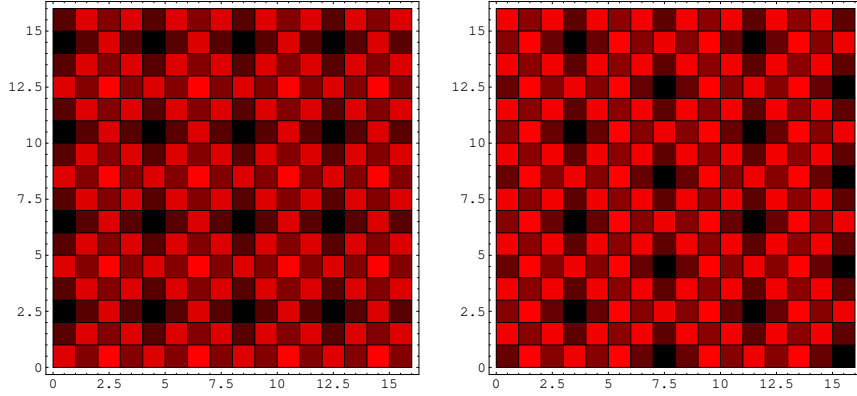


FIG. 12: Left panel: The pattern of the dual fluxes  $\delta B_d$  for  $p/q = 7/16$  with periodic boundary conditions in  $4 \times 4$  unit cell. The unit cell  $4 \times 4$  is repeated four times in horizontal and vertical directions for presentation purposes. The energy per site is  $-3.193$  in the units of  $t$  and the parameters of the model are the same as in the previous figure. The positive(negative) values of  $\delta B_d$  are shown in red (black). Right panel: the same but with  $8 \times 8$  unit cell. The square lattice is distorted towards the triangular lattice. The energy per site is  $-3.208t$  and is lower by 0.5% compared to the square arrangement.

$\frac{2\pi}{a_0}(\frac{3}{4}, 0)$  and  $\frac{2\pi}{a_0}(0, \frac{3}{4})$ . While it is tempting to associate the  $3/4$  peaks with an entirely independent type of order, we note that for a periodic lattice of identical  $4a_0 \times 4a_0$  tiles, the Fourier transform is a *discrete series* with wavevectors  $Q_{n_x, n_y} = \frac{1}{4} \frac{2\pi}{a_0}(n_x, n_y)$ , where  $n_x$  and  $n_y$  are integers, irrespective of how complex is the internal structure of each tile. For a general structure of the tile all of the harmonics  $(n_x, n_y)$  are present, and there is no *a priori* reason for the Fourier coefficients with  $n_x = 3$ ,  $n_y = 0$  to be particularly small. The presence of a large signal at  $Q_{3,0}$  is only natural, and no more unexpected than the weakness of Fourier harmonics at  $Q_{2,0}$  and  $Q_{0,2}$ .

Next, in order to describe and compare the Fourier transforms of spatially broadened LDOS patterns in Figs. (7-9) and tunneling LDOS observed in experiments<sup>9</sup>, we introduce a simple model which approximates each bright spot inside the primitive  $4a_0 \times 4a_0$  tile as

$$\eta(\mathbf{r}) = \exp \left[ J \left( \cos \frac{2\pi x}{4a_0} + \cos \frac{2\pi y}{4a_0} - 2 \right) \right].$$

While the specific functional form of the peak is not im-

portant, our choice is convenient since  $g(\mathbf{r})$  has a period of  $4a_0 \times 4a_0$  and a gaussian shape, centered at positions  $\mathbf{r} = (4N_x a_0, 4N_y a_0)$ , where  $N_x$  and  $N_y$  are integers. The width of the gaussians is  $\sim a_0/\sqrt{J}$ .

The real-space tunneling LDOS pattern of Hanaguri *et al.* can now be represented by a function

$$g(\mathbf{r}) = A\eta(\mathbf{r}) + B \sum_{\delta} \eta(\mathbf{r} + \delta) + C \sum_{\delta'} \eta(\mathbf{r} + \delta'), \quad (53)$$

where the first term represents the brightest peak of each tile, the term proportional to  $B$  represents the set of four second brightest peaks located at  $\delta = \pm(1 + \epsilon)a\hat{x}$ ,  $\pm(1 + \epsilon)a\hat{y}$  and the last term represents the weak peaks at  $\delta' = \pm a_0(1 + \epsilon)\hat{x} \pm a_0(1 + \epsilon)\hat{y}$  (see Fig. 14). Parameter  $\epsilon$  equals zero if the real-space LDOS peaks are centered at the Cu lattice sites, while  $\epsilon = 1/3$  if the maxima of all peaks, except for the central one, are displaced from their commensurate positions on top of Cu atoms – this is how the experimental data were interpreted in Ref. 9. We will show that for a wide range of parameters  $J, A, B, C$ , and arbitrary  $0 < \epsilon < 1/3$  the  $Q_{3,0}$  peaks are much stronger

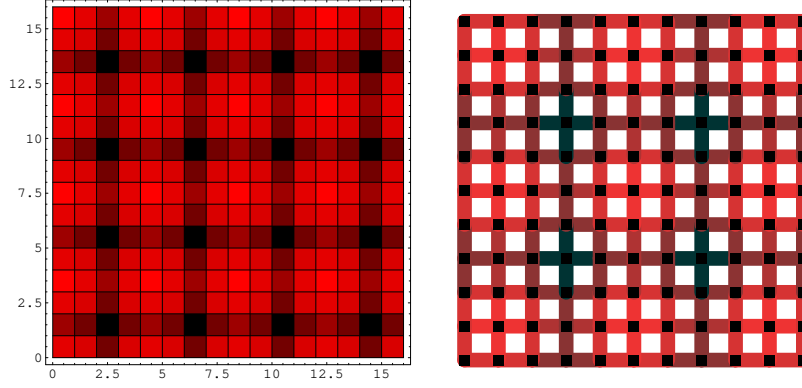


FIG. 13: Left panel: The pattern of the dual fluxes  $\delta B_d$  for the Hofstadter-Abrikosov problem at  $f = 7/16$  ( $x = 1/8$ ) obtained for the  $8 \times 8$  unit cell. The parameters of the model are  $\kappa_d^2 = 30.0$ ,  $\Gamma_0 = 6.0$ ,  $\Gamma_1 = -12.0$ ,  $m^2 = -1.0$ , and  $g = 2.0$ . The  $4 \times 4$  checkerboard symmetry of the pattern is precisely what is shown in Fig. 7. Right panel: The distribution of modulations in the pairing pseudogap  $\delta\Delta_{ij}$  corresponding to the pattern of fluxes shown on the left panel. This “tartan” pattern has the symmetry of Fig. 5 with “dual vortex holes” coinciding with black “crosses”.

$m$	$\epsilon = 0$	$\epsilon = 1/3$
$m \equiv 0 \pmod{4}$	$A + 4B + 4C$	$A + 4B + 4C$
$m \equiv 1 \pmod{4}$	$A + 2B$	$A + B - 2C$
$m \equiv 2 \pmod{4}$	$A - 4C$	$A + B - 2C$
$m \equiv 3 \pmod{4}$	$A + 2B$	$A + 4B + 4C$

TABLE I: Non-monotonic dependence  $\tilde{g}_{m,0}$  of the Fourier transformed LDOS  $g(\mathbf{r})$  defined in (53).

than peaks at  $Q_{2,0}$ , although to explain other features of Fig. 2 in Ref. 9, the “commensurate” choice  $\epsilon = 0$  appears to be more natural. For the momentum-space direction  $n = 0$  shown as black circles in Fig. 2 of Ref. 9, the Fourier coefficients are

$$g_{m,0} = \frac{1}{16a^2} \int_0^{4a_0} \int_0^{4a_0} dx dy G(x, y) e^{-i \frac{2\pi}{4a_0} m x}.$$

The integral is elementary and the result for  $g_{m,0}$  is

$$\left[ A + 2B + (2B + 4C) \cos \frac{2\pi(1 + \epsilon)m}{4} \right] I_0(J) I_m(J) e^{-2J}, \quad (54)$$

where  $I_m$  is the regular modified Bessel function.  $I_m(J)$ , shown for several values of  $J$  in Fig. 14, is a monotonically decreasing function of  $m$ . The non-monotonic part of  $g_{m,0}$ , denoted by  $\tilde{g}_{m,0}$ , is contained in the first factor of (54). When  $\epsilon = 0$  (commensurate position of the peaks), this factor is a periodic function of  $m$  with period four, while for  $\epsilon = 1/3$  the said period is equal to three. Table I summarizes the factors  $\tilde{g}_{m,0}$  for the two cases.

We start our analysis with the incommensurate case  $\epsilon = 1/3$ . The third column of Table I implies that in this case  $\tilde{g}_{1,0}$  and  $\tilde{g}_{2,0}$  are equal and smaller than the component  $\tilde{g}_{3,0}$ , as shown in the third column of the table. Experimentally, however, the Fourier component at

$Q_{1,0}$  (the  $1/4$  peak) is roughly of the same magnitude as  $Q_{3,0}$ , and it is the component at  $Q_{2,0}$  that is the weakest. To account for particularly small  $g_{2,0} \ll g_{1,0}$  one has to select the value of  $J$  such that the monotonic function  $I_m(J)$  decreases rapidly in the region between  $m = 1$  and  $m = 2$ , Fig. 14 indicates that this is the case for  $3 < J$ . This choice, however, also dramatically suppresses the Fourier transforms at  $m = 3$  and  $m = 4$ , both of which are rather large in experiments.

While the qualitative features of the Fourier transformed experimental LDOS could possibly be reconciled with  $\epsilon = 1/3$  by fine-tuning parameters  $A, B$ , and  $C$ , the situation might in fact be better described by assuming the *commensurate* location of the peaks, in registry with Cu atoms ( $\epsilon = 0$ ); see the second column the Table I. In this case, harmonic  $m = 2$  is *automatically* suppressed compared to the  $1/4$  and  $3/4$  Fourier components. The suppression of Fourier component at  $2/4$  can be qualitatively understood as follows: This Fourier component is determined by the overlap of the LDOS signal and  $\cos(2\frac{2\pi}{4a_0}x)$ . Obviously, the maxima of the LDOS signal correspond to alternating maxima and minima of  $\cos(2\frac{2\pi}{4a_0}x)$  and destructive interference of the two functions occurs. For harmonics  $1/4$  and  $3/4$  (and of course for  $4/4$ ) the overlaps are significant and their Fourier coefficients are larger. Peaks corresponding to larger values of  $m$  are strongly reduced due to the monotonic dependence  $I_m(J)$  of the Fourier transform on  $m$ . This suppression can serve as an estimate of parameter  $J$ : visually, the last discernible peak in Fig. 2 of Ref. 9 appears at  $Q_{5,0}$ , which places  $J$  in the range of  $5 - 10$  (see right panel of Fig. 14). In the right panel of Fig. 14 the spatial Fourier transforms of the LDOS (53) with parameters  $J = 7$ ,  $A = 1$ ,  $B = 0.5$ , and  $C = 0$  and commensurate placement of the peaks  $\epsilon = 0$  is shown. This example illustrates that the major features of the Fourier-transformed LDOS obtained by Hanaguri *et al.*<sup>9</sup> are ro-

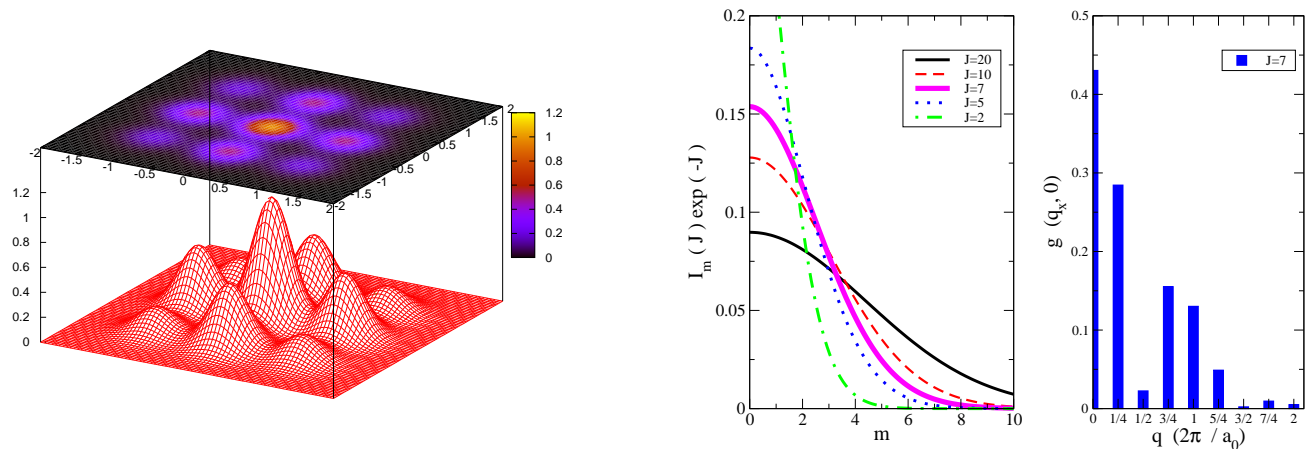


FIG. 14: Left panel: Function  $g(\mathbf{r})$  used to emulate the LDOS signal with parameters  $J = 7.0$ ,  $a = 1.0$ ,  $b = 0.5$  and  $c = 0.2$ . Center panel: Regular modified Bessel function  $I_m(J)$  shown as a function of its index  $m$  for several values of fixed  $J$ . Right panel: Fourier coefficients  $g(q_x, 0)$  for LDOS pattern shown in the left panel. The reader should compare this with the similar plot in Fig. 2 of Ref. 9.

bust properties of an elementary tile of size  $4a_0 \times 4a_0$  and nine peaks occupying *commensurate* locations at sites of the Cu lattice as depicted in our Figs. (7-9): the large magnitude of  $3/4$  peak is simply a higher harmonic describing the characteristic intra-tile structure.

## VII. CONCLUSIONS

Our main goal in this paper is to devise a more realistic description of a strongly quantum and thermally fluctuating  $d$ -wave superconductor, based on the theory of Ref. 5. Such description applies not only to long distance and low energy properties, which are the primary domain of<sup>5</sup>, but also to intermediate lengthscales, of order of several lattice spacings, and to energies up to the pseudogap scale  $\Delta$ . This enables us to use the theory to address the experimental observations of Refs. 8,9,10. The charge modulation observed in those experiments is attributed to the formation of the Cooper pair CDW, the dynamical origin of which is in strong quantum fluctuations of vortex-antivortex pairs. These quantum superconducting phase fluctuations reflect enhanced Mott-Hubbard correlations in underdoped cuprates as doping approaches zero. Quantum fluctuating  $hc/2e$  (anti)vortices “see” physical electron as a source of a half-quantum *dual* magnetic flux and the theory of the CPCDW can be formulated as the Abrikosov-Hofstadter problem in a type-II dual superconductor<sup>12</sup>. An XY-type model of such a dual superconductor appropriate for a lattice  $d$ -wave superconductor is constructed, both for thermal and quantum phase fluctuations. The specific translational symmetry breaking patterns that arise from the dual Abrikosov-Hofstadter problem are discussed for various dopings  $x$ , which determines the dual flux per unit cell of the  $\text{CuO}_2$  lattice via  $f = p/q = (1 - x)/2$ . In turn, the spatial modulation of the dual magnetic in-

duction  $\mathbf{B}_d$  corresponding to these Abrikosov-Hofstadter patterns is related to the modulation in the gap function of the lattice  $d$ -wave superconductor and is used to compute LDOS observed in STM experiments. A good agreement is found for  $x = 1/8$  ( $f = 7/16$ ), which is the dominant fraction of the Abrikosov-Hofstadter problem in the window of dopings where our theory applies.

## Acknowledgments

The authors thank J.C. Davis, M. Franz, J.E. Hoffman, S. Sachdev, A. Sudbø, O. Vafek, A. Yazdani and S.C. Zhang for useful discussions and correspondence and to S. Sachdev for generously sharing with us unpublished results of Ref. 17. A.M. also thanks P. Hirschfeld, B. Andersen, T. Nunner, and L.-Y. Zhu for numerous discussions. The final touches were applied to this paper while one of us (ZT) enjoyed hospitality of the Aspen Center for Physics. This work was supported in part by the NSF grant DMR00-94981.

## APPENDIX: TWO ALTERNATIVE DERIVATIONS OF DUAL ABRIKOSOV-HOFSTADTER HAMILTONIAN

In this Appendix we present two different and self-contained derivations of the dual Abrikosov-Hofstadter Hamiltonian (37,38), either one of which can serve as an alternative to the derivation given in the main text. The first approach is somewhat more detailed and in a sense more “microscopic” since it uses a quantum vortex-antivortex Hamiltonian as a springboard to derive the effective dual field theory (36). In turn, such vortex-antivortex Hamiltonian in principle can be derived from the (still unknown) fully microscopic theory of cuprates.

Incidentally, this derivation is the (2+1) dimensional analogue of the 3D case presented in the Appendix of Ref. 6. The second derivation follows the familiar Villain approximation to the XY model and applies it to our specific situation. The Villain approximation is less “realistic” but provides a transparent and systematic way of deriving dual representations of XY-like models.

In both derivations the starting point is the effective (2+1)D XY model of a quantum fluctuating  $d$ -wave superconductor:

$$L_{XY}^d = i \sum_i f_i \dot{\varphi}_i + \frac{K_0}{2} \sum_i \dot{\varphi}_i^2 - J \sum_{nn} \cos(\varphi_i - \varphi_j) - J_1 \sum_{rnnn} \cos(\varphi_i - \varphi_j) - J_2 \sum_{bnnn} \cos(\varphi_i - \varphi_j) + L_{\text{nodal}}[\cos(\varphi_i - \varphi_j)] + L_{\text{core}} \quad , \quad (\text{A.1})$$

where  $\varphi_i(\tau)$  is the fluctuating phase on a site of the blue lattice in Fig. 2, the first (imaginary) term is the charge Berry phase corresponding to the overall flux  $f$  through a plaquette the blue lattice,  $J$  is the nearest neighbor XY coupling,  $J_{1(2)}$  are the next nearest neighbor XY couplings along red (black) diagonals,  $L_{\text{nodal}}$  is the contribution of nodal fermions, and  $L_{\text{core}}$  denotes core contributions arising from small regions around vortices where the pairing pseudogap is significantly suppressed – this, for example, generally includes the mass term (25), the energy cost of core-core overlap, the Bardeen-Stephen core dissipation, etc. The reader should bear in mind that the last effect is small in cuprates, as explained in the main text, and will be neglected in the Appendix. Furthermore, we are neglecting vortex interactions with the spin of low energy nodal fermions, represented by the Berry gauge field  $a$ ; this is justified away from the critical point. The results below are easily adapted to the extended  $s$ -wave pairing symmetry. Similarly, both derivations are straightforwardly applied to a yet simpler case, a fluctuating  $s$ -wave superconductor:

$$L_{XY} = if \sum_i \dot{\phi}_i + \frac{K_0}{2} \sum_i \dot{\phi}_i^2 - J \sum_{nn} \cos(\phi_i - \phi_j) + L_{\text{core}} \quad , \quad (\text{A.2})$$

which was used in the main text as a pedagogical example.

Just as the starting points of two derivations coincide, their final product, the effective dual theory at long and intermediate lengthscales, will also turn out to be the same.

### 1. $\mathcal{H}_d$ from a “microscopic” vortex-antivortex Hamiltonian

The quantum partition function of a phase fluctuating superconductor is:

$$Z_{XY}^d = \int \mathcal{D}\varphi_i \exp\left(-\int_0^\beta d\tau L_{XY}^d[\varphi_i(\tau)]\right) \quad , \quad (\text{A.3})$$

where the functional integral  $\int \mathcal{D}\varphi_i(\tau)$  runs over phase variables  $\varphi_i(\tau)$  such that  $\exp(i\varphi_i(\tau))$  is periodic in the interval  $\tau \in [0, \beta]$ .

The difficulty in computing (A.3) is twofold: the fact that  $\varphi_i(\tau)$  is a *compact* phase variable, defined on an interval  $[0, 2\pi)$ , rather than an ordinary real field taking values in  $[-\infty, +\infty]$ , and the cosine functions in  $L_{XY}^d$  that couple phases on different sites in a non-linear fashion. To deal with the problem one approximates the cosines with quadratic forms. One popular approximation on a lattice is due to Villain and will be discussed in the next subsection. In continuum, the approximation amounts to replacing  $\cos(\varphi_i - \varphi_j) \rightarrow 1 - (a^2/2)(\nabla\varphi)^2 + \dots$ , where  $a$  is the lattice spacing and  $\varphi(x)$  is now a function in continuous (2+1) dimensional spacetime. Its compact character is enforced by writing  $\partial_\mu\varphi(x) \rightarrow \partial_\mu\chi(x) + (\partial_\mu\varphi(x))_v$ , where  $\chi$  is an ordinary real field and  $(\partial_\mu\varphi(x))_v$  is the part of the phase associated with vortices, defined via  $\nabla \times (\nabla\varphi(\mathbf{r}, \tau))_v = 2\pi \sum_\alpha \delta(\mathbf{r} - \mathbf{r}_\alpha^v(\tau)) - 2\pi \sum_\alpha \delta(\mathbf{r} - \mathbf{r}_\alpha^a(\tau))$ , with  $\{\mathbf{r}_\alpha^{v(a)}(\tau)\}$  being (anti)vortex positions. Simultaneously with this decomposition of  $\partial_\mu\varphi(x)$ ,  $\int \mathcal{D}\varphi_i$  is replaced by the functional integrations over  $\chi(x)$  and (anti)vortex positions  $\{\mathbf{r}_\alpha^{v(a)}(\tau)\}$ . We are assuming here that the (anti)vortices of topological charge  $\pm 1$  dominate the fluctuation behavior in the regime where the amplitude of the pseudogap  $\Delta$  is large and stiff, allowing us to safely neglect topological defects corresponding to vorticity  $\pm 2, \pm 3, \dots$  due to their higher core energies. This assumption simplifies the algebra considerably. Furthermore, this assumption is natural within the theory of Ref. 5: The proliferation of defects of high topological charge is equivalent to strong amplitude fluctuations and the eventual collapse of the pseudogap – as long as we are in the pseudogap regime the  $\pm 1$  (anti)vortices are the only relevant excitations. With these changes in place, the partition function (A.3) finally takes the form:

$$Z_{XY}^d \rightarrow \sum_{N_v=0}^{\infty} \sum_{N_a=0}^{\infty} \frac{1}{N_v! N_a!} \int \mathcal{D}\chi \prod_{\alpha, \gamma=1}^{N_v, N_a} \int_{\{\mathbf{r}_\alpha^v(0)\}=\{\mathbf{r}_\alpha^v(\beta)\}} \int_{\{\mathbf{r}_\gamma^a(0)\}=\{\mathbf{r}_\gamma^a(\beta)\}} \mathcal{D}\mathbf{r}_\alpha^v(\tau) \mathcal{D}\mathbf{r}_\gamma^a(\tau) \exp\left(-\int d^3x L_{XY}^d[\chi, \{\mathbf{r}_\alpha^{v(a)}(\tau)\}]\right) \quad , \quad (\text{A.4})$$

where  $\int d^3x = \int_0^\beta d\tau \int d^2r$  and the set  $\{\mathbf{r}_\alpha^{v(a)}(\tau)\}$  containing  $N_{v(a)}$  (anti)vortices at  $\tau = 0$  coincides with the one at  $\tau = \beta$ , to ensure proper periodicity of  $\exp(i\varphi(\mathbf{r}, \tau))$  in imaginary time. Lastly,

$$L_{XY}^d[\chi, \{\mathbf{r}_\alpha^{v(a)}(\tau)\}] = if(\mathbf{r})\dot{\varphi}_v + \frac{K_0}{2}(\dot{\chi} + \dot{\varphi}_v)^2 + \frac{\tilde{J}}{2}(\nabla\chi + \nabla\varphi_v)^2 + L_{\text{nodal}} + L_{\text{core}}^d[\{\mathbf{r}_\alpha^{v(a)}(\tau)\}] \quad , \quad (\text{A.5})$$

where  $f(\mathbf{r}) = \sum_i f_i \delta(\mathbf{r} - \mathbf{R}_i)$ ,  $\{\mathbf{R}_i\}$  are the sites of the blue lattice,  $\tilde{J} = J + J_1 + J_2$ ,  $K_0$  has been rescaled by

$a^2$ , and

$$\begin{aligned} \dot{\varphi}_v(\mathbf{r}, \tau) &= \sum_{\alpha} \frac{(\mathbf{r} - \mathbf{r}_{\alpha}^v(\tau)) \times \hat{z}}{|\mathbf{r} - \mathbf{r}_{\alpha}^v(\tau)|^2} \cdot \dot{\mathbf{r}}_{\alpha}^v - \\ &\sum_{\gamma} \frac{(\mathbf{r} - \mathbf{r}_{\gamma}^a(\tau)) \times \hat{z}}{|\mathbf{r} - \mathbf{r}_{\gamma}^a(\tau)|^2} \cdot \dot{\mathbf{r}}_{\gamma}^a = \int d^2 r' \frac{(\mathbf{r} - \mathbf{r}') \times \hat{z}}{|\mathbf{r} - \mathbf{r}'|^2} \cdot \mathbf{J}(\mathbf{r}, \tau), \\ \nabla \varphi_v(\mathbf{r}, \tau) &= - \sum_{\alpha} \frac{(\mathbf{r} - \mathbf{r}_{\alpha}^v(\tau)) \times \hat{z}}{|\mathbf{r} - \mathbf{r}_{\alpha}^v(\tau)|^2} \\ &+ \sum_{\gamma} \frac{(\mathbf{r} - \mathbf{r}_{\gamma}^a(\tau)) \times \hat{z}}{|\mathbf{r} - \mathbf{r}_{\gamma}^a(\tau)|^2} = - \int d^2 r' \frac{(\mathbf{r} - \mathbf{r}') \times \hat{z}}{|\mathbf{r} - \mathbf{r}'|^2} n(\mathbf{r}, \tau). \end{aligned} \quad (\text{A.6})$$

In (A.6) we found it useful to introduce vorticity density and current:  $n(\mathbf{r}, \tau) = \sum_{\alpha} \delta(\mathbf{r} - \mathbf{r}_{\alpha}^v(\tau)) - \sum_{\gamma} \delta(\mathbf{r} - \mathbf{r}_{\gamma}^a(\tau))$ ,  $\mathbf{J}(\mathbf{r}, \tau) = \sum_{\alpha} \dot{\mathbf{r}}_{\alpha}^v \delta(\mathbf{r} - \mathbf{r}_{\alpha}^v(\tau)) - \sum_{\gamma} \dot{\mathbf{r}}_{\gamma}^a \delta(\mathbf{r} - \mathbf{r}_{\gamma}^a(\tau))$ , in terms of which, when combined with vortex particle density and current  $\rho(\mathbf{r}, \tau) = \sum_{\alpha} \delta(\mathbf{r} - \mathbf{r}_{\alpha}^v(\tau)) + \sum_{\gamma} \delta(\mathbf{r} - \mathbf{r}_{\gamma}^a(\tau))$ ,  $\mathbf{j}(\mathbf{r}, \tau) = \sum_{\alpha} \dot{\mathbf{r}}_{\alpha}^v \delta(\mathbf{r} - \mathbf{r}_{\alpha}^v(\tau)) + \sum_{\gamma} \dot{\mathbf{r}}_{\gamma}^a \delta(\mathbf{r} - \mathbf{r}_{\gamma}^a(\tau))$ , we can write

$$\begin{aligned} L_{\text{core}}^d &= \frac{1}{2} \sum_{\alpha} M \left( \frac{d\mathbf{r}_{\alpha}^v}{d\tau} \right)^2 \delta(\mathbf{r} - \mathbf{r}_{\alpha}^v) + \\ &\frac{1}{2} \sum_{\gamma} M \left( \frac{d\mathbf{r}_{\gamma}^a}{d\tau} \right)^2 \delta(\mathbf{r} - \mathbf{r}_{\gamma}^a) + H_{\text{core}}^d, \end{aligned} \quad (\text{A.7})$$

where

$$\begin{aligned} H_{\text{core}}^d &= V(\mathbf{r})\rho(\mathbf{r}, \tau) + \frac{1}{2}\rho(\mathbf{r}, \tau) \int d^2 r' V^{(2)}(\mathbf{r}, \mathbf{r}')\rho(\mathbf{r}', \tau) \\ &+ \frac{1}{2}j_k(\mathbf{r}, \tau) \int d^2 r' V_{kl}^{(2)}(\mathbf{r}, \mathbf{r}')j_l(\mathbf{r}', \tau) \\ &+ \frac{1}{2}n(\mathbf{r}, \tau) \int d^2 r' \mathcal{V}^{(2)}(\mathbf{r}, \mathbf{r}')n(\mathbf{r}', \tau) \\ &+ \frac{1}{2}\mathbf{J}_k(\mathbf{r}, \tau) \int d^2 r' \mathcal{V}_{kl}^{(2)}(\mathbf{r}, \mathbf{r}')\mathbf{J}_l(\mathbf{r}', \tau) + (\dots). \end{aligned} \quad (\text{A.8})$$

(Anti)vortex mass terms appearing in (A.7) have been introduced already in Section IV (see the discussion surrounding Eq. (25)), while  $H_{\text{core}}^d$  represents a systematic expansion in vortex core density, including single core, two core terms and so on. All the short range terms that arise from expanding the cosine functions (A.1) in continuum limit have been absorbed into  $H_{\text{core}}^d$ , as was our habit throughout the text – in particular,  $V(\mathbf{r})$  is just the vortex potential on the blue lattice, containing crucial information on  $d$ -wave pairing, which is extensively discussed in Section III.

We can now integrate out  $\chi$ , the regular (XY “spin-wave”) part of the phase. The quadratic phase stiffness terms in (A.5) are decoupled as:

$$\begin{aligned} \frac{K_0}{2}(\dot{\chi} + \dot{\varphi}_v)^2 + \frac{\tilde{J}}{2}(\nabla\chi + \nabla\varphi_v)^2 &\rightarrow iW_0(\dot{\chi} + \dot{\varphi}_v) \\ &+ i\mathbf{W} \cdot (\nabla\chi + \nabla\varphi_v) + \frac{1}{2K_0}W_0^2 + \frac{1}{2\tilde{J}}\mathbf{W}^2 \end{aligned} \quad (\text{A.9})$$

via the Hubbard-Stratonovich vector field  $W = (W_0, \mathbf{W})$  (note that we have set the “dual speed of light”  $\sqrt{\tilde{J}/K_0}$  to unity). Integration by parts gives  $iW \cdot \partial\chi \rightarrow -i(\partial \cdot W)\chi$  and is followed by functional integration over  $\chi(x)$ , resulting in the local  $\delta$ -function constraint  $\delta(\partial \cdot W)$ . The constraint is solved by introducing a non-compact gauge field  $A_d$  such that  $W = \partial \times A_d$ , ensuring  $\partial \cdot W = \partial \cdot (\partial \times A_d) = 0$ . What remains of (A.9) is further transformed by another partial integration:

$$\begin{aligned} i(\partial \times A_d) \cdot (\partial\varphi)_v + \frac{1}{2K_0}(\partial \times A_d)_0^2 + \frac{1}{2\tilde{J}}(\partial \times A_d)_{\perp}^2 \\ \rightarrow -iA_d \cdot \partial \times (\partial\varphi)_v + \frac{1}{2K_0}(\partial \times A_d)_0^2 + \frac{1}{2\tilde{J}}(\partial \times A_d)_{\perp}^2, \end{aligned} \quad (\text{A.10})$$

where  $(\partial \times A_d)_{0,\perp}$  denotes temporal and spatial components of  $\partial \times A_d$ , respectively. Now observe that (A.6) implies  $\partial \times (\partial\varphi)_v = (2\pi n, 2\pi\mathbf{J})$ . This allows us to finally write the partition function of the quantum vortex-antivortex system as:

$$\begin{aligned} Z_v^d &= \sum_{N_v=0}^{\infty} \sum_{N_a=0}^{\infty} \frac{1}{N_v!N_a!} \prod_{\alpha, \gamma=1}^{N_v, N_a} \int_{\{\mathbf{r}_{\alpha}^v(0)\}=\{\mathbf{r}_{\alpha}^v(\beta)\}} \mathcal{D}\mathbf{r}_{\alpha}^v(\tau) \\ &\times \int_{\{\mathbf{r}_{\gamma}^a(0)\}=\{\mathbf{r}_{\gamma}^a(\beta)\}} \mathcal{D}\mathbf{r}_{\gamma}^a(\tau) \exp\left(-\int d^3x L_v^d\right), \end{aligned} \quad (\text{A.11})$$

where  $L_v^d$  equals

$$\begin{aligned} \frac{1}{2} \sum_{\alpha} M \left( \frac{d\mathbf{r}_{\alpha}^v}{d\tau} \right)^2 \delta(\mathbf{r} - \mathbf{r}_{\alpha}^v) + \frac{1}{2} \sum_{\gamma} M \left( \frac{d\mathbf{r}_{\gamma}^a}{d\tau} \right)^2 \delta(\mathbf{r} - \mathbf{r}_{\gamma}^a) \\ + L_{\text{nodal}} + H_{\text{core}}^d - 2\pi i A_{d0} n - i2\pi(\mathbf{A}_d^{(0)} + \mathbf{A}_d) \cdot \mathbf{J} \\ + \frac{1}{2K_0}(\partial \times A_d)_0^2 + \frac{1}{2\tilde{J}}(\partial \times A_d)_{\perp}^2, \end{aligned} \quad (\text{A.12})$$

and  $\nabla \times \mathbf{A}_d^{(0)} = \mathbf{B}_d^{(0)} = f(\mathbf{r})\hat{z}$ .

Eqs. (A.11, A.12) are an important result of this Appendix. We recognize  $Z_v^d$  as equivalent to a partition function of two species of non-relativistic quantum bosons expressed in the Feynman path integral representation over particle worldline trajectories. These vortex and antivortex bosons have identical mass  $M$  and carry dual charges  $+2\pi$  and  $-2\pi$ , respectively, through which they couple to a dynamical gauge field  $A_d$ . The dual photons of  $A_d$  mediate long range “electrodynamic” interactions between the bosons, which are just the familiar Biot-Savart interactions between (anti)vortices. In addition, the particles interact through an assortment of short range interactions contained in  $H_{\text{core}}^d$  (A.8). Furthermore,  $L_{\text{nodal}}$  describes the interactions generated by nodal Dirac-like fermions which will be included explicitly once we arrive at the dual representation of (A.12), as detailed in Section IV. Finally, the vortex potential  $V(\mathbf{r})$  contains important information about the underlying lattice structure and the symmetry of the order parameter, as emphasized throughout the text.

We have derived  $Z_v^d$  as a continuum limit approximation to the partition function  $Z_{XY}^d$  (A.3) of the quantum XY-type model (A.1). Actually, in real cuprates and in all other physical systems, the opposite is true: It is the quantum XY-type representation that is an approximation to  $Z_v^d$ .  $Z_v^d$  captures the general description of the quantum vortex-antivortex system, applicable to all superconductors and superfluids whose order parameter is a complex scalar. To appreciate this, imagine that for each given configuration of the phase, with (anti)vortex positions fixed in Euclidean spacetime, the microscopic action of a physical system is minimized with respect to the amplitude, after all other degrees of freedom have been integrated out. The subsequent summation over all distinct (anti)vortex positions leads to precisely  $Z_v^d$  as the final result (again, we remind the reader that the core dissipative terms will also generically appear in  $Z_v^d$  but, being small in underdoped cuprates, are neglected here as explained in the main text). In practice, this procedure is difficult to carry out explicitly and the actual values of various terms that enter  $Z_v^d$  are hard to determine from “first principles”. This is particularly true for core-core interaction terms appearing in  $H_{\text{core}}^d$ . For our purposes it will suffice to approximate  $V^{(2)}(\mathbf{r}, \mathbf{r}') \rightarrow g\delta(\mathbf{r} - \mathbf{r}')$ , where  $g > 0$ , and drop the rest.

There is one crucial feature which distinguishes  $Z_v^d$  from the standard Feynman partition function: The vortex and antivortex quantum bosons are *not conserved*. As particles make their way through imaginary time, vortices and antivortices can *annihilate* each other; similarly, they can also be *created* at an instant in time; this is depicted in Fig. 3. All such processes of creation and annihilation proceed in *pairs* of vortices and antivortices. Consequently, while the individual number of vortices and antivortices is not conserved, the *vorticity*, measured by dual charge  $e_d = \pm 2\pi$ , is *conserved* and the gauge symmetry associated with  $A_d$  is always maintained (unless, of course, it is spontaneously broken by a dual Higgs mechanism in dual superfluid). In other words, these nonrelativistic (anti)vortex bosons propagate through spacetime permeated by a vortex-antivortex condensate, of strength  $\Delta_v$ .

Feynman path integrals are beautiful but difficult to calculate with. Following the standard mapping<sup>47</sup> we can express  $Z_v^d$  as a functional integral over complex fields  $\Psi_v(\mathbf{r}, \tau)$  and  $\Psi_a(\mathbf{r}, \tau)$ , which are the eigenvalues of vortex and antivortex annihilation operators, respectively, in the

basis of coherent states:

$$\begin{aligned} Z_v^d \rightarrow & \int \mathcal{D}\Psi_v \mathcal{D}\Psi_a \int \mathcal{D}A_d \exp \left[ - \int d^3x (\Psi_v^* (\partial_\tau + ie_d A_{d0}) \Psi_v \right. \\ & + \Psi_a^* (\partial_\tau - ie_d A_{d0}) \Psi_a + \\ & + \frac{1}{2M} |(\nabla + ie_d \mathbf{A}_d^{(0)} + ie_d \mathbf{A}_d) \Psi_v|^2 \\ & + \frac{1}{2M} |(\nabla - ie_d \mathbf{A}_d^{(0)} - ie_d \mathbf{A}_d) \Psi_a|^2 - \mu_v (|\Psi_v|^2 + |\Psi_a|^2) \\ & + V(\mathbf{r}) (|\Psi_v|^2 + |\Psi_a|^2) + \Delta_v \Psi_v^* \Psi_a^* + \Delta_v^* \Psi_a \Psi_v \\ & \left. + \frac{g}{2} (|\Psi_v|^2 + |\Psi_a|^2)^2 + L_{\text{nodal}} + \frac{1}{2K_\mu} (\partial \times A_d)_\mu^2 \right] \quad , \quad (\text{A.13}) \end{aligned}$$

where the meaning of various terms is straightforward in light of our earlier discussion; we have consolidated the notation so that  $e_d = 2\pi$ ,  $K_\mu = (K_0, \vec{J}, \vec{J})$ , the chemical potential for vortices is  $\mu_v = \mu_a$ , and  $g$  describes the short range core-core repulsions. The “vortex-antivortex pairing” function  $\Delta_v$  is crucial since it regulates the frequency of vortex-antivortex pair creation and annihilation processes.

The form of  $Z_v^d$  can be further simplified by exploiting the vorticity conservation law. We observe that the action in (A.13) is invariant under gauge transformations:  $\Psi_v \rightarrow \exp(i\zeta) \Psi_v$ ,  $\Psi_a \rightarrow \exp(-i\zeta) \Psi_a$ ,  $A_d \rightarrow A_d - (\partial\zeta)/e_d$ . This prompts us to introduce bosonic “spinors”  $\bar{\Psi} = (\Psi_v^*, \Psi_a)$  which carry a conserved dual charge  $e_d$  and couple minimally to  $A_d$ :

$$\begin{aligned} Z_v^d \rightarrow & \int \mathcal{D}\bar{\Psi} \mathcal{D}A_d \mathcal{D}\sigma \exp \left[ - \int d^3x (\bar{\Psi} \mathcal{L} \Psi \right. \\ & \left. + L_{\text{nodal}} + \frac{1}{2g} \sigma^2 + \frac{1}{2K_\mu} (\partial \times A_d)_\mu^2 \right] \quad , \quad (\text{A.14}) \end{aligned}$$

where

$$\begin{aligned} \mathcal{L} = & \begin{bmatrix} (\partial_\tau + ie_d A_{d0}) & \Delta_v \\ \Delta_v^* & -(\partial_\tau + ie_d A_{d0}) \end{bmatrix} \\ & + \left( -\frac{1}{2M} (\nabla + ie_d \mathbf{A}_d^{(0)} + ie_d \mathbf{A}_d)^2 - \mu_v + V(\mathbf{r}) + i\sigma \right) \mathbf{1} \quad , \quad (\text{A.15}) \end{aligned}$$

and a Hubbard-Stratonovich scalar field  $\sigma$  was deployed to decouple short range repulsion. Now we set  $A_d \rightarrow 0$  and ignore  $L_{\text{nodal}}$ —they will be easily restored later—and note that the integration over vortex matter fields  $\Psi$  gives:

$$\begin{aligned} Z_v^d \rightarrow & \int \mathcal{D}\sigma \exp \left( - \int d^3x \frac{1}{2g} \sigma^2 \right) \times \\ \det & \begin{bmatrix} \partial_\tau - \frac{1}{2M} \nabla^2 - \mu_v + V(\mathbf{r}) + i\sigma & \Delta_v \\ \Delta_v^* & -\partial_\tau - \frac{1}{2M} \nabla^2 - \mu_v + V(\mathbf{r}) + i\sigma \end{bmatrix} \quad (\text{A.16}) \end{aligned}$$

The above partition function has a transition at  $\mu_v = -|\Delta_v|$  (we are assuming that the minimum of  $V(\mathbf{r})$  occurs at zero, with  $E_c^r$ , or  $E_c^b$  as the case may be, having



been absorbed into  $\mu_v$ ). For  $\mu_v < -|\Delta_v|$  the system of (anti)vortex bosons is in its “normal” state, with  $\langle \Psi \rangle = 0$ . For  $\mu_v > -|\Delta_v|$  (anti)vortex bosons condense and  $\langle \Psi \rangle$  becomes finite. This is nothing but the dual description of the superconducting transition discussed in the main text. In the general vicinity of the transition it is useful to introduce  $m^2 = \mu_v^2 - |\Delta_v|^2$ , where now  $m^2 > 0$  and  $m^2 < 0$  indicate dual normal and superfluid states, respectively. Focusing on distances longer than  $\sqrt{\Delta_v M}$  and energies lower than  $\Delta_v$ , the determinant in (A.16) can be further reduced to:

$$\det \left[ -\partial_\tau^2 - \frac{|\Delta_v| + V(\mathbf{r}) + i\sigma}{2M} \nabla^2 + m^2 - \frac{1}{M} [(\nabla^2 V) + i(\nabla^2 \sigma)] + 2|\Delta_v|(V(\mathbf{r}) + i\sigma) + (V(\mathbf{r}) + i\sigma)^2 \right] + (\dots) , \quad (\text{A.17})$$

with additional terms  $(\dots)$  contributing unimportant derivatives.

By setting  $V(\mathbf{r})$  and  $\sigma(x)$  to zero, we observe that the above expression assumes the form of the partition function determinant for a system of *relativistic* quantum bosons of mass  $m$ :  $\det \left[ -\partial_\tau^2 - c^2 \nabla^2 + m^2 c^4 \right]$ , with the speed of “light”  $c = \sqrt{|\Delta_v|/2M}$  set to unity henceforth. The terms involving  $V(\mathbf{r})$  and  $\sigma(x)$  describe the underlying potential and various short range interactions of these relativistic bosons. We therefore can reexpress the determinant (A.17) as a functional integral over the relativistic boson field  $\Phi(x)$ ; this is a faithful representation of the original (anti)vortex partition function at distances longer than  $\sqrt{\Delta_v M}$  and energies lower than  $\Delta_v$ :

$$\begin{aligned} \mathcal{Z}_v^d \rightarrow \mathcal{Z}_d = \int \mathcal{D}\Phi \int \mathcal{D}A_d \int \mathcal{D}\sigma \\ \exp \left[ - \int d^3x \left( |\partial + i2\pi A_d \Phi|^2 + m^2(\mathbf{r})|\Phi|^2 \right. \right. \\ \left. \left. + 2|\Phi|^2 \left[ |\Delta_v| + V(\mathbf{r}) - \frac{\nabla^2}{2M} \right] (i\sigma) + \frac{|\mathbf{D}\Phi|^2}{M} (i\sigma) \right. \right. \\ \left. \left. + \left[ \frac{1}{2g} - |\Phi|^2 \right] \sigma^2 + \mathcal{L}_{\text{nodal}} + \frac{1}{2K_\mu} (\partial \times A_d)_\mu^2 \right] \right], \quad (\text{A.18}) \end{aligned}$$

where  $m^2(\mathbf{r}) = m^2 + 2|\Delta_v|V(\mathbf{r}) + V(\mathbf{r})^2 - (\nabla^2 V(\mathbf{r})/M)$  and we have restored  $\mathcal{L}_{\text{nodal}}$  and dual gauge field  $A_d$ , through covariant derivatives  $\partial \rightarrow D = (D_0, \mathbf{D}) = (\partial_0 + i2e_d A_{d0}, \nabla + ie_d \mathbf{A}_d^{(0)} + ie_d \mathbf{A}_d)$ . The minimal coupling of  $A_d$  is mandated by dual charge conservation:  $\Phi \rightarrow \exp(i\zeta)\Phi$ ,  $A_d \rightarrow A_d - (\partial\zeta)/e_d$ .

The dual partition function  $\mathcal{Z}_d$  (A.18) is the final result of this subsection. It describes the system of relativistic quantum bosons of mass  $m$  and charge  $e_d = 2\pi$  in a magnetic field  $\mathbf{B}_d = \nabla \times \mathbf{A}_d^{(0)}$ . The virtual particle-antiparticle creation and annihilation processes in the vacuum of this theory are nothing but quantum vortex-antivortex pair excitations evolving in imaginary time (see Fig. 3). In the “normal” vacuum,  $m^2 > 0$ , the average size of such pairs is  $\sim m^{-1}$ . This is just the superconducting ground state of physical underdoped cuprates. For  $m^2 < 0$ , this “normal” vacuum is unstable to a Higgs phase, with a finite dual condensate  $\langle \Phi \rangle$ . The vortex-antivortex pairs unbind as infinite loops of virtual particle-antiparticle excitations of  $\Phi$  permeate this dual

Higgs vacuum – this is the pseudogap state of cuprates. The integration over the Hubbard-Stratonovich field  $\sigma$  produces a short range repulsion  $\frac{1}{2}(4|\Delta_v|^2)g|\Phi|^4$  followed by an assortment of other short range interactions including  $V(\mathbf{r})$ , powers of  $|\Phi|$  higher than quartic and various derivatives. All these additional interactions are irrelevant in the sense of long distance behavior but might play some quantitative role at intermediate lengthscales. For simplicity, we shall mostly ignore them in this paper. Finally, with the change of notation  $4|\Delta_v|^2 g \rightarrow g$  and  $\mathcal{L}_{\text{nodal}}$  incorporated into the self-action for  $A_d$  as detailed in Section IV, the dual Lagrangian in (A.18) reduces to  $\mathcal{L}_d$  (36). The arguments in the text can then be followed to arrive at  $\mathcal{H}_d$  (37,38).

## 2. $\mathcal{H}_d$ in the Villain approximation

A useful approximation to the ordinary XY model is due to Villain. In this approximation the exponential of the cosine function is replaced by an infinite sum of the exponentials of parabolas. We will illustrate this approximation first for the 2D case and follow up with the (2+1)D quantum XY-like model.

### a. Classical (thermal) phase fluctuations

Here we apply the Villain approximation to our classical XY model of a phase fluctuating two-dimensional  $d$ -wave superconductor (14). As we will see presently, the final Coulomb gas representation coincides with (23) – however, the advantage of the Villain approximation is that it will allow us to obtain explicit expressions for the core energies  $E_c^{r(b)}$  in terms of the coupling constants of the original Hamiltonian (14).

Denoting the sites of the blue lattice by  $\boldsymbol{\rho} = (x, y)$ , the partition function of the model can be written as

$$\begin{aligned} Z = \int \left( \prod_{\boldsymbol{\rho}} d\phi_{\boldsymbol{\rho}} \right) \exp \sum_{\boldsymbol{\rho}} \left[ J (\cos(\nabla_{\hat{x}} \phi_{\boldsymbol{\rho}}) + \cos(\nabla_{\hat{y}} \phi_{\boldsymbol{\rho}})) \right. \\ \left. + J_{12}(\boldsymbol{\rho}) (\cos(\phi_{\boldsymbol{\rho}+\hat{x}+\hat{y}} - \phi_{\boldsymbol{\rho}}) + \cos(\phi_{\boldsymbol{\rho}+\hat{y}} - \phi_{\boldsymbol{\rho}+\hat{x}})) \right] \quad (\text{A.19}) \end{aligned}$$

where the lattice operator  $\nabla$  is defined according to  $\nabla_{\delta} f(\mathbf{r}) = f_{\mathbf{r}+\delta} - f_{\mathbf{r}}$ , and coefficients  $J_{12}(\boldsymbol{\rho})$  denote  $J_1$  (or  $J_2$ ) if  $\boldsymbol{\rho}$  is in the lower left corner of a red (or black) plaquette.

In Villain approximation the exponent of a cosine is replaced by a sum of Gaussian exponents that has the same periodicity  $2\pi$ :

$$\exp[\beta \cos \gamma] \approx R_V(\beta) \sum_{n=-\infty}^{+\infty} \exp \left[ -\frac{\beta_V(\beta)}{2} (\gamma - 2\pi n)^2 \right] . \quad (\text{A.20})$$

The fitting functions  $\beta_V(\beta)$  and  $R_V(\beta)$  are determined by the requirement that the lowest Fourier coefficients of the two functions coincide. In particular, the function  $\beta_V(\beta)$  has the following asymptotic behavior for low and high temperatures:

$$\beta_V(\beta) \approx \begin{cases} \beta & \text{for } \beta \gg 1 \\ \left(2 \ln \frac{\beta}{2}\right)^{-1} & \text{for } \beta \ll 1 \end{cases} \quad (\text{A.21})$$

The sum over  $n$  in (A.20) can be transformed by decoupling the quadratic term in the exponent via the Hubbard-Stratonovich transformation:

$$\exp[\beta \cos \gamma] \propto \sum_{n=-\infty}^{\infty} \exp\left[-\frac{1}{2\beta_V(\beta)} n^2 + i\gamma n\right] . \quad (\text{A.22})$$

By introducing integer fields  $u_x(\boldsymbol{\rho})$ ,  $u_y(\boldsymbol{\rho})$  and  $w_{\pm}(\boldsymbol{\rho})$  to apply (A.22) to the cosine terms in (A.19) we obtain:

$$Z = \sum_{u_{\alpha}} \sum_{w_{\pm}} \int \prod_{\boldsymbol{\rho}} d\phi_{\boldsymbol{\rho}} e^{-\sum_{\boldsymbol{\rho}} \left[ \frac{u_{\alpha}^2(\boldsymbol{\rho})}{2J'} + \frac{w_{\pm}^2(\boldsymbol{\rho}) + w_{\mp}^2(\boldsymbol{\rho})}{2J'_{12}(\boldsymbol{\rho})} \right]} \times e^{i \sum_{\boldsymbol{\rho}} [u_{\alpha}(\boldsymbol{\rho}) \nabla_{\alpha} \phi_{\boldsymbol{\rho}} + w_{+}(\boldsymbol{\rho}) (\phi_{\boldsymbol{\rho}+\hat{x}+\hat{y}} - \phi_{\boldsymbol{\rho}}) + w_{-}(\boldsymbol{\rho}) (\phi_{\boldsymbol{\rho}+\hat{y}} - \phi_{\boldsymbol{\rho}+\hat{x}})]} , \quad (\text{A.23})$$

where  $\alpha = x, y$ , and coefficients  $J_{12}(\boldsymbol{\rho})$  and  $J'$  are defined as

$$J' = \beta_V(J) \quad (\text{A.24})$$

$$J_{12}(\boldsymbol{\rho}) = \beta_V(J_{12}(\boldsymbol{\rho})) . \quad (\text{A.25})$$

The integration over the angles  $\phi_{\boldsymbol{\rho}}$  can be performed after applying the discrete analog of the integration by parts to the sums in the last exponent in (A.23):

$$\begin{aligned} \sum_x f(\boldsymbol{\rho}) \nabla_x g(\boldsymbol{\rho}) &= \sum_x f(\boldsymbol{\rho}) (g(\boldsymbol{\rho} + \hat{x}) - g(\boldsymbol{\rho})) \\ &= \sum_x (f(\boldsymbol{\rho} - \hat{x}) - f(\boldsymbol{\rho})) g(\boldsymbol{\rho}) = - \sum_x \bar{\nabla} f(\boldsymbol{\rho}) g(\boldsymbol{\rho}) . \end{aligned} \quad (\text{A.26})$$

Note that we distinguish between the ‘‘right difference’’ operator  $\nabla$  and ‘‘left difference’’ operator  $\bar{\nabla}$ . Integration over the phases  $\phi_{\boldsymbol{\rho}}$  yields the following expression for the partition function:

$$\sum_{u_x, u_y, w_{\pm}} e^{-\sum_{\boldsymbol{\rho}} \left[ \frac{u_x^2(\boldsymbol{\rho}) + u_y^2(\boldsymbol{\rho})}{2J'} + \frac{w_{\pm}^2(\boldsymbol{\rho}) + w_{\mp}^2(\boldsymbol{\rho})}{2J'_{12}(\boldsymbol{\rho})} \right]} \delta(\bar{\nabla} \cdot \mathbf{v}(\boldsymbol{\rho}) + \dots) . \quad (\text{A.27})$$

where  $\bar{\nabla} \cdot \mathbf{v}(\boldsymbol{\rho})$  denotes two-dimensional lattice divergence of  $\mathbf{v}(\boldsymbol{\rho})$  and dots denote

$$(w_{+}(\boldsymbol{\rho}) - w_{+}(\boldsymbol{\rho} - \hat{x} - \hat{y})) + (w_{-}(\boldsymbol{\rho} - \hat{x}) - w_{-}(\boldsymbol{\rho} - \hat{y})) .$$

We rewrite the constraint appearing as the Kronecker delta function in the sum as

$$\bar{\nabla} \cdot (\mathbf{v} + \mathbf{w}[w_{+}, w_{-}]) = 0 ,$$

where  $\mathbf{w} = (w_x, w_y)$  denote the following linear combinations of integer fields  $w_{\pm}(\boldsymbol{\rho})$ :

$$w_x = \frac{w_{+}(\boldsymbol{\rho}) + w_{+}(\boldsymbol{\rho} - \hat{y})}{2} - \frac{w_{-}(\boldsymbol{\rho}) + w_{-}(\boldsymbol{\rho} - \hat{y})}{2} \quad (\text{A.28})$$

$$w_y = \frac{w_{+}(\boldsymbol{\rho}) + w_{+}(\boldsymbol{\rho} - \hat{x})}{2} + \frac{w_{-}(\boldsymbol{\rho}) + w_{-}(\boldsymbol{\rho} - \hat{x})}{2} . \quad (\text{A.29})$$

The constraint can then be resolved as

$$\mathbf{v} = \mathbf{b} - \mathbf{w}[w_{+}, w_{-}] ,$$

where

$$\mathbf{b} = (\bar{\nabla}_y \Lambda, -\bar{\nabla}_x \Lambda) \quad (\text{A.30})$$

and  $\Lambda(\boldsymbol{\rho})$  has the meaning of the time-like component of a vector potential. At this point it is useful to pause and establish a simple geometrical interpretation of the various fields we have introduced. Variables  $u_x(\boldsymbol{\rho})$  and  $u_y(\boldsymbol{\rho})$  are coupled to the phase differences  $\phi_{\boldsymbol{\rho}+\hat{x}} - \phi_{\boldsymbol{\rho}}$  and  $\phi_{\boldsymbol{\rho}+\hat{y}} - \phi_{\boldsymbol{\rho}}$  and therefore they reside on the links emanating from  $\boldsymbol{\rho}$  in positive  $x$  and  $y$  directions respectively. Integers  $\Lambda(\boldsymbol{\rho})$ , on the other hand are related to link variable  $u_x(\boldsymbol{\rho})$  through the difference  $\Lambda(\boldsymbol{\rho}) - \Lambda(\boldsymbol{\rho} - \hat{y})$ . Consequently we must associate  $\Lambda(\boldsymbol{\rho})$  with the centers of the blue plaquettes, which coincide with either red or black sites. Nevertheless, we will continue to use notation  $\Lambda(\boldsymbol{\rho})$  tacitly implying that  $\boldsymbol{\rho}$  refers to the lower left corner of the (red or black) plaquette associated with  $\Lambda$ . Having resolved the constraint, we find that the partition function  $Z$  can be written in terms of integer-valued fields  $w_{\pm}(\boldsymbol{\rho})$  and  $\Lambda(\boldsymbol{\rho})$  only:

$$\sum_{\Lambda, w_{\pm}} \exp \sum_{\boldsymbol{\rho}} \left[ -\frac{(\mathbf{b}[\Lambda] - \mathbf{w}[w_{\pm}])_{\perp}^2}{2J'} - \frac{w_{+}^2(\boldsymbol{\rho}) + w_{-}^2(\boldsymbol{\rho})}{2J'_{12}(\boldsymbol{\rho})} \right] . \quad (\text{A.31})$$

To obtain the description in terms of continuous rather than integer-valued fields  $\Lambda(\boldsymbol{\rho})$ , we use the Poisson summation formula:

$$\sum_{\Lambda=-\infty}^{\infty} f(\Lambda) = \int_{-\infty}^{\infty} d\Lambda \sum_{l=-\infty}^{\infty} e^{2\pi i l \Lambda} f(\Lambda) . \quad (\text{A.32})$$

The partition function  $Z$  assumes the following form:

$$\int_{-\infty}^{\infty} \prod_{\boldsymbol{\rho}} d\Lambda(\boldsymbol{\rho}) \sum_{\mathbf{l}(\boldsymbol{\rho})} \exp \sum_{\boldsymbol{\rho}} 2\pi i \mathbf{l}(\boldsymbol{\rho}) \Lambda(\boldsymbol{\rho}) \} \exp\{F[\mathbf{b}[\Lambda(\boldsymbol{\rho})]]\} , \quad (\text{A.33})$$

where we have defined a functional  $\exp\{F[\mathbf{b}(\boldsymbol{\rho})]\}$  according to

$$\sum_{w_{\pm}} \exp \left[ \sum_{\boldsymbol{\rho}} \left( -\frac{(\mathbf{b} - \mathbf{w}[w_{\pm}])_{\perp}^2}{2J'} - \frac{w_{+}^2(\boldsymbol{\rho}) + w_{-}^2(\boldsymbol{\rho})}{2J'_{12}(\boldsymbol{\rho})} \right) \right] . \quad (\text{A.34})$$

In the limit when constants  $J_1$  and  $J_2$  are infinitesimally small, only the configurations  $w_{\pm}(\boldsymbol{\rho}) = 0$  contribute to the  $F[\mathbf{b}]$ . This limit, which corresponds to the usual 2D XY model, is described by partition function  $Z_0$  given by

$$\int_{-\infty}^{\infty} \prod_{\boldsymbol{\rho}} d\Lambda(\boldsymbol{\rho}) \sum_{l(\boldsymbol{\rho})} \exp \left[ \sum_{\boldsymbol{\rho}} \left( 2\pi i l(\boldsymbol{\rho}) \Lambda(\boldsymbol{\rho}) - \frac{(\bar{\nabla}_{\alpha} \Lambda)^2}{2J'} \right) \right]. \quad (\text{A.35})$$

For finite  $J_{12}$  we must resort to approximate evaluation of the functional  $F(b(\boldsymbol{\rho}))$ :

$$\exp\{F[b_x(\boldsymbol{\rho}), b_y(\boldsymbol{\rho})]\} = \sum_{w_{\pm}} \exp \left[ - \sum_{\boldsymbol{\rho}} \left( \frac{(b_{\alpha} - w_{\alpha})^2}{2J'} + \frac{w_{+}^2(\boldsymbol{\rho}) + w_{-}^2(\boldsymbol{\rho})}{2J'_{12}(\boldsymbol{\rho})} \right) \right]. \quad (\text{A.36})$$

The quadratic terms containing  $\mathbf{b}$  can be decoupled using the Hubbard-Stratonovich transformation:

$$e^{F[\mathbf{b}(\boldsymbol{\rho})]} = \int \prod_{\boldsymbol{\rho}} dZ_x(\boldsymbol{\rho}) dZ_y(\boldsymbol{\rho}) \times \sum_{w_{\pm}} \exp \left[ \sum_{\boldsymbol{\rho}} \left( - \frac{J' Z_{\alpha}^2(\boldsymbol{\rho})}{2} + iZ_{\alpha}(\boldsymbol{\rho}) (b_{\alpha}(\boldsymbol{\rho}) - w_{\alpha}(\boldsymbol{\rho})) - \frac{w_{+}^2(\boldsymbol{\rho}) + w_{-}^2(\boldsymbol{\rho})}{2J'_{12}(\boldsymbol{\rho})} \right) \right], \quad (\text{A.37})$$

where  $\alpha = x, y$ . Using explicit expressions for  $w_{\alpha}$  we obtain

$$e^{F[\mathbf{b}]} = \int \prod_{\boldsymbol{\rho}} dZ_x(\boldsymbol{\rho}) dZ_y(\boldsymbol{\rho}) \times \sum_{w_{\pm}} \exp \left[ \sum_{\boldsymbol{\rho}} \left( - \frac{J' Z_{\alpha}^2(\boldsymbol{\rho})}{2} - \frac{w_{+}^2(\boldsymbol{\rho}) + w_{-}^2(\boldsymbol{\rho})}{2J'_{12}(\boldsymbol{\rho})} + iZ_{\alpha}(\boldsymbol{\rho}) b_{\alpha}(\boldsymbol{\rho}) - \frac{i}{2} w_{+}(\boldsymbol{\rho}) (Z_x(\boldsymbol{\rho}) + Z_x(\boldsymbol{\rho} + \hat{y}) + Z_y(\boldsymbol{\rho}) + Z_y(\boldsymbol{\rho} + \hat{x})) - \frac{i}{2} w_{-}(\boldsymbol{\rho}) (-Z_x(\boldsymbol{\rho}) - Z_x(\boldsymbol{\rho} + \hat{y}) + Z_y(\boldsymbol{\rho}) + Z_y(\boldsymbol{\rho} + \hat{x})) \right) \right]. \quad (\text{A.38})$$

The sums over  $w_{\pm}(\boldsymbol{\rho})$  can be performed by employing the Villain approximation (A.20) backward. Note that the coupling constants  $J'_{\pm}$  are restored to the original

values of coupling constants  $J_{\pm}$ :

$$e^{F[\mathbf{b}(\boldsymbol{\rho})]} = \int \prod_{\boldsymbol{\rho}} dZ_x(\boldsymbol{\rho}) dZ_y(\boldsymbol{\rho}) \times \exp \left[ \sum_{\boldsymbol{\rho}} \left( - \frac{J' Z_{\alpha}^2(\boldsymbol{\rho})}{2} + iZ_{\alpha}(\boldsymbol{\rho}) b_{\alpha}(\boldsymbol{\rho}) + J_{12}(\boldsymbol{\rho}) \left( \cos \frac{Z_x(\boldsymbol{\rho}) + Z_x(\boldsymbol{\rho} + \hat{y}) + Z_y(\boldsymbol{\rho}) + Z_y(\boldsymbol{\rho} + \hat{x})}{2} + \cos \frac{-Z_x(\boldsymbol{\rho}) - Z_x(\boldsymbol{\rho} + \hat{y}) + Z_y(\boldsymbol{\rho}) + Z_y(\boldsymbol{\rho} + \hat{x})}{2} \right) \right) \right]. \quad (\text{A.39})$$

To quadratic order, the expression in the exponent is

$$\sum_{\boldsymbol{\rho}} \left[ - \frac{J' Z_{\alpha}^2(\boldsymbol{\rho})}{2} + iZ_{\alpha}(\boldsymbol{\rho}) b_{\alpha}(\boldsymbol{\rho}) - J_{12}(\boldsymbol{\rho}) \times \frac{(Z_x(\boldsymbol{\rho}) + Z_x(\boldsymbol{\rho} + \hat{y}))^2 + (Z_y(\boldsymbol{\rho}) + Z_y(\boldsymbol{\rho} + \hat{x}))^2}{4} \right]. \quad (\text{A.40})$$

Note that  $Z_x$  and  $Z_y$  components are completely decoupled at the quadratic level. To proceed, one can double the unit cell, in which case the expression in the exponent becomes diagonal in the momentum space. Alternatively, one can use an equivalent, but technically simpler procedure of keeping the original unit cell. In this latter case, the momentum space problem reduces to the diagonalization of a  $2 \times 2$  matrix connecting modes at wavevectors  $\mathbf{q}$  and  $\mathbf{q} - \mathbf{g}$ , where  $\mathbf{g} = \pi(\hat{x} + \hat{y})$ .

It is convenient to represent  $J_{12}(\boldsymbol{\rho})$  as

$$J_{12}(\boldsymbol{\rho}) = \frac{J_1 + J_2}{2} + e^{i\mathbf{g}\boldsymbol{\rho}} \frac{J_1 - J_2}{2} \equiv \bar{J} + \delta J e^{i\mathbf{g}\boldsymbol{\rho}}.$$

After Fourier transformation, the exponent in (A.40) becomes

$$iZ_x(\mathbf{q}) b_x(-\mathbf{q}) - Z_x(\mathbf{q}) Z_x(-\mathbf{q}) \frac{J' + \bar{J}(1 + \cos q_y)}{2} - \frac{i\delta J}{2} \sin q_y Z_x(\mathbf{g} - \mathbf{q}) Z_x(\mathbf{q}) + (x \leftrightarrow y). \quad (\text{A.41})$$

Since  $Z_{\alpha}(\boldsymbol{\rho})$  and  $b_{\alpha}(\boldsymbol{\rho})$  are real, their Fourier components satisfy

$$Z_{\alpha}(-\mathbf{q}) = Z_{\alpha}^*(\mathbf{q}) \quad (\text{A.42})$$

$$b_{\alpha}(-\mathbf{q}) = b_{\alpha}^*(\mathbf{q}). \quad (\text{A.43})$$

In the last expression for the partition function we found that the terms with  $Z_x$  and  $Z_y$  decouple and we thus can integrate over  $Z_x(\boldsymbol{\rho})$  and  $Z_y(\boldsymbol{\rho})$  separately.

The expressions in this and especially the next subsection can be significantly economized by using a check mark to denote two-component vectors:

$$\check{b}(\mathbf{q}) = \begin{pmatrix} b(\mathbf{q}) \\ b(\mathbf{q} - \mathbf{g}) \end{pmatrix}$$

Using this notation, the contribution due to  $Z_x(\boldsymbol{\rho})$  can be written as

$$\frac{i}{2}\check{b}_x^T(-\mathbf{q})\check{Z}_x(\mathbf{q}) - \frac{1}{4}\check{Z}_x^T(-\mathbf{q})(\dots)\check{Z}_x(\mathbf{q}). \quad (\text{A.44})$$

where  $(\dots) = J' + \bar{J} + \bar{J} \cos q_y \sigma_3 + \delta J \sin q_y \sigma_2$  and superscript  $T$  denotes the transpose of a matrix. Now  $Z_\alpha$  can be integrated out. Apart from the overall normalization constant,  $F[\mathbf{b}]$  is given by:

$$F[\mathbf{b}(\boldsymbol{\rho})] = -\frac{1}{4} \int \frac{d\mathbf{q}}{(2\pi)^2} [\check{b}_x^T(-\mathbf{q})G(q_y)\check{b}_x(\mathbf{q}) + (x \leftrightarrow y)], \quad (\text{A.45})$$

where matrix  $G$  is defined as

$$G = \frac{1}{\Delta(q_y)}(J' + \bar{J} - \bar{J} \cos q_y \sigma_z - \delta J \sin q_y \sigma_2) \quad (\text{A.46})$$

and the determinant  $\Delta$  equals

$$\Delta(q_y) = J'(J' + 2\bar{J}) + (\bar{J}^2 + (\delta J)^2) \sin^2 q_y. \quad (\text{A.47})$$

When  $\bar{J} = \delta J = 0$  we find

$$F[\mathbf{b}(\mathbf{q})] \rightarrow -\frac{1}{2J'} b_\alpha(\mathbf{q}) b_\alpha(-\mathbf{q}),$$

which restores the limit of an ordinary 2D XY model (A.35).

Returning to the partition function (A.33) and using the expression (A.45) for  $F[\mathbf{b}]$  we just found, we are now in position to integrate out the gauge field  $\Lambda(\boldsymbol{\rho})$  and obtain the analogue of the Coulomb gas representation for our model. Note that (A.30) implies

$$b_x(\mathbf{q}) = (1 - e^{-iq_y}) \Lambda(\mathbf{q}) \quad (\text{A.48})$$

$$b_y(\mathbf{q}) = -(1 - e^{-iq_x}) \Lambda(\mathbf{q}). \quad (\text{A.49})$$

The partition function now becomes

$$Z = \sum_{\mathbf{l}(\boldsymbol{\rho})} \int_{-\infty}^{\infty} \prod_{\boldsymbol{\rho}} d\Lambda(\boldsymbol{\rho}) \times \exp \left[ \int \frac{d\mathbf{q}}{(2\pi)^2} \left( i\pi \check{l}^T(-\mathbf{q}) \check{\Lambda}(\mathbf{q}) - \check{\Lambda}(-\mathbf{q}) \check{M} \check{\Lambda}(\mathbf{q}) \right) \right], \quad (\text{A.50})$$

where  $2 \times 2$  matrix  $\check{M}$  is given by

$$\check{M} = \frac{1}{2\Delta(q_y)} \left( (1 - \sigma_3 \cos q_y) [J' + \bar{J}(1 - \sigma_3 \cos q_y)] + \sigma_1 \delta J \sin^2 q_y \right) + (x \leftrightarrow y). \quad (\text{A.51})$$

After integration over  $\Lambda(\boldsymbol{\rho})$  we obtain

$$Z = \sum_{\mathbf{l}(\boldsymbol{\rho})} \exp \left[ -\frac{\pi^2}{4} \int \frac{d\mathbf{q}}{(2\pi)^2} \check{l}^T(-\mathbf{q}) M(\mathbf{q}) \check{l}(\mathbf{q}) \right], \quad (\text{A.52})$$

where matrix  $M$  is the inverse of  $\check{M}$ . The elements of matrix  $M$  satisfy the following simple identities:

$$M_{11}(\mathbf{q}) = M_{22}(\mathbf{q} - \mathbf{g}) \quad (\text{A.53})$$

$$M_{12}(\mathbf{q}) = M_{21}(\mathbf{q}). \quad (\text{A.54})$$

Consequently, the integrand in the exponent of partition function (A.52) can be written as

$$2 \left( l(-\mathbf{q}) M_{11}(\mathbf{q}) l(\mathbf{q}) + l(\mathbf{g} - \mathbf{q}) M_{12}(\mathbf{q}) l(\mathbf{q}) \right). \quad (\text{A.55})$$

The explicit form of  $M = \check{M}^{-1}$  is rather cumbersome. Fortunately, we will only need the leading and subleading order terms in the long wavelength ( $q \rightarrow 0$ ) expansion:

$$M_{11}(\mathbf{q}) = \frac{4(J' + 2\bar{J})}{q_x^2 + q_y^2} + \frac{(J' - 4\bar{J} + 18\delta J)(q_x^4 + q_y^4) + 12\delta J q_x^2 q_y^2}{3J'(q_x^2 + q_y^2)^2} + O(q^2) \quad (\text{A.56})$$

$$M_{12}(\mathbf{q}) = -\delta J + O(q^2). \quad (\text{A.57})$$

The terms of order  $O(q^2)$  correspond to  $M(\boldsymbol{\rho} - \boldsymbol{\rho}')$  decreasing at least as fast as  $|\boldsymbol{\rho} - \boldsymbol{\rho}'|^{-4}$ . Returning to the real space representation, we obtain

$$\sum_{\mathbf{l}(\boldsymbol{\rho})} \exp \left\{ -\frac{\pi^2}{2} \sum_{\boldsymbol{\rho}, \boldsymbol{\rho}'} (l(\boldsymbol{\rho}) M_{11}(\boldsymbol{\rho} - \boldsymbol{\rho}') l(\boldsymbol{\rho}') + e^{i\mathbf{g} \cdot \boldsymbol{\rho}} l(\boldsymbol{\rho}) M_{12}(\boldsymbol{\rho} - \boldsymbol{\rho}') l(\boldsymbol{\rho}')) \right\}, \quad (\text{A.58})$$

where

$$M_{\alpha\beta}(\boldsymbol{\rho} - \boldsymbol{\rho}') = \int_{-\pi}^{\pi} \frac{dq_x}{2\pi} \int_{-\pi}^{\pi} \frac{dq_y}{2\pi} e^{i\mathbf{q} \cdot (\boldsymbol{\rho} - \boldsymbol{\rho}')} M_{\alpha\beta}(\mathbf{q}). \quad (\text{A.59})$$

The two terms in the exponent of (A.58) are easy to interpret. Recall that integers  $l(\boldsymbol{\rho})$  coupled to  $\Lambda(\boldsymbol{\rho})$  effectively reside at the centers of the plaquettes of the blue lattice corresponding to either black or red sites in Fig. 2. The terms containing  $M_{11}$  clearly describe the average interaction between two plaquettes *irrespective* of their ‘‘color’’, while the terms with  $M_{12}$  reflect the difference between the red and black sites. For example, the strength of interaction between two black sites separated by two lattice spacings with  $\boldsymbol{\rho} = 0$  and  $\boldsymbol{\rho} = 2\hat{x}$  will be different from interaction between two red sites at  $\boldsymbol{\rho} = \hat{x}$ ,  $\boldsymbol{\rho}' = 3\hat{x}$  due to the factor  $\exp(i\mathbf{g} \cdot \boldsymbol{\rho})$  that multiplies  $M_{12}$ .

At large distances the Fourier transform can be evaluated by comparison to the standard lattice Green’s function in two dimensions. The difference

$$M_{11}(\mathbf{q}) - 4(J' + 2\bar{J}) \frac{1}{4 - 2\cos q_x - 2\cos q_y}$$

is finite at  $\mathbf{q} = 0$ , and therefore the Fourier transform of this difference vanishes at large distances. Thus

$$M_{11}(\boldsymbol{\rho}) = 4(J' + 2\bar{J}) \times \int_{-\pi}^{\pi} \frac{dq_x}{2\pi} \int_{-\pi}^{\pi} \frac{dq_y}{2\pi} \frac{e^{i\boldsymbol{\rho}\mathbf{q}}}{4 - 2\cos q_x - 2\cos q_y} + \dots \quad (\text{A.60})$$

Using the well known asymptotic behavior of the last integral<sup>36</sup>, we find

$$M_{11}(\boldsymbol{\rho} - \boldsymbol{\rho}') = M_{11}(0) - \frac{4(J' + 2\bar{J})}{2\pi} [\ln |\boldsymbol{\rho} - \boldsymbol{\rho}'| + () + \dots] \quad , \quad (\text{A.61})$$

where  $C_1$  can be related to the Euler-Mascheroni constant  $\gamma \approx 0.5772$  as  $C_1 = \gamma + \ln(2\sqrt{2})$ . Note that  $M_{11}(\boldsymbol{\rho})$  formally logarithmically diverges because  $M_{11}(\mathbf{q})$  is proportional to  $q^{-2}$  at small momenta. The difference,  $M_{11}(\boldsymbol{\rho}) - M_{11}(0)$ , however, is finite. The overall infinite additive constant has a simple physical interpretation, just like for an ordinary two-dimensional XY model, as will become clear in a moment.

The real space expression for  $M_{12}$  can be easily calculated directly:

$$M_{12}(\boldsymbol{\rho} - \boldsymbol{\rho}') = -\delta J \delta_{\boldsymbol{\rho}\boldsymbol{\rho}'} + \dots, \quad (\text{A.62})$$

where  $\dots$  denotes terms that decrease at least as fast as  $|\boldsymbol{\rho} - \boldsymbol{\rho}'|^{-4}$ . Combining (A.59), (A.61), and (A.62), we obtain the following expression, after separating off the terms with  $\boldsymbol{\rho} = \boldsymbol{\rho}'$ :

$$Z = \sum_{l(\boldsymbol{\rho})} \exp \left[ -\frac{\pi^2}{2} \left( M_{11}(0) \sum_{\boldsymbol{\rho}} l^2(\boldsymbol{\rho}) + \sum_{\boldsymbol{\rho} \neq \boldsymbol{\rho}'} M_{11}(\boldsymbol{\rho} - \boldsymbol{\rho}') l(\boldsymbol{\rho}) l(\boldsymbol{\rho}') - \delta J \sum_{\boldsymbol{\rho}} e^{i\mathbf{g} \cdot \boldsymbol{\rho}} l^2(\boldsymbol{\rho}) \right) \right]. \quad (\text{A.63})$$

By applying the long distance expansion of  $M_{11}(\boldsymbol{\rho})$  in the sum containing terms with  $\boldsymbol{\rho} \neq \boldsymbol{\rho}'$  we find that the partition function  $Z$  becomes

$$\sum_{l(\boldsymbol{\rho})} \exp \left[ -\frac{\pi^2}{2} \left( M_{11}(0) \left( \sum_{\boldsymbol{\rho}} l(\boldsymbol{\rho}) \right)^2 - \delta J \sum_{\boldsymbol{\rho}} e^{i\mathbf{g} \cdot \boldsymbol{\rho}} l^2(\boldsymbol{\rho}) - \frac{4(J' + 2\bar{J})}{2\pi} \sum_{\boldsymbol{\rho} \neq \boldsymbol{\rho}'} l(\boldsymbol{\rho}) l(\boldsymbol{\rho}') (\ln |\boldsymbol{\rho} - \boldsymbol{\rho}'| + C_1) \right) \right]. \quad (\text{A.64})$$

We now return to the discussion of the formally divergent constant  $M_{11}(0)$ . This divergence is a reflection of the logarithmic dependence of a single vortex energy on the system size. If the number of the sites  $N$  were finite, we would have obtained a constant of order  $\ln N$  for  $M_{11}(0)$  instead of an outright divergence. Although finite, this constant becomes large in the thermodynamic limit  $N \rightarrow \infty$ , with the effect of suppressing all configurations of the integer-valued field  $l(\boldsymbol{\rho})$  except those that satisfy

$$\sum_{\boldsymbol{\rho}} l(\boldsymbol{\rho}) = 0 \quad . \quad (\text{A.65})$$

This is nothing but the charge neutrality condition in the partition function of a 2D Coulomb plasma. Restricting

ourselves only to such configurations, we obtain:

$$Z = \sum_{l(\boldsymbol{\rho})} \exp \left[ \frac{\pi^2}{2} \left( \frac{4(J' + 2\bar{J})}{2\pi} \sum_{\boldsymbol{\rho} \neq \boldsymbol{\rho}'} l(\boldsymbol{\rho}) l(\boldsymbol{\rho}') (\ln |\boldsymbol{\rho} - \boldsymbol{\rho}'| + C_1) + \delta J \sum_{\boldsymbol{\rho}} e^{i\mathbf{g} \cdot \boldsymbol{\rho}} l^2(\boldsymbol{\rho}) \right) \right]. \quad (\text{A.66})$$

A further simplification is achieved by noticing that

$$\sum_{\boldsymbol{\rho} \neq \boldsymbol{\rho}'} l(\boldsymbol{\rho}) l(\boldsymbol{\rho}') = \left( \sum_{\boldsymbol{\rho}} l(\boldsymbol{\rho}) \right)^2 - \sum_{\boldsymbol{\rho}} l^2(\boldsymbol{\rho}) \quad .$$

Since the first term on the right hand side vanishes by virtue of (A.65), the partition function equals

$$Z = \sum_{l(\boldsymbol{\rho})} \exp \left[ \frac{\pi^2}{2} \left( \frac{4(J' + 2\bar{J})}{2\pi} \sum_{\boldsymbol{\rho} \neq \boldsymbol{\rho}'} l(\boldsymbol{\rho}) l(\boldsymbol{\rho}') \ln |\boldsymbol{\rho} - \boldsymbol{\rho}'| - \frac{4C_1(J' + 2\bar{J})}{2\pi} \sum_{\boldsymbol{\rho}} l^2(\boldsymbol{\rho}) + \delta J \sum_{\boldsymbol{\rho}} e^{i\mathbf{g} \cdot \boldsymbol{\rho}} l^2(\boldsymbol{\rho}) \right) \right]. \quad (\text{A.67})$$

This is the Coulomb gas representation of our model describing charges  $l(\boldsymbol{\rho})$  residing on black and red plaquettes and interacting with long-ranged forces. Condition (A.65) therefore is simply an expression of the overall neutrality of the system – only the configurations with the same number of vortices and antivortices contribute to the partition function.

The Hamiltonian of the system can be finally recast as

$$\mathcal{H}_v^d = -\pi(J' + J_1 + J_2) \sum_{\boldsymbol{\rho} \neq \boldsymbol{\rho}'} l(\boldsymbol{\rho}) l(\boldsymbol{\rho}') \ln |\boldsymbol{\rho} - \boldsymbol{\rho}'| + E_c^r \sum_{\boldsymbol{\rho} \in \mathcal{R}} l^2(\boldsymbol{\rho}) + E_c^b \sum_{\boldsymbol{\rho} \in \mathcal{B}} l^2(\boldsymbol{\rho}) \quad , \quad (\text{A.68})$$

where the core energies of the vortices on red ( $\mathcal{R}$ ) and black ( $\mathcal{B}$ ) plaquettes are expressed through the original parameters of the model as

$$E_c^r = \pi C_1 (J' + J_1 + J_2) - \frac{\pi^2}{4} (J_1 - J_2) \quad (\text{A.69})$$

$$E_c^b = \pi C_1 (J' + J_1 + J_2) + \frac{\pi^2}{4} (J_1 - J_2) \quad . \quad (\text{A.70})$$

The Hamiltonian (A.68) is of the form equivalent to Eq. (23) derived in the main text from the continuum formulation. Note that in the “low temperature” limit  $J \gg 1$ , coefficients  $J$  and  $J' = \beta_V(J)$  coincide (see Eq. (A.21)), and the agreement with the continuum formulation is complete: the effective strength of the long range interaction between vortices is

$$\tilde{J} = J + J_1 + J_2 \quad .$$

b. *Quantum phase fluctuations*

The derivation in 2+1 dimensions follows closely the steps of the two-dimensional case considered in the previous subsection. Denoting the imaginary time by  $\tau$ , the partition function of the model is

$$Z = \int \prod_{\rho} \mathcal{D}\phi_{\mathbf{r}}(\tau) \exp \left[ - \int_0^{\beta} d\tau \sum_{\rho} L(\rho, \tau) \right],$$

where  $\rho$  is defined precisely like in the 2D case and  $\mathbf{r} = (\rho, \tau)$ . The Lagrangian of our quantum model is defined as

$$\begin{aligned} -L(\rho, \tau) = & -\frac{K_0}{2} \dot{\phi}_{\mathbf{r}}^2 + i\bar{f}\dot{\phi}_{\mathbf{r}} + J(\cos(\nabla_x \phi_{\mathbf{r}}) + \cos(\nabla_y \phi_{\mathbf{r}})) \\ & + J_{12}(\rho)(\cos(\phi_{\mathbf{r}+\hat{x}+\hat{y}} - \phi_{\mathbf{r}}) + \cos(\phi_{\mathbf{r}+\hat{y}} - \phi_{\mathbf{r}+\hat{x}})). \end{aligned} \quad (\text{A.71})$$

The sign of the Berry phase is chosen to be positive for later convenience; obviously the partition function is not affected by the change. It is convenient to replace the integrals over continuous variable  $\tau$  by sums over discrete  $\tau_n$  (abbreviated often as  $\tau$  below) separated by intervals of “length”  $\epsilon$ . For brevity, we will use  $\phi_{\mathbf{r}+\hat{\tau}}$  to denote  $\phi(\rho, \tau + \epsilon)$ .

The terms containing time derivatives can be transformed as follows:

$$\begin{aligned} & \exp \left[ \int d\tau \sum_{\rho} \left( -\frac{K_0}{2} \dot{\phi}_{\rho, \tau}^2 + i\bar{f}\dot{\phi}_{\rho, \tau} \right) \right] \\ & = \exp \left[ \sum_{\mathbf{r}} -\frac{K_0\epsilon}{2} \left( \frac{\phi_{\mathbf{r}+\tau} - \phi_{\mathbf{r}}}{\epsilon} \right)^2 + \sum_{\mathbf{r}} i\bar{f}\epsilon \frac{\phi_{\mathbf{r}+\tau} - \phi_{\mathbf{r}}}{\epsilon} \right]. \end{aligned} \quad (\text{A.72})$$

After completing the square we have

$$\exp \sum_{\mathbf{r}} \left[ -\frac{K_0}{2\epsilon} \left( \phi_{\mathbf{r}+\tau} - \phi_{\mathbf{r}} - i\frac{\bar{f}}{K_0}\epsilon \right)^2 - \frac{\epsilon\bar{f}^2}{2K_0} \right].$$

Note that this expression can be formally replaced by a sum

$$\sum_{m(\mathbf{r})} \exp \sum_{\mathbf{r}} \left[ -\frac{K_0}{2\epsilon} (\nabla_{\tau} \phi_{\mathbf{r}} - i\frac{\bar{f}}{K_0}\epsilon - 2\pi m(\mathbf{r}))^2 - \frac{\epsilon\bar{f}^2}{2K_0} \right],$$

since, clearly, only the term  $m = 0$  survives in the limit of small  $\epsilon$ . The latter form is convenient because now the Poisson identity

$$\begin{aligned} & \sum_{n=-\infty}^{\infty} \exp \left[ -\frac{a}{2} n^2 + in\phi \right] \\ & = \sqrt{\frac{2\pi}{a}} \sum_{m=-\infty}^{\infty} \exp \left[ -\frac{(\phi - 2\pi m)^2}{2a} \right] \end{aligned} \quad (\text{A.73})$$

can be applied. The result is

$$\begin{aligned} & \exp \left[ \int d\tau \sum_{\rho} \left( -\frac{K_0}{2} \dot{\phi}_{\rho, \tau}^2 + i\bar{f}\dot{\phi}_{\rho, \tau} \right) \right] \\ & \propto \sum_{u_{\tau}(\mathbf{r})} \exp \left[ \sum_{\mathbf{r}} \left( -\frac{\epsilon}{2K_0} u_{\tau}(\mathbf{r})^2 \right. \right. \\ & \quad \left. \left. + iu_{\tau}(\mathbf{r})(\phi_{\mathbf{r}+\hat{\tau}} - \phi_{\mathbf{r}} - \frac{i\bar{f}\epsilon}{K_0}) - \epsilon \frac{\bar{f}^2}{2K_0} \right) \right], \end{aligned} \quad (\text{A.74})$$

where  $u_{\tau}(\mathbf{r})$  is an integer-valued field. Using the identity the partition function  $Z$  can now be rewritten as

$$\begin{aligned} & \sum_{\mathbf{u}} \sum_{w_{\pm}} \int \prod_{\mathbf{r}} d\phi_{\mathbf{r}} \exp \left[ i \sum_{\mathbf{r}} \left( u_i(\mathbf{r}) \nabla_i \phi_{\mathbf{r}} \right. \right. \\ & \quad \left. \left. + w_+(\mathbf{r})(\phi_{\mathbf{r}+\hat{x}+\hat{y}} - \phi_{\mathbf{r}}) + w_-(\mathbf{r})(\phi_{\mathbf{r}+\hat{y}} - \phi_{\mathbf{r}+\hat{x}}) \right) \right] \times \\ & \exp \left[ - \sum_{\mathbf{r}} \left( \frac{u_{\alpha}^2(\mathbf{r})}{2J'} + \frac{w_+^2(\mathbf{r}) + w_-^2(\mathbf{r})}{2J'_{12}(\rho)} + \frac{\epsilon(u_{\tau} - \bar{f})^2}{2K_0} \right) \right]. \end{aligned} \quad (\text{A.75})$$

The reader should bear in mind that throughout the appendix the Greek indices exclusively denote the space-like components  $x, y$  of a three-vector, while latin indices denote both space-like and time-like components, as the case may be. The coefficients  $J'$  and  $J'_{12}(\rho)$  are defined as

$$J' = \beta_V(\epsilon J) \quad (\text{A.76})$$

$$J_{12}(\rho) = \beta_V(J_{12}(\epsilon\rho)) \quad (\text{A.77})$$

We now proceed to transform the above expression by shifting the differences of the phases  $\phi_r$  onto the difference of the fields  $\mathbf{u}(\mathbf{r})$  and  $w_{\pm}(\mathbf{r})$  by using discrete integration by parts (A.26), just as it was done in the two-dimensional case:

$$\begin{aligned} Z = & \sum_{\mathbf{u}} \sum_{w_{\pm}} \int \prod_{\mathbf{r}} \left[ d\phi_{\mathbf{r}} \delta \left( \nabla \cdot \mathbf{u}(\mathbf{r}) + (w_+(\mathbf{r}) \right. \right. \\ & \quad \left. \left. - w_+(\mathbf{r} - \hat{x} - \hat{y}) + (w_-(\mathbf{r} - \hat{x}) - w_-(\mathbf{r} - \hat{y})) \right) \right] \\ & \exp \left[ - \sum_{\mathbf{r}} \left( \frac{u_{\alpha}^2(\mathbf{r})}{2J'} + \frac{\epsilon(u_{\tau} - \bar{f})^2}{2K_0} + \frac{w_+^2(\mathbf{r}) + w_-^2(\mathbf{r})}{2J'_{12}(\rho)} \right) \right], \end{aligned} \quad (\text{A.78})$$

where bold letters stand for *three-dimensional* vectors and  $\nabla \cdot \mathbf{u}$  denotes *three-dimensional* divergence.

In the absence of the next-nearest coupling terms represented by  $w_{\pm}$ , the  $\delta$ -function constraint in (A.78) is resolved by  $\mathbf{u} = \nabla \times \mathbf{a}$ , where the lattice curl is defined as

$$u_i = \epsilon_{ijk} \nabla_j \Lambda_k(\mathbf{r} - \mathbf{e}_k), \quad \mathbf{e} = (\hat{x}, \hat{y}, \hat{\tau}).$$

In our case of a  $d$ -wave superconductor and finite  $w_{\pm}$ , we rewrite the constraint as

$$\nabla \cdot (\mathbf{u}(\mathbf{r}) + \mathbf{w}[w_+, w_-]) = 0, \quad (\text{A.79})$$

where  $\mathbf{w} = (w_x, w_y, 0)$  and  $w_{x(y)}$  are defined in the previous subsection section (A.28). The solution is clearly

$$\mathbf{u} = \bar{\nabla} \times \mathbf{\Lambda} - \mathbf{w}[w_+, w_-] .$$

One can easily check that the choice of  $\mathbf{\Lambda}$  is not unique: for arbitrary scalar function  $\xi(\mathbf{r})$

$$\begin{aligned} [\bar{\nabla} \times (\mathbf{\Lambda} + \nabla \xi(\mathbf{r}))]_i - [\bar{\nabla} \times \mathbf{\Lambda}]_i &= \\ = \epsilon_{ijk} \bar{\nabla}_j \nabla_k \xi(\mathbf{r} - \boldsymbol{\delta}_k) &= \epsilon_{ijk} \bar{\nabla}_j \bar{\nabla}_k \xi(\mathbf{r}) = 0 \end{aligned} \quad (\text{A.80})$$

This gauge invariance implies that a gauge-fixing term must be introduced when replacing the sums over integer field  $\mathbf{u}$  by summation over  $\mathbf{\Lambda}$  in order to avoid multiple-counting. The next step is most easily derived in the temporal gauge:

$$\delta(\Lambda_3) \equiv \prod_{\mathbf{r}} \delta_{\Lambda_3(\mathbf{r}), 0} .$$

Afterwards, the results will be generalized to an arbitrary gauge-fixing condition. We proceed by rewriting the partition function as

$$\begin{aligned} Z &= \sum_{\mathbf{\Lambda}} \sum_{w_{\pm}} \exp \left[ - \sum_{\mathbf{r}} \left( \frac{(\bar{\nabla} \times \mathbf{\Lambda} - \mathbf{F}[w_{\pm}]_{\perp})^2}{2J'} \right. \right. \\ &\quad \left. \left. + \frac{\epsilon}{2K_0} ((\bar{\nabla} \times \mathbf{\Lambda})_0 - \bar{f})^2 + \frac{w_{\pm}^2(\mathbf{r}) + w_{\pm}^2(\mathbf{r})}{2J'_{12}(\boldsymbol{\rho})} \right) \right] \delta_{\Lambda_3(\mathbf{r}), 0} \end{aligned} \quad (\text{A.81})$$

and apply the Poisson formula in order to obtain a theory depending on continuous rather than integer valued gauge field  $\mathbf{\Lambda}$ :

$$\begin{aligned} \sum_{\mathbf{\Lambda}(\mathbf{r})} \delta_{\Lambda_3, 0} f(\Lambda_1(\mathbf{r}), \Lambda_2(\mathbf{r}), \Lambda_3(\mathbf{r})) &= \prod_{\mathbf{r}} \int d\Lambda_1(\mathbf{r}) d\Lambda_2(\mathbf{r}) \times \\ &\quad \sum_{l_1(\mathbf{r}), l_2(\mathbf{r})} e^{2\pi i \sum_{\mathbf{r}} l_{\alpha}(\mathbf{r}) \Lambda_{\alpha}(\mathbf{r})} f(\Lambda_1(\mathbf{r}), \Lambda_2(\mathbf{r}), 0) \\ &= \prod_{\mathbf{r}} \int_{-\infty}^{\infty} d\Lambda_1(\mathbf{r}) d\Lambda_2(\mathbf{r}) d\Lambda_3(\mathbf{r}) \delta(\Lambda_3) \times \\ &\quad \sum_{\mathbf{l}(\mathbf{r})} \delta_{\bar{\nabla} \cdot \mathbf{l}} e^{2\pi i \sum_{\mathbf{r}} l_j(\mathbf{r}) \Lambda_j(\mathbf{r})} f(\Lambda_1(\mathbf{r}), \Lambda_2(\mathbf{r}), \Lambda_3(\mathbf{r})) . \end{aligned} \quad (\text{A.82})$$

In performing the last step, we formally introduced  $l_3 \Lambda_3$  and an additional sum over  $l_3(\mathbf{r})$ . The delta function  $\delta(\Lambda_3(\mathbf{r}))$  ensures that the exponent is not affected. All terms in the sum over  $l_3$  are therefore equal, and in order to avoid multiple-counting we need to impose a constraint, chosen as  $\bar{\nabla} \cdot \mathbf{l} = 0$ , by assigning

$$l_3 = -(\bar{\nabla}_3)^{-1} (\bar{\nabla}_1 l_1 + \bar{\nabla}_2 l_2) .$$

Note that the result of applying operator  $(\bar{\nabla}_3)^{-1}$  to an integer field is another integer. The integer-valued field  $\mathbf{l}(\mathbf{r})$  with zero divergence describes non-backtracking closed

loops on the 2+1 space-time lattice. The field  $\mathbf{\Lambda}(\mathbf{r})$  is now continuous and the temporal gauge condition

$$\Theta_{\tau}[\mathbf{\Lambda}] = \prod_{\mathbf{r}} \delta(\Lambda_3(\mathbf{r}))$$

can be replaced<sup>36</sup> by an arbitrary gauge-fixing condition  $\Theta[\mathbf{\Lambda}]$ ; examples are  $\bar{\nabla} \cdot \mathbf{\Lambda} = 0$  (Landau gauge) or  $\bar{\nabla}_{\perp} \cdot \mathbf{\Lambda}_{\perp} = 0$  (radiation gauge):

$$\begin{aligned} \sum_{\mathbf{\Lambda}(\mathbf{r})} \delta_{\Lambda_3, 0} f(\Lambda_1(\mathbf{r}), \Lambda_2(\mathbf{r}), \Lambda_3(\mathbf{r})) &= \\ \int_{-\infty}^{\infty} \prod_{\mathbf{r}} d\mathbf{\Lambda}(\mathbf{r}) \Theta[\mathbf{\Lambda}(\mathbf{r})] \sum_{\mathbf{l}(\mathbf{r})} e^{2\pi i \sum_{\mathbf{r}} \mathbf{l}(\mathbf{r}) \cdot \mathbf{\Lambda}(\mathbf{r})} f(\mathbf{\Lambda}(\mathbf{r})) \delta_{\bar{\nabla} \cdot \mathbf{l}} . \end{aligned} \quad (\text{A.83})$$

This final identity allows us to rewrite our partition function as

$$\begin{aligned} Z &= \int_{-\infty}^{\infty} \prod_{\mathbf{r}} d\mathbf{\Lambda}(\mathbf{r}) \Theta[\mathbf{\Lambda}(\mathbf{r})] e^{\sum_{\mathbf{r}} F[(\bar{\nabla} \times \mathbf{\Lambda})_{\perp}]_{\times}} \\ &\quad \sum_{\mathbf{l}(\mathbf{r})} \delta_{\bar{\nabla} \cdot \mathbf{l}} e^{\sum_{\mathbf{r}} [2\pi i \mathbf{l}(\mathbf{r}) \cdot \mathbf{\Lambda}(\mathbf{r}) - (\epsilon/2K_0) ((\bar{\nabla} \times \mathbf{\Lambda})_0 - \bar{f})^2]} \end{aligned} \quad (\text{A.84})$$

where  $F[(\bar{\nabla} \times \mathbf{\Lambda})_{\perp}]$  has already been calculated in (A.45) and can be used as is, provided that proper definitions (A.77) of  $J'$  and  $J'_{12}(\boldsymbol{\rho})$  are replaced.

The remaining steps leading to the ‘‘Coulomb’’ gas representation of 3D vortex loops are conceptually similar to the 2D case from the previous subsection. The algebra, however, is considerably more involved. We therefore will go slowly and first wade through the derivation for the simple case  $J_1 = J_2 = 0$ . This is just the ordinary (2+1)D XY model, appropriate for our  $s$ -wave pedagogical exercise from the main text and the beginning of this Appendix (A.2). Only the configurations  $w_{\pm}(\mathbf{r}) = 0$  contribute to the functional  $F[(\bar{\nabla} \times \mathbf{\Lambda})_{\perp}]$  (A.45) and we recover the usual<sup>13</sup> anisotropic 3D XY model in a uniform magnetic field  $\mathbf{H} = \bar{f} \hat{\tau}$ :

$$\begin{aligned} Z_0 &= \int_{-\infty}^{\infty} \prod_{\mathbf{r}} d\mathbf{\Lambda}(\mathbf{r}) \Theta[\mathbf{\Lambda}(\mathbf{r})] \sum_{\mathbf{l}(\mathbf{r})} \delta_{\bar{\nabla} \cdot \mathbf{l}} \times \\ &\quad e^{\sum_{\mathbf{r}} \left[ 2\pi i \mathbf{l}(\mathbf{r}) \cdot \mathbf{\Lambda}(\mathbf{r}) - \frac{(\bar{\nabla} \times \mathbf{\Lambda})_{\perp}^2}{2J'} - \frac{\epsilon}{2K_0} \left( (\bar{\nabla} \times \mathbf{\Lambda})_0 - \bar{f} \right)^2 \right]} . \end{aligned} \quad (\text{A.85})$$

To obtain the lattice loop gas representation, we need to integrate out the gauge field  $\mathbf{\Lambda}$ . The most transparent connection with the results for the 2D model is obtained by using the radiation gauge  $\bar{\nabla}_{\alpha} \Lambda_{\alpha} = 0$ :

$$\sum_{\mathbf{r}} (\bar{\nabla} \times \mathbf{\Lambda})_0^2 = \sum_{\mathbf{r}} [\bar{\nabla}_x \Lambda_y(\mathbf{r} - \hat{y}) - \bar{\nabla}_y \Lambda_x(\mathbf{r} - \hat{x})]^2 \quad (\text{A.86})$$

Expanding the square and shifting the difference opera-



tors via (A.26) we have

$$\begin{aligned} \sum_{\mathbf{r}} (\bar{\nabla} \times \Lambda)_0^2 &= \sum_{\mathbf{r}} -\Lambda_y(\mathbf{r} - \hat{y}) \nabla_x \bar{\nabla}_x \Lambda_y(\mathbf{r} - \hat{y}) \\ &- \Lambda_x(\mathbf{r} - \hat{x}) \nabla_y \bar{\nabla}_y \Lambda_x(\mathbf{r} - \hat{x}) - 2 \nabla_y \Lambda_y(\mathbf{r} - \hat{y}) \nabla_x \Lambda_x(\mathbf{r} - \hat{x}) \\ &= \sum_{\mathbf{r}} -\Lambda_\mu(\mathbf{r}) \nabla_\nu \bar{\nabla}_\nu \Lambda_\mu(\mathbf{r}) - (\bar{\nabla}_\mu \Lambda_\mu(\mathbf{r}))^2 . \end{aligned} \quad (\text{A.87})$$

We introduce the following notation for the lattice analogues of wavevectors  $q_j$  appearing from discrete left-sided or right-sided derivatives after Fourier transformation:

$$Q_j(\mathbf{q}) = \frac{e^{iq_j} - 1}{i} \quad (\text{A.88})$$

$$\bar{Q}_j(\mathbf{q}) = \frac{1 - e^{-iq_j}}{i} \quad (\text{A.89})$$

$$Q_j^{\mathbf{g}}(\mathbf{q}) = Q_j(\mathbf{q} - \mathbf{g}) = \frac{-e^{-iq_j} - 1}{i} \quad (\text{A.90})$$

$$\bar{Q}_j^{\mathbf{g}}(\mathbf{q}) = \bar{Q}_j(\mathbf{q} - \mathbf{g}) = \frac{1 + e^{-iq_j}}{i} . \quad (\text{A.91})$$

$$(\text{A.92})$$

The arguments of  $Q_j$  and  $\bar{Q}_j$  is assumed to be  $\mathbf{q}$  unless specified otherwise.

We define the Fourier transformation as

$$f(\mathbf{r}) = \frac{1}{\beta} \sum_{q_0} \int \frac{d\mathbf{q}_\perp}{(2\pi)^2} e^{i\mathbf{q}\cdot\mathbf{r}} f(\mathbf{q})$$

where the sum over frequencies  $q_0$  runs through  $q_0 = 0, \frac{2\pi}{\beta}, \dots, \frac{2\pi}{\epsilon}$  and the integrals over  $q_x, q_y$  extend from  $-\pi$  to  $\pi$ . Using the definition and properties that follow from it

$$f(\mathbf{q}) = \epsilon \sum_{q_0} \int \frac{d\mathbf{q}_\perp}{(2\pi)^2} e^{-i\mathbf{q}\cdot\mathbf{r}} f(\mathbf{q}) \quad (\text{A.93})$$

$$f^2(\mathbf{r}) = \frac{1}{\beta\epsilon} \sum_{q_0} \int \frac{d\mathbf{q}_\perp}{(2\pi)^2} f(\mathbf{q}) f(-\mathbf{q}) , \quad (\text{A.94})$$

we obtain in the radiation gauge:

$$\begin{aligned} \sum_{\mathbf{r}} (\bar{\nabla} \times \Lambda)_0^2 &= - \sum_{\mathbf{r}} \Lambda_\mu(\mathbf{r}) \nabla_\nu \bar{\nabla}_\nu \Lambda_\mu(\mathbf{r}) \\ &= \sum_{q_0} \int \frac{d\mathbf{q}_\perp}{\beta\epsilon(2\pi)^2} \Lambda_\mu(-\mathbf{q}) Q_\nu \bar{Q}_\nu \Lambda_\mu(\mathbf{q}) , \end{aligned} \quad (\text{A.95})$$

Similarly,

$$\begin{aligned} \sum_{\mathbf{r}} (\bar{\nabla} \times \Lambda)_\perp^2 &= \sum_{\mathbf{r}} \left( -\Lambda_0(\mathbf{r}) \bar{\nabla}_\mu \nabla_\mu \Lambda_0(\mathbf{r}) \right. \\ &\left. - \Lambda_\mu(\mathbf{r}) \bar{\nabla}_0 \nabla_0 \Lambda_\mu(\mathbf{r}) - 2 \nabla_0 \Lambda_0(\mathbf{r} - \hat{\tau}) \nabla_\alpha \Lambda_\alpha(\mathbf{r} - \mathbf{e}_\alpha) \right) , \end{aligned} \quad (\text{A.96})$$

where the last term vanishes due to our choice of the gauge. In the momentum space we have:

$$\begin{aligned} \sum_{\mathbf{r}} (\bar{\nabla} \times \Lambda)_\perp^2 &= \sum_{q_0} \int \frac{d\mathbf{q}_\perp}{\beta\epsilon(2\pi)^2} \left( \Lambda_0(-\mathbf{q}) \Lambda_0(\mathbf{q}) Q_\mu \bar{Q}_\mu \right. \\ &\left. + \Lambda_\mu(-\mathbf{q}) \Lambda_\mu(\mathbf{q}) Q_0 \bar{Q}_0 \right) . \end{aligned} \quad (\text{A.97})$$

The above definitions are generally valid but now we focus again on the simple case of  $J_1 = J_2 = 0$ . The partition function  $Z_0$ , given by (A.85), can be written as

$$\begin{aligned} Z_0 &= \sum_{\mathbf{l}(\mathbf{r})} \delta_{\bar{\nabla}\cdot\mathbf{l}} e^{\sum_{\mathbf{r}} 2\pi i \mathbf{l}(\mathbf{r}) \cdot \Lambda_f(\mathbf{r})} \int_{-\infty}^{\infty} \prod_{\mathbf{r}} d\Lambda(\mathbf{r}) \times \\ &\delta[\bar{\nabla}_\alpha \Lambda_\alpha] e^{\sum_{\mathbf{r}} \left[ 2\pi i \mathbf{l}(\mathbf{r}) \cdot \Lambda(\mathbf{r}) - \frac{(\bar{\nabla} \times \Lambda)_\perp^2}{2J'} - \frac{\epsilon}{2K_0} (\bar{\nabla} \times \Lambda)_0^2 \right]} . \end{aligned} \quad (\text{A.98})$$

In arriving at the expression above we performed a shift of variable  $\Lambda \rightarrow \Lambda + \Lambda_f$ , where  $\Lambda_f$  is a time independent vector potential corresponding to a constant and uniform magnetic field  $\bar{f}\hat{\tau}$ . After Fourier transformation the expression in the exponent can be written as

$$\begin{aligned} \sum_{q_0} \int \frac{d\mathbf{q}_\perp}{\beta\epsilon(2\pi)^2} \left[ 2\pi i \mathbf{l}(\mathbf{q}) \cdot \Lambda(-\mathbf{q}) - \frac{\Lambda_0(-\mathbf{q}) \Lambda_0(\mathbf{q}) Q_\mu \bar{Q}_\mu}{2J'} \right. \\ \left. - \Lambda_\mu(-\mathbf{q}) \Lambda_\mu(\mathbf{q}) \left( \frac{1}{2J'} Q_0 \bar{Q}_0 + \frac{1}{2K'} Q_\nu \bar{Q}_\nu \right) \right] . \end{aligned} \quad (\text{A.99})$$

Note that temporal and space-like components are independent and can be integrated out separately. Integration over  $\Lambda_0$  is trivial and yields

$$\begin{aligned} \exp \left[ -2\pi^2 J' \sum_{q_0} \int \frac{dq_x dq_y}{\beta\epsilon(2\pi)^2} \frac{l_0(-\mathbf{q}) l_0(\mathbf{q})}{Q_\mu \bar{Q}_\mu} \right] \\ = \exp \left[ -2\pi^2 J' \sum_{q_0} \int \frac{dq_x dq_y}{\beta\epsilon(2\pi)^2} \frac{l_0(-\mathbf{q}) l_0(\mathbf{q})}{4 - 2 \cos q_x - 2 \cos q_y} \right] . \end{aligned} \quad (\text{A.100})$$

The remaining integral

$$\begin{aligned} \int_{-\infty}^{\infty} \prod_{\mathbf{q}} d\Lambda(\mathbf{q}) \delta[\bar{Q}_\alpha \Lambda_\alpha] \exp \left[ \sum_{\mathbf{r}} \left( 2\pi i l_\nu(-\mathbf{q}) \Lambda_\nu(\mathbf{q}) \right. \right. \\ \left. \left. - \left( \frac{1}{2J'} Q_0 \bar{Q}_0 + \frac{1}{2K'} Q_\nu \bar{Q}_\nu \right) \Lambda_\mu(-\mathbf{q}) \Lambda_\mu(\mathbf{q}) \right) \right] \end{aligned} \quad (\text{A.101})$$

can be computed by switching to 2D transverse and longitudinal components of  $\Lambda$ , which we define on the lattice as

$$\Lambda_L(\mathbf{q}) = i \frac{\bar{Q}_x \Lambda_x(\mathbf{q}) + \bar{Q}_y \Lambda_y(\mathbf{q})}{Q_\perp} \quad (\text{A.102})$$

$$\Lambda_T(\mathbf{q}) = i \frac{-Q_y \Lambda_x(\mathbf{q}) + Q_x \Lambda_y(\mathbf{q})}{Q_\perp} , \quad (\text{A.103})$$

where

$$Q_\perp = \sqrt{\bar{Q}_\alpha Q_\alpha} = \sqrt{\bar{Q}_x Q_x + \bar{Q}_y Q_y} .$$

The  $\Lambda_x(\mathbf{r})$  and  $\Lambda_y(\mathbf{r})$  can be expressed through the transverse and longitudinal components of the gauge field  $\Lambda$  as

$$\Lambda_x(\mathbf{q}) = -i \frac{Q_x \Lambda_L(\mathbf{q}) - \bar{Q}_y \Lambda_T(\mathbf{q})}{Q_\perp} \quad (\text{A.104})$$

$$\Lambda_y(\mathbf{q}) = -i \frac{Q_y \Lambda_L(\mathbf{q}) + \bar{Q}_x \Lambda_T(\mathbf{q})}{Q_\perp} . \quad (\text{A.105})$$

Now observe that the Jacobian of the transformation  $(\Lambda_x, \Lambda_y) \rightarrow (\Lambda_L, \Lambda_T)$  is unity, 2D divergence of  $\Lambda$  is proportional to  $\Lambda_L$  as expected:

$$\bar{Q}_\alpha \Lambda_\alpha = -i \Lambda_L Q_\perp ,$$

and

$$l_\alpha(-\mathbf{q}) \Lambda_\alpha(\mathbf{q}) = l_T(-\mathbf{q}) \Lambda_T(\mathbf{q}) + l_L(\mathbf{q}) \Lambda_L(\mathbf{q}) .$$

The integral (A.101) can be written as

$$\int_{-\infty}^{\infty} \prod_{\mathbf{q}} d\Lambda_T(\mathbf{q}) \exp \left[ \sum_{\mathbf{q}_0} \int \frac{dq_x dq_y}{\beta \epsilon (2\pi)^2} \left( 2\pi i l_T(-\mathbf{q}) \Lambda_T(\mathbf{q}) - \left( \frac{1}{2J'} Q_0 \bar{Q}_0 + \frac{1}{2K'} Q_\alpha \bar{Q}_\alpha \right) \Lambda_T(-\mathbf{q}) \Lambda_T(\mathbf{q}) \right) \right] , \quad (\text{A.106})$$

which finally gives

$$Z_0 \propto \sum_{\mathbf{l}(\mathbf{r})} \delta_{\bar{\nabla} \cdot \mathbf{l}} \exp \left[ -\pi^2 \sum_{\mathbf{q}_0} \int \frac{dq_x dq_y}{\epsilon \beta (2\pi)^2} \left( 2J' \frac{l_0(-\mathbf{q}) l_0(\mathbf{q})}{\bar{Q}_\alpha Q_\alpha} + \frac{l_T(-\mathbf{q}) l_T(\mathbf{q})}{\frac{1}{2J'} \bar{Q}_0 Q_0 + \frac{1}{2K'} \bar{Q}_\alpha Q_\alpha} \right) \right] . \quad (\text{A.107})$$

This is the desired vortex loop gas representation of our model. Rather than integrating out the gauge field  $\Lambda$  in (A.85), one can partially perform the sum over over the integers  $\mathbf{l}(\mathbf{r})$  and arrive at yet another (dual) representation of partition function  $Z$ . The constraint  $\bar{\nabla} \cdot \mathbf{l}(\mathbf{r}) = 0$  in the partition function  $Z_0$  (A.85) is rewritten using auxiliary variables  $\alpha(\mathbf{r})$  as

$$\begin{aligned} \sum_{\mathbf{l}(\mathbf{r})} \delta_{\bar{\nabla} \cdot \mathbf{l}, 0} \exp \left[ -\frac{\sum_{\mathbf{r}} \mathbf{l}^2(\mathbf{r})}{2\beta_V(\beta')} + 2\pi i \sum_{\mathbf{r}} \mathbf{l}(\mathbf{r}) \cdot \Lambda(\mathbf{r}) \right] &= \\ \sum_{\mathbf{l}(\mathbf{r})} \prod_{\mathbf{r}} \int_0^{2\pi} d\alpha(\mathbf{r}) \exp \left[ -\frac{1}{2\beta_V(\beta')} \sum_{\mathbf{r}} \mathbf{l}^2(\mathbf{r}) + 2\pi i \sum_{\mathbf{r}} \mathbf{l}(\mathbf{r}) \cdot \Lambda(\mathbf{r}) + i \sum_{\mathbf{r}} \alpha(\mathbf{r}) \bar{\nabla} \cdot \mathbf{l}(\mathbf{r}) \right] &= \\ \sum_{\mathbf{l}(\mathbf{r})} \prod_{\mathbf{r}} \int_0^{2\pi} d\alpha(\mathbf{r}) \exp \left[ -\frac{1}{2\beta_V(\beta')} \sum_{\mathbf{r}} \mathbf{l}^2(\mathbf{r}) + i \sum_{\mathbf{r}} \mathbf{l}_i(2\pi \Lambda_i(\mathbf{r}) - \nabla_i \alpha(\mathbf{r})) \right] &\approx \\ \prod_{\mathbf{r}} \int_0^{2\pi} d\alpha(\mathbf{r}) \exp \left[ \sum_{\mathbf{r}, i} \beta' \cos(\nabla_i \alpha(\mathbf{r}) - 2\pi \Lambda_i) \right] . & \quad (\text{A.108}) \end{aligned}$$

The last equation describes a lattice superconductor. Note that the partition function (A.85) does not contain quadratic terms  $\mathbf{l}^2(\mathbf{r})$ . Instead, one introduces a vortex core energy term

$$-\frac{1}{2\beta_V(\beta')} \sum_{\mathbf{r}} \mathbf{l}^2(\mathbf{r})$$

by hand, and then, in the final lattice superconductor representation, a limit  $\beta \rightarrow \infty$  is taken. Such a system is called a frozen superconductor. Alternatively, terms proportional to  $\mathbf{l}^2$  can be kept finite. Such ‘‘unfrozen lattice superconductor’’ is equivalent to an ensemble of vortex loops, namely an XY-model augmented with an additional core energy that makes formation of vortices more difficult. Thus, applying (A.108) to (A.85) we obtain the partition function  $Z_0$  describing lattice superconductor in a field  $\bar{f}$  coupled to fluctuating gauge field  $\Lambda$ :

$$\begin{aligned} \prod_{\mathbf{r}} \int_0^{2\pi} d\alpha(\mathbf{r}) \int_{-\infty}^{\infty} d\Lambda(\mathbf{r}) \Theta[\Lambda(\mathbf{r})] \times \\ \exp \left[ \sum_{\mathbf{r}, i} \beta' \cos(\nabla_i \alpha(\mathbf{r}) - 2\pi \Lambda_i) - \sum_{\mathbf{r}} \left( \frac{1}{2J'} (\bar{\nabla} \times \Lambda)_\perp^2 + \frac{1}{2K'} ((\bar{\nabla} \times \Lambda)_0 - \bar{f})^2 \right) \right] . \quad (\text{A.109}) \end{aligned}$$

The last step of our derivation is the standard<sup>36</sup> Ginzburg-Landau expansion of the action and for completeness we reproduce here the derivation following Kleinert<sup>36</sup>.

First, we introduce a complex field  $U_{\mathbf{r}} = \exp(i\alpha(\mathbf{r}))$  and define covariant derivative operators  $D_i, \bar{D}_i$  according to

$$D_x \Phi(\mathbf{r}) = \Phi(\mathbf{r} + \hat{x}) e^{-2\pi i \Lambda_x} - \Phi(\mathbf{r}) \quad (\text{A.110})$$

$$\bar{D}_x \Phi(\mathbf{r}) = \Phi(\mathbf{r}) - \Phi(\mathbf{r} - \hat{x}) e^{2\pi i \Lambda_x(\mathbf{r} - \hat{x})} . \quad (\text{A.111})$$

The following identity, which expresses the cosine in (A.109) through  $U_{\mathbf{r}}$ , can be proved easily:

$$\sum_{\mathbf{r}} \cos(\nabla_x \alpha(\mathbf{r}) - 2\pi \Lambda_x) = \sum_{\mathbf{r}} U_{\mathbf{r}}^* \left( 1 + \frac{1}{2} \bar{D}_x D_x \right) U_{\mathbf{r}} .$$

Thus, for a given fixed configuration of dual gauge field  $\Lambda$  in (A.109), the sum over all configurations of angular variables  $\alpha(\mathbf{r})$  is

$$Z_{XY}[\Lambda] = \int \mathcal{D}\alpha(\mathbf{r}) e^{\sum_{\mathbf{r}, i} \beta' \cos(\nabla_i \alpha(\mathbf{r}) - 2\pi \Lambda_i)}$$

and can be transformed into

$$Z_{XY}[\Lambda] = \int \mathcal{D}\alpha \exp \left[ 3\beta' \sum_{\mathbf{r}} U_{\mathbf{r}}^* \hat{D} U_{\mathbf{r}} \right] . \quad (\text{A.112})$$

where  $\hat{D} = (1 + \frac{1}{6} \bar{D}_i D_i)$ . Operator  $\hat{D}$  is Hermitian, and therefore allows decomposition  $\hat{D} = \hat{K}^2$ . Let us show

that  $Z_{XY}$  is proportional to

$$\int \mathcal{D}[\alpha, \Phi, \Phi^*] e^{-\frac{1}{12\beta'} \sum_{\mathbf{r}} |\Phi_{\mathbf{r}}|^2 + \frac{1}{2} \sum_{\mathbf{r}, \mathbf{r}'} (\Phi_{\mathbf{r}}^* \hat{\mathcal{K}}_{\mathbf{r}\mathbf{r}'} U_{\mathbf{r}'} + U_{\mathbf{r}}^* \hat{\mathcal{K}}_{\mathbf{r}\mathbf{r}'} \Phi_{\mathbf{r}'})} . \quad (\text{A.113})$$

where notation

$$\int \mathcal{D}[\Phi, \Phi^*] \dots = \prod_{\mathbf{r}} \int_{-\infty}^{\infty} d\text{Re}\Phi_{\mathbf{r}} d\text{Im}\Phi_{\mathbf{r}} \dots$$

is used. To establish the equivalence, we group the terms in the exponent as

$$-\frac{1}{12\beta'} (\Phi_{\mathbf{r}}^* - 6\beta' \sum_{\mathbf{r}'} U_{\mathbf{r}'}^* \hat{\mathcal{K}}_{\mathbf{r}'\mathbf{r}}) (\Phi_{\mathbf{r}} - 6\beta' \sum_{\mathbf{r}'} \hat{\mathcal{K}}_{\mathbf{r}'\mathbf{r}} U_{\mathbf{r}'}) + 3\beta' \sum_{\mathbf{r}} \sum_{\mathbf{r}''} U_{\mathbf{r}''}^* \hat{\mathcal{K}}_{\mathbf{r}''\mathbf{r}} \hat{\mathcal{K}}_{\mathbf{r}\mathbf{r}''} U_{\mathbf{r}''} . \quad (\text{A.114})$$

After a shift of variables and integrating out the auxiliary fields  $\Phi_{\mathbf{r}}$  the result coincides with (A.112) up to an unimportant proportionality factor. To obtain the equivalent description in terms of field  $\Phi$ , we now integrate over the angular variables  $\alpha_{\mathbf{r}}$ . To simplify notation, we define  $\chi_1 = \hat{\mathcal{K}}\Phi/2$  and  $\chi_2 = \hat{\mathcal{K}}^T\Phi^*/2$ , or more explicitly,

$$\begin{cases} \chi_1(\mathbf{r}) = \frac{1}{2} \sum_{\mathbf{r}'} \hat{\mathcal{K}}_{\mathbf{r}\mathbf{r}'} \Phi_{\mathbf{r}'} \\ \chi_2(\mathbf{r}) = \frac{1}{2} \sum_{\mathbf{r}'} \hat{\mathcal{K}}_{\mathbf{r}'\mathbf{r}} \Phi_{\mathbf{r}'}^* \end{cases} .$$

Integration over the phases in (A.112) now amounts to calculation of disentangled integrals at separate  $\mathbf{r}$ :

$$\int d\alpha(\mathbf{r}) e^{e^{i\alpha(\mathbf{r})} \chi_2(\mathbf{r}) + e^{-i\alpha(\mathbf{r})} \chi_1(\mathbf{r})} = 2\pi I_0(\sqrt{4\chi_1(\mathbf{r})\chi_2(\mathbf{r})}) ,$$

where  $I_0$  denotes the modified Bessel function. Thus, omitting non-essential overall prefactors the expression for  $Z_{XY}[\mathbf{A}]$  assumes the following form:

$$\int \mathcal{D}[\Phi, \Phi^*] e^{-\frac{1}{12\beta'} \sum_{\mathbf{r}} |\Phi_{\mathbf{r}}|^2 + \sum_{\mathbf{r}} \ln I_0(\sqrt{4\chi_1(\mathbf{r})\chi_2(\mathbf{r})})} .$$

Finally, after applying the Taylor expansion

$$\ln I_0(x) = \frac{x^2}{4} - \frac{x^4}{64} + \dots ,$$

and retaining only the leading terms, we obtain

$$Z_0 = \int \prod_{\mathbf{r}} d\Phi(\mathbf{r}) d\Phi^*(\mathbf{r}) d\mathbf{A}(\mathbf{r}) \Theta[\mathbf{A}(\mathbf{r})] \times \exp \left[ - \sum_{\mathbf{r}} \left( \frac{1}{24} (\overline{D}_i \Phi)^* (D_i \Phi) + \frac{1}{4} \left( \frac{1}{3\beta'} - 1 \right) |\Phi(\mathbf{r})|^2 + \frac{|\Phi(\mathbf{r})|^4}{64} + \frac{1}{2J'} (\overline{\nabla} \times \mathbf{A})_{\perp}^2 + \frac{1}{2K'} ((\overline{\nabla} \times \mathbf{A})_0 - \overline{f})^2 \right) \right] . \quad (\text{A.115})$$

The partition function (A.115) is the desired dual representation of our initial anisotropic  $XY$  model with the Berry phase, in the simple case  $J_1 = J_2 = 0$ .

Armed with the experience from the above derivation we now return to the partition function  $Z$  of the full-fledged model (A.84) containing  $J_1$  and  $J_2$ . As we will demonstrate, the effect of the next nearest neighbor interactions will be rather modest: to the leading order only the term proportional to  $|\Phi(\mathbf{r})|^2$  will be modified. The prefactors of this term will be modulated, having different values on the red and the black plaquettes.

To arrive at the dual representation of  $Z$ , we seek a gauge that will ensure the decoupling of the temporal and spatial components of  $\Lambda(\mathbf{q})$ , similarly to the radiation gauge in the simple example above. The bilinear terms in  $\Lambda_{\mu}$  appearing in the exponent can be classified as following: first, there is a contribution from the term  $(\overline{\nabla} \times \mathbf{A})_0^2$  which in an arbitrary (yet unknown) gauge has been already calculated in (A.87)

$$-\frac{1}{2K'} \left( \Lambda_{\mu}(-\mathbf{q}) \Lambda_{\mu}(\mathbf{q}) \overline{Q}_{\nu} Q_{\nu} - Q_{\nu} \overline{Q}_{\mu} \Lambda_{\mu}(-\mathbf{q}) \Lambda_{\nu}(\mathbf{q}) \right) . \quad (\text{A.116})$$

To facilitate the bookkeeping of various terms resulting from  $F[(\overline{\nabla} \times \mathbf{A})_{\perp}]$  we use the following set of identities:

$$\check{b}_x^T(-\mathbf{q}) = -ie^{iq_0} \check{\Lambda}_0^T(-\mathbf{q}) \begin{pmatrix} Q_y & 0 \\ 0 & Q_y^{\mathbf{g}} \end{pmatrix} + ie^{iq_y} Q_0 \check{\Lambda}_x^T(-\mathbf{q}) \sigma_3 \quad (\text{A.117})$$

$$\check{b}_x(\mathbf{q}) = -ie^{iq_0} \begin{pmatrix} \overline{Q}_y & 0 \\ 0 & \overline{Q}_y^{\mathbf{g}} \end{pmatrix} \check{\Lambda}_0(\mathbf{q}) - ie^{-iq_y} \overline{Q}_0 \sigma_3 \check{\Lambda}_x(\mathbf{q}) . \quad (\text{A.118})$$

The expressions for  $\check{b}_y(\mathbf{q})$  can be obtained by replacing  $x \leftrightarrow y$  and the overall change of sign. Using these identities the bilinear form

$$\check{b}_x^T(-\mathbf{q}) \begin{pmatrix} G_{11}(q_y) & G_{12}(q_y) \\ G_{21}(q_y) & G_{22}(q_y) \end{pmatrix} \check{b}_x(\mathbf{q}) + (x \leftrightarrow y)$$

can be written as a sum of two groups: the diagonal terms are

$$\check{\Lambda}_0^T(-\mathbf{q}) \begin{pmatrix} \overline{Q}_y Q_y G_{11}(q_y) & \overline{Q}_y^{\mathbf{g}} Q_y G_{12}(q_y) \\ \overline{Q}_y^{\mathbf{g}} Q_y^{\mathbf{g}} G_{21}(q_y) & \overline{Q}_y^{\mathbf{g}} Q_y^{\mathbf{g}} G_{22}(q_y) \end{pmatrix} \check{\Lambda}_0(\mathbf{q}) + \check{\Lambda}_y^T(-\mathbf{q}) \begin{pmatrix} \overline{Q}_0 Q_0 G_{11}(q_y) & -\overline{Q}_0 Q_0 G_{12}(q_y) \\ -\overline{Q}_0 Q_0 G_{21}(q_y) & \overline{Q}_0 Q_0 G_{22}(q_y) \end{pmatrix} \check{\Lambda}_y(\mathbf{q}) + (x \leftrightarrow y) . \quad (\text{A.119})$$

In addition, we obtain cross-terms that couple the spatial and temporal components of  $\check{\Lambda}_i$

$$Q_0 \check{\Lambda}_0^T(-\mathbf{q}) \left( P(q_y) \check{\Lambda}_y(\mathbf{q}) + P(q_x) \check{\Lambda}_x(\mathbf{q}) \right) + c.c. , \quad (\text{A.120})$$

where *c.c.* denotes complex conjugation and matrices  $P(q_\alpha)$  are defined as

$$P(q_\alpha) = \begin{pmatrix} -\bar{Q}_\alpha G_{11}(q_\alpha) & \bar{Q}_\alpha G_{12}(q_\alpha) \\ \bar{Q}_\alpha^\mathbf{g} G_{21}(q_\alpha) & -\bar{Q}_\alpha^\mathbf{g} G_{22}(q_\alpha) \end{pmatrix} .$$

Note that the terms diagonal in  $\Lambda_0$  are exactly what we encountered in (A.51) when we considered the 2D example. The off-diagonal terms can be eliminated altogether by choosing a gauge defined by the following relation between  $\Lambda_x(\mathbf{q})$  and  $\Lambda_y(\mathbf{q})$ :

$$P(q_y)\check{\Lambda}_y(\mathbf{q}) + P(q_x)\check{\Lambda}_x(\mathbf{q}) = 0 . \quad (\text{A.121})$$

The matrix equation can be resolved by  $\check{\Lambda}_y(\mathbf{q}) = \Gamma(\mathbf{q})\check{\Lambda}_x(\mathbf{q})$  where matrix  $\Gamma$  is defined as  $\Gamma(\mathbf{q}) = -P^{-1}(q_y)P(q_x)$ . The spatial part of the action in momentum space becomes

$$\sum_{q_0} \int \frac{dq_x dq_y}{\beta\epsilon(2\pi)^2} \left[ i\pi \left( \check{l}_x^T(-\mathbf{q}) + \check{l}_y^T(-\mathbf{q})\Gamma(\mathbf{q}) \right) \check{\Lambda}_x(\mathbf{q}) - \check{\Lambda}_x(-\mathbf{q})\check{X}(\mathbf{q})\check{\Lambda}_x(\mathbf{q}) \right] , \quad (\text{A.122})$$

where  $2 \times 2$  matrix  $\check{X}$  is defined as

$$\begin{aligned} & \frac{1}{4K'} \left[ \begin{pmatrix} Q_\perp^2 & 0 \\ 0 & (Q_\perp^\mathbf{g})^2 \end{pmatrix} + \Gamma^T(-\mathbf{q}) \begin{pmatrix} Q_\perp^2 & 0 \\ 0 & (Q_\perp^\mathbf{g})^2 \end{pmatrix} \Gamma(\mathbf{q}) \right] \\ & + \frac{1}{4} \left[ \begin{pmatrix} G_{11}(q_x) & -G_{12}(q_x) \\ -G_{21}(q_x) & G_{22}(q_x) \end{pmatrix} \right. \\ & \left. + \Gamma^T(-\mathbf{q}) \begin{pmatrix} G_{11}(q_x) & -G_{12}(q_x) \\ -G_{21}(q_x) & G_{22}(q_x) \end{pmatrix} \Gamma(\mathbf{q}) \right] . \quad (\text{A.123}) \end{aligned}$$

Note that we omitted the second term in (A.116) as it is only of the order  $Q_\perp^6$  and can be safely neglected for extracting the long distance behavior. After integrating out  $\Lambda_x$ , we obtain

$$\begin{aligned} & \exp \left[ -\frac{\pi^2}{4} \sum_{q_0} \int \frac{dq_x dq_y}{\beta\epsilon(2\pi)^2} \times \right. \\ & \left. \left( \check{l}_x^T(-\mathbf{q}) + \check{l}_y^T(-\mathbf{q})\Gamma(\mathbf{q}) \right) X \left( \check{l}_x(\mathbf{q}) + \Gamma^T(-\mathbf{q})\check{l}_y(\mathbf{q}) \right) \right] , \quad (\text{A.124}) \end{aligned}$$

where  $X = \check{X}^{-1}$ . Expanding this expression in the region of small momenta as in (A.55) and retaining only the leading order terms, as in the two-dimensional example, we find

$$\begin{aligned} & -\pi^2 \sum_{q_0} \int \frac{dq_x dq_y}{\beta\epsilon(2\pi)^2} \frac{1}{\frac{1}{2\tilde{J}}q_0^2 + \frac{1}{2K'}q_{\perp^2}} \times \\ & \frac{\left( q_y l_x(-\mathbf{q}) - q_x l_y(-\mathbf{q}) \right) \left( q_y l_x(\mathbf{q}) - q_x l_y(\mathbf{q}) \right)}{q_\perp^2} . \quad (\text{A.125}) \end{aligned}$$

Observe that there are no cross-terms that couple modes at wavevectors  $\mathbf{q}$  and  $\mathbf{q} - \mathbf{g}$  to the order of  $q^0$  and  $q^{-2}$ . The spatial part of the action after integrating out the gauge fields is equivalent to the result (A.107) obtained in the framework of simple model  $Z_0$  where  $J'$  is replaced by the effective coupling constant  $\tilde{J} = J' + J_1 + J_2$ .

Combining (A.125) and (A.68), the final form of the action  $Z$  in terms of closed vortex loops  $\mathbf{l}(\mathbf{r})$  can be written as

$$\begin{aligned} Z = \sum_{\mathbf{l}(\mathbf{r})} \delta_{\nabla \cdot \mathbf{l}} \exp \left[ \sum_{\mathbf{r}} \left( 2\pi i \mathbf{l}(\mathbf{r}) \cdot \mathbf{A}_f(\mathbf{r}) - E'_c(\boldsymbol{\rho}) l_0^2(\mathbf{r}) \right) \right. \\ \left. - \pi^2 \sum_{q_0} \int \frac{dq_x dq_y}{\beta\epsilon(2\pi)^2} \left( 2\tilde{J} \frac{l_0(-\mathbf{q})l_0(\mathbf{q})}{q_\perp^2} \right. \right. \\ \left. \left. + \frac{1}{\frac{1}{2\tilde{J}}q_0^2 + \frac{1}{2K'}q_{\perp^2}} l_T(\mathbf{q})l_T(-\mathbf{q}) \right) \right] , \quad (\text{A.126}) \end{aligned}$$

where  $E'_c(\boldsymbol{\rho}) = \pm\pi^2(J_1 - J_2)/4$  depending on whether  $\boldsymbol{\rho}$  corresponds to a black or a red plaquette.

We had intentionally used momentum representation for the last two terms in the exponent. It is important to recognize that these terms are precisely what one would have obtained for the usual 3D XY model with no next nearest neighbors interaction and the effective nearest neighbors coupling constant equal to  $\tilde{J} = J' + J_1 + J_2$ . Thus, we may introduce a dual gauge field  $\mathbf{A}(\mathbf{r})$  and present the partition function as

$$\begin{aligned} Z = \sum_{\mathbf{l}(\mathbf{r})} \int_{-\infty}^{\infty} \prod_{\mathbf{r}} d\mathbf{A}(\mathbf{r}) \Theta[\mathbf{A}(\mathbf{r})] \delta_{\nabla \cdot \mathbf{l}} \times \\ \exp \left[ \sum_{\mathbf{r}} \left( 2\pi i \mathbf{l}(\mathbf{r}) \cdot (\mathbf{A}(\mathbf{r}) + \mathbf{A}_f(\mathbf{r})) \right) \right. \\ \left. - E'_c(\boldsymbol{\rho}) l^2(\mathbf{r}) - \frac{(\nabla \times \mathbf{A})_\perp^2}{2\tilde{J}} - \frac{(\nabla \times \mathbf{A})_0^2}{2K'} \right] . \quad (\text{A.127}) \end{aligned}$$

By shifting  $\mathbf{A} \rightarrow \mathbf{A} - \mathbf{A}_f$  back we obtain

$$\begin{aligned} Z = \int_{-\infty}^{\infty} \prod_{\mathbf{r}} d\mathbf{A}(\mathbf{r}) \Theta[\mathbf{A}(\mathbf{r})] \exp \left[ \sum_{\mathbf{r}} \left( 2\pi i \mathbf{l}(\mathbf{r}) \cdot \mathbf{A}(\mathbf{r}) \right) \right. \\ \left. - E'_c(\boldsymbol{\rho}) l^2(\mathbf{r}) - \frac{(\nabla \times \mathbf{A})_\perp^2}{2\tilde{J}} - \frac{[(\nabla \times \mathbf{A})_0 - \bar{f}]^2}{2K'} \right] . \quad (\text{A.128}) \end{aligned}$$

Note that in the absence of the next nearest neighbors interactions, a similar expression (A.85) contained no quadratic terms  $\mathbf{l}^2(\mathbf{r})$  and the core energy  $-\frac{1}{\beta_V(\beta')}\mathbf{l}^2(\mathbf{r})$  was introduced by hand. In the present case, the difference  $\Delta E'_c$  of the core energies on the black and red sites is *finite* due to the anisotropic next nearest neighbors interactions. However, the average magnitude is still zero within our model, and here we also need to introduce a constant average core energy term  $\frac{1}{\beta_V(\beta'_0)}\mathbf{l}^2(\mathbf{r})$ . Thereby we replace  $E'_c(\boldsymbol{\rho})$  in (A.128) by

$$\frac{1}{\beta_V(\beta'(\boldsymbol{\rho}))} \rightarrow \frac{1}{\beta_V(\beta'_0)} + E'_c(\boldsymbol{\rho}) ,$$

where the function  $\beta'(\boldsymbol{\rho})$  is implicitly defined by this equation.

The remaining steps repeat the derivation leading from (A.108) to (A.115) with the replacement  $\beta' \rightarrow \beta'(\boldsymbol{\rho})$  and result in the Ginzburg-Landau expansion of our dual theory:

$$Z = \int \prod_{\mathbf{r}} d\Phi(\mathbf{r}) d\Phi^*(\mathbf{r}) d\mathbf{\Lambda}(\mathbf{r}) \Theta[\mathbf{\Lambda}(\mathbf{r})] \times \exp \left[ - \sum_{\mathbf{r}} \left\{ \frac{1}{24} (\overline{D}_i \Phi)^* (D_i \Phi) + \frac{1}{4} \left( \frac{1}{3\beta'(\boldsymbol{\rho})} - 1 \right) |\Phi(\mathbf{r})|^2 + \frac{1}{64} |\Phi(\mathbf{r})|^4 + \frac{1}{2J'} (\overline{\nabla} \times \mathbf{\Lambda})_{\perp}^2 + \frac{1}{2K'} ((\overline{\nabla} \times \mathbf{\Lambda})_0 - \overline{f})^2 \right\} \right]. \quad (\text{A.129})$$

This is our final result – the partition function (A.129) represents the Ginzburg-Landau functional of a dual type-II superconductor appropriate for our model and subjected to a constant dual magnetic field  $\overline{f}$ .

- 
- <sup>1</sup> J. Corson, R. Mallozzi, J. Orenstein, J. N. Eckstein, and I. Bozovic, *Nature* **398**, 221 (1999).
- <sup>2</sup> Z. A. Xu, N. P. Ong, Y. Wang, T. Kakeshita, and S. Uchida, *Nature* **406**, 486 (2000); Y. Wang, S. Ono, Y. Onose, G. Gu, Y. Ando, Y. Tokura, S. Uchida, and N. P. Ong, *Science* **299**, 86 (2003).
- <sup>3</sup> J. C. Campuzano *et al.*, unpublished.
- <sup>4</sup> V. J. Emery and S. A. Kivelson, *Nature* **374**, 434 (1995).
- <sup>5</sup> M. Franz and Z. Tešanović, *Phys. Rev. Lett.* **87**, 257003 (2001); Z. Tešanović, O. Vafek, and M. Franz, *Phys. Rev. B* **65**, 180511 (2002); M. Franz, Z. Tešanović, and O. Vafek, *ibid.* **66**, 054535 (2002).
- <sup>6</sup> Z. Tešanović, *Phys. Rev. B* **59**, 6449 (1999).
- <sup>7</sup> I. F. Herbut, *Phys. Rev. Lett.* **88**, 047006 (2002); B.H. Seradjeh and I. F. Herbut, *Phys. Rev. B* **66**, 184507 (2002).
- <sup>8</sup> M. Vershinin, S. Misra, S. Ono, Y. Abe, Y. Ando, and A. Yazdani, *Science* **303**, 1995 (2004).
- <sup>9</sup> T. Hanaguri *et al.*, to appear in *Nature*; K. McElroy, D.-H. Lee, J. E. Hoffman, K. M. Lang, E. W. Hudson, H. Eisaki, S. Uchida, J. Lee, J. C. Davis, cond-mat/0404005; J. E. Hoffman, E. W. Hudson, K. M. Lang, V. Madhavan, H. Eisaki, S. Uchida, and J. C. Davis, *Science* **295**, 466 (2002).
- <sup>10</sup> C. Howald, H. Eisaki, N. Kaneko, M. Greven, and A. Kapitulnik, *Phys. Rev. B* **67**, 014533 (2003); M. A. Steiner and A. Kapitulnik, cond-mat/0406227.
- <sup>11</sup> H. D. Chen, O. Vafek, A. Yazdani, and S. C. Zhang, *Phys. Rev. Lett.* **93**, 187002 (2004).
- <sup>12</sup> Z. Tešanović, *Phys. Rev. Lett.* **93**, 217004 (2004).
- <sup>13</sup> M. P. A. Fisher and D. H. Lee, *Phys. Rev. B* **39**, 2756 (1989).
- <sup>14</sup> H. D. Chen, S. Capponi, F. Alet, and S. C. Zhang, cond-mat/0312660; H. D. Chen, C. Wu, and S. C. Zhang, *Phys. Rev. Lett.* **92**, 107002 (2004).
- <sup>15</sup> E. Altman and A. Auerbach, *Phys. Rev. B* **65**, 104508 (2002).
- <sup>16</sup> While the Cooper and the real-space pairs correspond to two distinct limiting behaviors there is still a sense in which they are two sides of the same coin: in both cases charge modulation arises primarily from the particle-particle channel. Similarly, a recent preprint, P. W. Anderson, cond-mat/0406038, also examines the effect on the LDOS of the modulations in the particle-particle channel. This puts these works in the category different from theories which focus on non-uniformities in the particle-hole channel, for example H. C. Fu, J. C. Davis, and D. H. Lee, cond-mat/0403001. Other prominent examples of such theories are J. Zaanen and O. Gunnarson, *Phys. Rev. B* **40**, 7391 (1989); K. Machida, *Physica C* **158**, 192 (1989); S. A. Kivelson, I. P. Bindloss, E. Fradkin, V. Oganesyan, J. M. Tranquada, A. Kapitulnik, and C. Howald, *Rev. Mod. Phys.* **75**, 1201 (2003); S. Chakravarty, R. B. Laughlin, D. K. Morr, and C. Nayak, *Phys. Rev. B* **63**, 094503 (2001); Y. Zhang, E. Demler, and S. Sachdev, *Phys. Rev. B* **66**, 094501 (2002). A useful general study of a non-uniform superconductor is found in D. Podolsky, E. Demler, K. Damle, and B.I. Halperin, *Phys. Rev. B* **67**, 094514 (2003).
- <sup>17</sup> A Hofstadter-type problem is also at the root of various inhomogeneous phases of quantum spin-dimer models; see L. Balents, L. Bartosch, A. Burkov, S. Sachdev, and K. Sengupta, cond-mat/0408329 and references therein. For early discussions of valence-bond-solids in such quantum spin-dimer models see S. Sachdev and N. Read, *Int. J. Mod. Phys. B* **5**, 219 (1991) and M. Vojta and S. Sachdev, *Phys. Rev. Lett.* **83**, 3916 (1999).
- <sup>18</sup> O. Vafek, A. Melikyan, M. Franz, and Z. Tešanović, *Phys. Rev. B* **63**, 134509 (2001) and references therein.
- <sup>19</sup> M. Sutherland, D. G. Hawthorn, R. W. Hill, F. Ronning, S. Wakimoto, H. Zhang, C. Proust, E. Boaknin, C. Lupien, L. Taillefer, R. Liang, D. A. Bonn, W. N. Hardy, R. Gagnon, N. E. Hussey, T. Kimura, M. Nohara, H. Takagi, cond-mat/0301105.
- <sup>20</sup> There is a large and growing field-theory literature on non-compact, parity-preserving QED<sub>3</sub>, which is the low-energy limit of (9). Those interested will find T. Appelquist and L. C. R. Wijewardhana, hep-ph/0403250, C. S. Fischer, R. Alkofer, T. Dahm, and P. Maris, hep-ph/0407104, S. J. Hands, J. B. Kogut, L. Scorzato, and C. G. Strouthos, hep-lat/0404013, and J. Alexandre, K. Farakos, and N. E. Mavromatos, hep-ph/0407265 to provide good overview of frontier issues and useful source of additional references.
- <sup>21</sup> Representing  $a_\mu$  as a U(1) gauge field constitutes the “nat-

ural” gauge choice for this problem due to the following fundamental feature of a spin-singlet superconductor: consider a system made up of two *distinct* species of fermions, “up” ( $u$ ) and “down” ( $d$ ). The normal part has the form consisting entirely of bilinears  $u^\dagger u$  and  $d^\dagger d$  so that  $u$  and  $d$  flavors are *separately* conserved. Note that we are not at all concerned here with the symmetry with respect to rotations between  $u$  and  $d$  – such symmetry may or may not be present and the relevant symmetry of the normal part is just the global  $U_u(1) \times U_d(1)$ . The inclusion of pairing terms of the form  $ud$  and  $d^\dagger u^\dagger$  (but not  $uu$  or  $dd$  and their complex conjugates!) breaks this symmetry by violating the conservation law for the *total* fermion number, the sum of “up” and “down” flavors. There remains, however, an intact *continuous*  $U_{u-d}(1)$  symmetry associated with the *relative* fermion number, the difference between “up” and “down” flavors. This continuous symmetry signals the remaining conservation law (spin conservation in spin-singlet superconductors). Actually, our lattice  $d$ -wave superconductor model (13) is a simple illustration of this general feature: consider screening the bond phase factor of  $\Delta_{ij}$  by site phase factors arising from the gauge transformed electron fields  $c_{i\sigma}$ : there are  $2N$  bond phase factors  $\exp(i\theta_{ij})$  versus only  $N$  site phases  $\exp(-i\varphi_i)$ . The most natural solution is to introduce  $2N$  site phase factors  $\exp(-i\varphi_{i\uparrow})$  and  $\exp(-i\varphi_{i\downarrow})$  and attach them via gauge transformation to  $c_{i\uparrow}$  and  $c_{i\downarrow}$ . In this way one can completely eliminate the *center-of-mass*  $\exp(i\theta_{ij})$ <sup>18</sup> from (13) by a judicious choice of  $\exp(i\varphi_{i\sigma})$ :  $\exp(i\theta_{ij})\exp(-i\varphi_{i\uparrow} - i\varphi_{j\downarrow}) \rightarrow \exp(-ia_{ij})$ ;  $\exp(i\theta_{ij})\exp(-i\varphi_{i\downarrow} - i\varphi_{j\uparrow}) \rightarrow \exp(ia_{ij})$ , where  $a_{ij}$  is a bond phase antisymmetric under  $\uparrow \leftrightarrow \downarrow$  exchange. This is nothing but the tight-binding lattice version of the FT transformation and leads directly to the  $U(1)$  representation of the Berry gauge field  $a \leftrightarrow a_{ij}$ . Here  $\exp(2ia_{ij})$  is determined by  $\exp(i\varphi_{i\uparrow} - i\varphi_{j\uparrow} - i\varphi_{i\downarrow} + i\varphi_{j\downarrow})$ , where  $\exp(i\varphi_{i\sigma})$  are found in terms of *center-of-mass*  $\theta_{ij}$ ’s from  $\exp(i\varphi_{i\uparrow} + i\varphi_{j\uparrow} + i\varphi_{i\downarrow} + i\varphi_{j\downarrow}) \leftrightarrow \exp(2i\theta_{ij})$ . Note also that the hopping term in the Hamiltonian acquires a gauge field factor  $\exp(i\varphi_{i\uparrow(\downarrow)} - i\varphi_{j\uparrow(\downarrow)})$  for spin  $\uparrow$  ( $\downarrow$ ) fermions, with  $\varphi_{i\uparrow(\downarrow)} - \varphi_{j\uparrow(\downarrow)}$  being the lattice equivalents of the gauge fields  $v_{A(B)}$  featured in the continuum FT transformation. Since  $a_{ij}$  is ultimately given by the (half of) phase differences  $(\varphi_{i\uparrow} - \varphi_{j\uparrow}) - (\varphi_{i\downarrow} - \varphi_{j\downarrow})$  – expressed in terms of  $\theta_{ij}$ ’s – its configurations are non-compact, *i.e.* monopole free, by construction. Note that these arguments do not generally apply to superconductors which are not spin-singlet. For example, if we have a single flavor of spinless fermions  $f$ , the normal part made up of  $f^\dagger f$  bilinears has only a single  $U(1)$  symmetry – pairing terms of the form  $f^\dagger f^\dagger$  and  $ff$  (in the odd angular momentum channel) break this  $U(1)$  symmetry down to *discrete*  $Z_2$ .

<sup>22</sup> In short, the gauge theory (1, 9) is non-compact by construction. Recently, there has been much interest in quantum spin systems where the underlying effective gauge theory is compact but its monopole (instanton) configurations are dynamically irrelevant at a critical point or in a critical phase. In such cases, one is again back to a non-compact QED<sub>3</sub> with massless bosons or fermions; see M. Hermele, T. Senthil, M. P. A. Fisher, P. A. Lee, N. Nagaosa, and X.-G. Wen, cond-mat/0404751 and references therein.

<sup>23</sup> This chirally symmetric “algebraic Fermi liquid” phase has unusual thermodynamic and transport properties; see O. Vafek and Z. Tešanović, Phys. Rev. Lett. **91**, 237001 (2003). For example, its specific heat  $\sim T^2$ , just as in a

neighboring superconducting state (see Fig. 1). This translates into heat transport similar to that of a nodal  $d$ -wave superconductor, *i.e.* the critical pseudogap state is a “thermal metal”. On the other hand, since vortex-antivortex pairs are unbound, the same state is also a “charge insulator”, as emphasized in Ref.<sup>5</sup> and detailed in this manuscript. This implies breakdown of the Wiedemann-Franz law in the pseudogap state. The  $T^2$  specific heat and heat transport are due to spin excitations carried by nodal BdG fermions. Remarkably, the pseudogap is also a “spin dielectric” in the sense that Pauli spin susceptibility vanishes as  $\chi \sim q^2$ , in contrast to  $\chi \sim q$  in a superconductor. Consequently, the Wilson ratio also vanishes as temperature goes to zero.

<sup>24</sup> In general, the Hamiltonian (14) will also contain terms which do not involve the standard XY phase differences of bond phases but are instead due to  $\Delta_{ij}$  itself being a “hopping term” in a  $d$ -wave superconductor (unlike the case of a simple  $s$ -wave superconductor). The leading such term is  $K \cos(\theta_{12} - \theta_{23} + \theta_{34} - \theta_{41})$  around a plaquette of the CuO<sub>2</sub> lattice. Such terms are down by a factor  $\sim \Delta^2/t^{*2}$  relative to the XY terms kept in (14) and one can neglect them in cuprates, where  $\Delta$  remains significantly smaller than  $t^*$  for most of the underdoped regime, judged by the ratio of  $v_\Delta$  to  $v_F$ <sup>19</sup>. However, such terms might become important, along with many other longer range terms excluded from (14) and (36), in the calculation of vortex core energies later in the text since  $K$  is not necessarily smaller than  $J_1 - J_2$ .

<sup>25</sup> D. R. Nelson, in Phase Transitions and Critical Phenomena, edited by C. Domb and J. L. Lebowitz, (Academic Press, London, 1983), Vol. 7, p. 1.

<sup>26</sup> J. V. Jose, L. P. Kadanoff, S. Kirkpatrick and D. R. Nelson, Phys. Rev. B **16**, 1217 (1977).

<sup>27</sup> The vortex core mass  $M$  can be computed in a specific microscopic model, say a  $d$ -wave BCS model of vortex quantum tunneling (A. Mizel, unpublished); also, see J. H. Han, J. S. Kim, M. J. Kim, and P. Ao, cond-mat/0407156 and references therein. Similarly, one can also envision computing the mass with a Gutzwiller correlated BCS wavefunction.

<sup>28</sup> Ch. Renner, B. Revaz, K. Kadowaki, I. Maggio-Aprile, and Ø. Fischer, Phys. Rev. Lett. **80**, 3606 (1998); E. W. Hudson, S. H. Pan, A. K. Gupta, K.-W. Ng, and J. C. Davis, Science, **285**, 88 (1999); S. H. Pan, E. W. Hudson, A. K. Gupta, K.-W. Ng, H. Eisaki, S. Uchida, and J. C. Davis, Phys. Rev. Lett. **85**, 1536 (2000).

<sup>29</sup> M. Franz and Z. Tešanović, Phys. Rev. B **63**, 064516 (2001).

<sup>30</sup> H. Tsuchiura, M. Ogata, Y. Tanaka, and S. Kashiwaya, Phys. Rev. B **68**, 012509 (2003) and references therein.

<sup>31</sup> Q.-H. Wang, J. H. Han and D.-H. Lee, Phys. Rev. Lett. **87**, 167004 (2001).

<sup>32</sup> P. A. Lee and X.-G. Wen, Phys. Rev. B **63**, 224517 (2001).

<sup>33</sup> L. B. Ioffe and A. J. Millis, Phys. Rev. B **66**, 094513 (2002).

<sup>34</sup> Viewing cuprates as entirely analogous to superfluid <sup>4</sup>He, however, should be studiously avoided as emphasized elsewhere in this paper – the essential role of gapless fermions, the Galilean invariance being broken by the CuO<sub>2</sub> lattice, the conversion of the Goldstone mode to gapped plasmon in superconductors are but a few examples of the calamities that will be visited upon those who take the similarities too far.

<sup>35</sup> In transport calculations a small empirical Bardeen-

Stephen core dissipation should be included for better quantitative accuracy.

<sup>36</sup> H. Kleinert, *Gauge Fields in Condensed Matter* (World Scientific, Singapore, 1989).

<sup>37</sup> A. A. Abrikosov, Zh. Eksp. Teor. Fiz. **32**, 1442 (1957); Sov. Phys. JETP **5**, 1174 (1957).

<sup>38</sup> Since we are discussing an  $s$ -wave case here, the pseudogap  $\Delta$  in the fermionic action would have to be changed from a  $d_{x^2-y^2}$ - to an  $s$ -wave form.

<sup>39</sup> J. M. Singer, M. H. Pedersen, T. Schneider, H. Beck, and H.-G. Matuttis, Phys. Rev. B **54**, 1286 (1996) and references therein.

<sup>40</sup> Although  $\delta\Delta_{ij} \leftrightarrow \delta n_i + \delta n_j$  remains a useful approximation and will be used occasionally in this paper.

<sup>41</sup> A more explicit argumentation for the  $\delta\mathbf{B}_d(\mathbf{r}) \leftrightarrow \delta\Delta_{ij}$  correspondence goes as follows: Note that  $\delta\Delta_{ij}$  as defined in (33) is nothing but the Hubbard-Stratonovich field decoupling the  $\hat{\theta}_{ij}^2$  term in the action. By the reasoning of the previous ‘‘pedagogical’’ subsection this immediately makes  $\delta\Delta_{ij}$  equivalent to the modulation of the dual induction  $\mathbf{B}_d$ . But why should this modulation be translated into the modulation of the pairing gap amplitude  $\Delta_{ij}$  as our notation seems to imply? Consider the spatial region where  $\mathbf{B}_d$  is larger (smaller) than its average. This region attracts (repels) dual vortices, i.e. vortices in the dual field  $\Phi$ . Consequently, the amplitude of  $\Phi$  is reduced (enhanced) in this region which translates into the (anti)vortices in  $\theta_{ij}$  itself staying away from (being drawn to) the same region. This, by the analyticity of the complex gap function  $\Delta_{ij}$  near a (anti)vortex position, finally implies that its amplitude must be larger (smaller) than its average in the regions where  $\mathbf{B}_d$  is larger (smaller) than its average. Con-

sequently,  $\delta\mathbf{B}_d(\mathbf{r}) \leftrightarrow \delta\Delta_{ij}$  to the leading order, where  $\delta\Delta_{ij}$  indeed assumes the meaning of the modulation in the  $d$ -wave pairing amplitude, up to an overall factor which can only be determined from a fully microscopic theory. In the present paper, this overall factor should be treated as an adjustable parameter. Finally, note that the above reasoning does not imply that  $|\Delta_{ij}|$  is the operator canonically conjugate to  $\theta_{ij}$ . Rather, it simply relates the modulation in the ground state expectation value of such (unknown) operator to  $\delta\Delta_{ij}$ .

<sup>42</sup> N. R. Cooper, S. Komineas, and N. Read, cond-mat/0404112.

<sup>43</sup> M. Franz, I. Affleck, and M. H. S. Amin, Phys. Rev. Lett. **79**, 1555 (1997).

<sup>44</sup> Again, we should remind the reader that this dual Lagrangian contains the contribution from the charge channel but ignores the spin. The coupling to the spin channel, associated with nodal fermions, enters through the Berry gauge field  $a_\mu$  and its contribution to  $\mathcal{L}_d$  is important near a critical point but not otherwise. In the parlance of effective field theory  $\mathcal{L}_d$  describes the ‘‘high energy’’ physics of charge sector relative to the ‘‘low energy’’ physics of spin. Of course, the effect of  $a$  remains *essential* for the low energy fermiology throughout the pseudogap state.

<sup>45</sup> E. Brown, Phys. Rev **133**, A1038 (1964).

<sup>46</sup> J. Zak, Phys. Rev. **134**, A1602 (1964); **134**, A1607 (1964).

<sup>47</sup> J. W. Negele and H. Orland, *Quantum Many-Particle Systems* (Addison-Wesley, New York, 1988).

<sup>48</sup> Only five of the six parameters are independent:  $\delta\Delta_{ij}$  are related to dual fluxes  $\delta B_d$ , whose average over a unit cell is zero.